CANADIAN SPACE AGENCY

CLASS GRANT & CONTRIBUTION PROGRAM TO SUPPORT RESEARCH, AWARENESS AND LEARNING IN SPACE SCIENCE AND TECHNOLOGY

Final Report for the Grant Agreement dated September 4, 2012

Generating the complete WINDII dataset and CMAM simulations of future investigations

Centre for Research in Earth and Space Science

York University

Young-Min Cho
Victor Fomichev
Marianna Shepherd
Brian Solheim

Approved by: Gordon G. Shepherd, Principal Investigator

October 10, 2013

EXECUTIVE SUMMARY

The Wind Imaging Interferometer (WINDII), a joint project of the Canadian Space Agency (CSA), the Centre National d'Etudes Spatiales (CNES) and the National Aeronautics and Space Administration (NASA) was launched on NASA's Upper Atmosphere Research Satellite (UARS) in September, 1991. The data were processed at the NASA Goddard Space Flight Center, using software provided by the Principal Investigators. This processing ceased in 1997 when the mission (originally planned for 30 months) experienced budgetary limitations. The WINDII software was then transported at York University from a VAX/VMS environment to a UNIX environment. This was successfully accomplished, but the processing of the data acquired subsequently was not implemented before WINDII support terminated with the turnoff of the WINDII instrument in 2003. The objectives of this Grant Agreement were to update the data processing system to regain compatibility with current compilers and computers, to process the as yet unprocessed data, to test the validity of the newly processed data by comparisons with the old, and to make comparisons with the newly developed Canadian Middle Atmosphere Model (CMAM) simulations of airglow emission rates.

All of this has been successfully carried out. A fully updated processing system has been created, with the ability to make any future changes in software required as a result of new studies carried out by anyone in the Canadian research community. The new results have been validated against the earlier results, and comparisons have been made with the CMAM model for the new time period. This latter part of the mission was found to have differed from the earlier part in two significant ways. First, the satellite altitude was no longer maintained at its specified value of 585 km, as the fuel reserve no longer allowed it. This lowered altitude gave greater exposure to the bright Earth, allowing increased light to penetrate the baffle system, enhancing the scattered light for daytime observations. Second, the WINDII team agreed to operate the instrument without temperature control, in order to contribute to the reduction of operational power required. The resulting temperature change caused a shift in the phase of the Michelson interferometer that shifted the phase corresponding to zero wind, causing a bias in the wind measurements. The effects of these influences have been investigated.

The original Science Data Production Processing Software (SDPPS) worked well for the $O(^1S)$ and $O(^1D)$ atomic oxygen winds temperatures and emission rates. It also produced good results for the OH and O_2 Atm Band emissions, but their winds were not considered publishable. The ionized atomic oxygen O^+ emission rates, of great potential value were also questionable. All of these limitations can be challenged with the capability now available. Good progress has already been made with the O^+ emission.

Comparison of $O(^1S)$ emission rate vertical profiles show good agreement between WINDII and the CMAM in terms of shape and peak altitude, but the peak emission rates are higher for WINDII than for the CMAM. The primary focus of the CMAM simulations is the variation with solar activity, measured as the F10.7 solar radio flux measured by NRC. Both the CMAM and WINDII show weak correlation between the raw observed emission rate and solar flux, but when the seasonal variation is removed from the data, both show strong correlation with the solar flux.

CONTENTS

1: Introduction:

This is the final report on a combined study of the previously unanalyzed WINDII data and new CMAM simulations that together extend and project new resources for Canadian space science. This work was done under the CSA Class Grant and Contribution Program under a grant to York University entitled "Generating the complete WINDII dataset and CMAM simulations of future investigations". The work began on September 1, 2012 and was completed on August 31, 2013. For a review of WINDII history and accomplishments see Shepherd et al. (1912).

The challenge for the WIND Imaging Interferometer (WINDII) activity was to begin with code, compilers and computers last run about ten years ago and update this code so that it would run with current compilers on modern computers. This turned out to be a major task, owing to a lack of compatibility between the evolutions of these elements during the intervening years. However, this was accomplished, with the originally unappreciated consequence that the primary achievement was "to regain complete control of the WINDII software". That means that any future desired changes in the WINDII software can be readily made. The entire WINDII dataset was run with the new updated software, and while the new data, between 1997 and 2003, are important, a major outcome was the regeneration of the Level 1 data that had not been previously saved for all of the data. That opens up major new opportunities for the extension of the WINDII data into new scientific territory. Effectively the "Imaging" in "WIND Imaging Interferometer" is now accessible and can be exploited through the Level 1 data. An example is the high resolution images of Polar Mesospheric Clouds that are now available. However, the "real" outcome of this work is the delivery of the WINDII extended archival dataset.

For the Canadian Middle Atmosphere Model (CMAM) the challenge was to simulate the data and diagnose the model results for the whole length of the WINDII flight (1991-2003). The WINDII airglow data have been compared with the results obtained from the extended CMAM for the different levels of solar activity, in different latitudinal zones and seasons. For this comparison, the extended CMAM dataset obtained during the CMAM30 project (funded by CSA) have been diagnosed. The extended CMAM extends from the ground up to about 200-300 km depending on solar cycle and includes comprehensive lower and middle atmosphere physics and chemistry and the most important physical and chemical processes of the lower thermosphere. The photochemical module of the extended CMAM is fully interactive and consists of comprehensive neutral chemistry for the upper atmosphere (stratosphere, mesosphere and thermosphere) and basic ionospheric chemistry for the mesosphere-thermosphere domain. For the CMAM30 project, the extended CMAM was run in a nudged configuration, called CMAM Simplified Assimilation System (CMAM-SAS), where the model is nudged to wind and temperature observations below the stratopause level thus providing a realistic day-to-day dynamical forcing in the lower part of the domain. Thus the extended CMAM-SAS is able to produce a realistic variability of many airglow emissions from the mesosphere and lower thermosphere involving O-related and H-related species. Calculations of the airglow fields have been performed online assuming photochemical equilibrium between the excitation and quenching processes at each grid point for the excited molecular and/or atomic levels responsible for a given airglow process.

The modelling component of the current project was undertaken under the leadership of Professor John C. McConnell who now tragically is no longer with us. While the work was successfully completed by other team members, his loss to the project impacted on the team in so many different ways that must be recognized, though not recorded here.

In summary this project had two sets of objectives, specific objectives, and overarching objectives. The specific objectives were:

a. Completing the analysis of the full WINDII dataset and validating it.
b. Conducting the reanalysis of the previously processed data in order to re-generate the Level 1 data.
c. Generating a full archival set of WINDII data for future use.
d. Through modelling and WINDII-TIMED data analysis, to commence analysis of solar cycle effects datasets.

The overarching objectives are to describe clearly the new dataset available to the community and to provide an update on the modelling capability. The report includes a projection of future capability for Canadian space science of the whole-atmosphere based on this newly acquired expertise in data acquisition and modelling. For basic background on airglow measurements see Appendix E.

2. The original WINDII processing system

2.1 Background

The WINDII measurements were originally processed using the SDPPS (Scientific Data Production Processing Software) package developed in France to run on a VAX/VMS computer at the Goddard Space Flight Center. The resulting data were transferred to the WINDII Operations Centre at York University over a dedicated communications line. When the NASA operations ended because of budgetary limitations, the SDPPS was moved to York University, where it was ported to operate in a desktop Linux workstation environment. For the Linux/VAX porting project, the SDPPS was separated into three segments; WOADEP, JOBIT, and WINSLIN. WOADEP (Windii Orbit/Attitude Data Extraction Program) converts the raw UARS orbit/attitude data to a compatible file format as an input to the SDPPS process. It is an IDL program that runs a FORTRAN program, OA_EXTRACT, in the VAX environment. JOBIT (JOBstream IniTialisation Software) is a GUI interface IDL program that creates a job script file which allows users to run the SDPPS programs. WINSLIN (WINdii Sdpps for LINux) contains the FORTRAN programs and libraries from the WINDII SDPPS for Level 1 and Level 2 data processing. The processing steps are illustrated in Graphic 1 below.

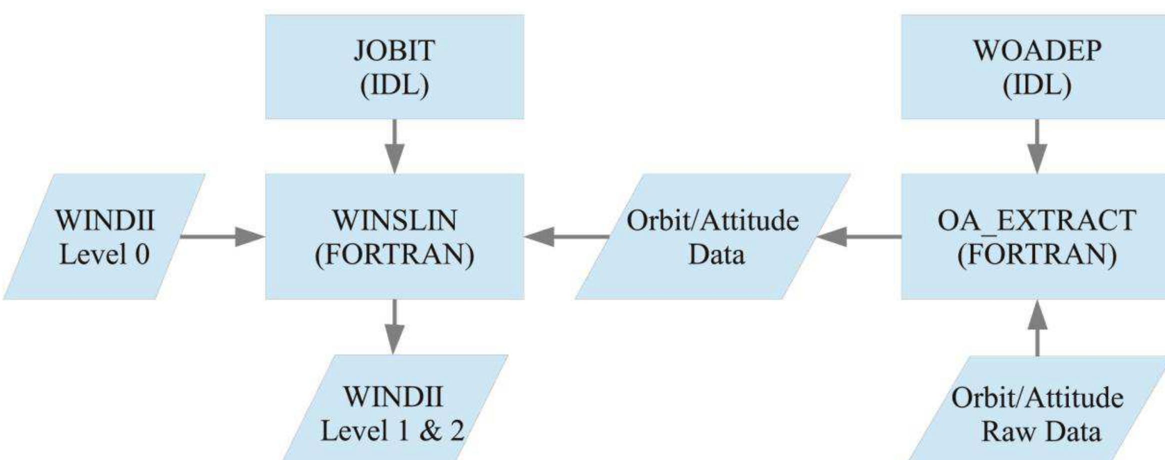

Graphic 1: The WINDII processing steps

2.2 Original data processing system

The WINDII data were processed on a 32-bit Linux operating system. The WINSLIN and OA_EXTRACT Fortran programs were compiled under Absoft Fortran version 8.2 and run on the 32-bit Linux system.

3. The new WINDII processing system

3.1 Background

The original computer system for WINDII data processing has been changed from a 32-bit based Linux system to a 64-bit system. We could use precompiled 32-bit execution files under the new 64-bit system using 32-bit compatibility libraries. However, we realized that some parts of the source codes needed to be changed for the new data set. Thus to modify and run the WINSLIN Fortran programs, we needed to recompile the Fortran source codes under the new 64-bit system. We also needed to check compile options, because the Fortran compiler was changed from version 8.2 to 13. Compiler options are different not only for different compilers, but also among versions of a given compiler.

3.2 New data processing system

The current computer system for WINDII data processing purchased under this grant is a openSUSE Linux 12.2 64-bit system with kernel version of 3.4.33-2.24-desktop. The WINSLIN Fortran programs have been modified under Absoft Fortran version 13 with different compile options on the 64-bit Linux system.

3.3 Implemented modifications

3.3.1 Compile option modifications

[Previous compile options]

f77Opts = -f -s -C -N51 -W -O2 -N3 -N33 -B19 -V -B111 -g -c

[Not valid in Absoft Fortran 13]

N3: includes record length info for sequential unformatted files

N33: causes structure fields to be "packed"

N51: for Direct Access files, RECL = # 32 bit words in a record. RECL will be interpreted as the number of 32 bit words in a record for “unformatted, Direct” access files. Without this option RECL defines the number of bytes in a record.

B19: more than one symbolic name references a variable's memory location. It can occur when pointers are used, when variables in COMMON are also passed as arguments or when two dummy arguments are the same actual argument.

B111: issue instructions to ensure the integrity of FPU(Floating-Point Unit) stack. This option is useful for tracking down mistyped functions and functions that are incorrectly referenced in subroutine CALL statement.

[Solutions for missing compile options]

N3 & N51: no need (by default options in the latest version)

N33, B19, & B111: ignored

Affected files:

/common_for/Makefile, /lss/Makefile, /nag/Makefile, /o2/Makefile, /sa/Makefile, /utl/Makefile, /yu/Makefile, /level1/Make_ci, /level1/Make_co, /level1/Make_da, /level1/Make_ps, /level1/Makefile, /level2/Make_ra, /level2/Make_rc, /level2/Make_rd, /level2/Make_rp, /level2/Make_yu, /level2/Makefile

3.3.2 Source code modifications

[Parameter statement]

Parentheses are required for the definition of the parameter statement in the new compiler.

Parameter xxxx='1234' → Parameter (xxxx='1234')

Affected file: /utl/ssdef_tmp.inc, /sa/uoas_messages.inc

[Structure component dereference operator]

The previous Fortran compiler uses a '.' (period) as a structure field component dereference operator, but it is replaced by '%' (percent) in the latest compiler. The use of a period may cause certain Fortran 90/95 conforming programs to be misinterpreted (a period is used to delineate user defined operators and some intrinsic operators). As an example of a structure 'A' having several record levels, A.B.C → A%B%C. Fortran User Guide (R.2.) suggested using an option "YNDFP=1", but it does not work.

Affected files:

/common_for/ch_cl_cdb.f, ch_op_cdb.f, ch_open_ipf.f, ss_init_sfdu.f

/lss/lss_asgiun.f, lss_clear_job.f, lss_get_jobparam.f, lss_openl0.f, lss_pginit.f, lss_pgterm.f, lss_read_emaf.f, lss_readl0.f

/sa/sa_star_init.f, yoa_ephem.f, yoa_get_lukey.f, yoa_sat_att.f, yoa_sat_orb.f

/level1/ci_close.f, ci_get_param.f, ci_open.f, co_process_close.f, co_process_init.f, daa_get_pardecom.f, daa_ini.f, daa_ini_o2.f, dag_min.f, dag_ter.f, dag_ter_o2.f, ps_close.f, ps_open.f, waa_cloself.f, wcb_asgaux.f

/level2/ra_close.f, ra_extract.f, ra_open.f, rc_close.f, rc_open.f, rd_close.f, rd_open.f, rp_close.f, rp_open.f, yu_rc_close.f, yu_rc_open.f

[99 continuation line limit]

Fortran95 and Fortran77 allow 99 continuation lines (1 initial and 98 continuation lines), but the source code '/winslin/yu/yu_ch_adj_models.f' has more than the continuation limit in the data block. For example, 'rate 2' data has 120 continuation lines and 'rate 6' has 146 continuation lines. These data blocks were separated from the yu_ch_adj_models.f code, and the data files were read at the beginning of the code.

[Change RECL length due to -N51 missing option]

As explained in Section 2.3.1, the N51 option set 32-bit (or 3-bytes) words as the number in a record. The N51 option is not available in the new compiler, so we need to define the number of bytes in a record. This affects the files.f file which defines record lengths of various data. The previous FILES_RECLEN numbers for direct access files are multiplied by 4. For examples, DATA FILES_RECLEN (C_WI_CDBI) /194/ is replaced by DATA FILES_RECLEN (C_WI_CDBI) /776/.

Affected file: /common_for/files.f

[Open statement option]

“Unformatted” → “Binary”

Affected files:

/common/ch_op_cdb.f

/lss/lss_openl0.f

/yu/yu_rc_open.f

/level1/ci_open.f, ci_close.f, co_process_init.f, co_process_close.f, daa_ini.f, daa_ini_o2.f, ps_open.f, ps_close.f

/level2/ra_open.f, ra_close.f, rc_open.f, rc_close.f, rd_open.f, rd_close.f, rp_open.f, rp_close.f, yu_rc_open.f, yu_rc_close.f

[Read statement option]

IOSTAT option is needed by read statement, “IOSTAT=IOS”

Affected files: /common_for/ss_r_header.f

[Function and Subroutine definition]

INTEGER*4 Function → INTEGER*2 Function

Previous: INTEGER*4 Function lss_2byte(b1,b2)

New: INTEGER*2 Function lss_2byte(b1,b2)

Affected file: /lss/lss_2byte.f

fdate_ → fdate

Previous: SUBROUTINE fdate_, CALL fdate_

New: SUBROUTINE fdate, CALL fdate

Affected file: /lss/lss_pginit.f, /level1/daf_win_init.f, daf_winlog.f

getarg_ → getarg

Previous: SUBROUTINE getarg_, CALL getarg_

New: SUBROUTINE getarg, CALL getarg

Affected file: /utl/getarg.f, /level1/ci_control.f, co_control.f, da_decom.f, ps_control.f, /level2/ra_extract.f, rc_combine.f, rd_deconvolute.f, rp_produce.f, yu_rc_combine.f

[Array data storage]

Previous: DATA (TRACE_STAR(I:I),I=1, C_WI_TRSTAR) /C_WI_TRSTAR*'*'/

New: DATA TRACE_STAR(1:C_WI_TRSTAR) /'*'/

Affected file: /common_for/tr_rc.f

[Year digit correction for 2000 later]

The original SDPPS did not allow for years beyond 1999, indicated as a two digit “99”.

The IF statement is added as below for adjusting years from 2000 to 2010.

IF ((year .GE. 100).AND.(year .LE. 110)) THEN

year=year+1900

ENDIF

Affected file: /lss/lss_vms2udtf.f

[Data type: Byte*1]

Unsigned Byte as expressed by Byte*1 is not available in the new compiler. It is replaced by Byte.

Affected files: /lss/lss_openl0.f, lss_read_emaf.f

[ENCODE function]

The ENCODE function writes to a character variable, array, or array element, but Fortran13 does not support the ENCODE statement. The statement is replaced by a READ statement involving internal files (CHARACTER variables and arrays).

Previous: ENCODE(23,100,asc_time) day_of_month, month, year, hour, min,...

New: WRITE(UNIT=asc_time,100) day_of_month, month, year, hour, min,...

Affected file: /lss/lss_udtf2vms.f

[Month indication, Upper case]

The name format for month was changed on February 20, 1999 in the c_ipf.dat file. From that date onwards the abbreviation for month should be in an all capital characters format.

Previous: 20-Feb-1999 15:27:22.00 south : Yaw on day 99051, UARS 2719

New: 20-FEB-1999 15:27:22.00 south : Yaw on day 99051, UARS 2719

Affected file: /cdbv5/c_ipf.dat

[ISHFT → JISHFT]

JISHFT(I,SHIFT) returns a value corresponding to “*I*” with all of the bits shifted SHIFT places. A value of SHIFT greater than zero corresponds to a left shift, a value of zero corresponds to no shift, and a value less than zero corresponds to a right shift. The return value is of type INTEGER and of the same kind as I. The PDEC001 value is INTEGER*4 type, so arguments should be the same type of PDEC001.

Previous: PDEC001 =
JISHFT((ZI4_TBIT.AND.XMSK_TI_MSK(ZIR_BIT,ZI_LAST_BIT)),XMSK_TI_SHI(ZI_LAST_BIT))

New:

INTEGER*4 DUMP_INDICATOR

DUMP_INDICATOR=(ZI4_TBIT .AND. XMSK_TI_MSK(ZIR_BIT,ZI_LAST_BIT))

PDEC001 = JISHFT(DUMP_INDICATOR,XMSK_TI_SHI(ZI_LAST_BIT))

Affected file: /level1/pdec001.f, pdec005.f

[MOD → JMOD]

JMOD returns the integer*4 remainder of its two integer*4 arguments, but defined variables were integer*2.

Previous: INTEGER*2 year, day_of_year, curyear

New: INTEGER*4 year, day_of_year, curyear

Affected file: utl_con_udtf.f

[not → .not.]

The intrinsic function of 'not' is replaced by '.not.'.

Previous: IF((not((CAC_N_F .EQ. 4) .AND.

New: IF((.not.((CAC_N_F .EQ. 4) .AND.

Affected file: /level2/ra_app_cor_tem.f

[sngl → REAL]

The sngl intrinsic function is replaced by REAL.

Previous: PA.Zmax = sngl(ANS)

New: PA.Zmax = REAL(ANS)

Affected file: /level2/yu_pk_alt_find.f

[Structure name]

The structure name of LUKEY is conflicted with local variables.

Previous: STRUCTURE /LUKEY/

New: STRUCTURE /LUKEY_new/

Affected file: /sa/YOA_STRUC_DEF.INC

Previous: RECORD /LUKEY/ LUKey_In

New: RECORD /LUKEY_new/ LUKey_In

Affected file: yoa_get_lukey.f

[Comment out]

All characters following C after the definition of *include 'wi_trace.frm'* are commentary in the previous version. In the new version, all characters after an exclamation mark, **!**, are commentary, and are ignored by the compiler.

Previous: include 'wi_trace.frm' C Trace format

New: include 'wi_trace.frm' !C Trace format

Affected file:

/common_for/ch_lin_corr.f

/sa/sa_get_orbit.f

4. Evaluation of the results of the new processing

4.1 Comparisons of old and new data processing

The WINSLIN package for WINDII data analysis has been fully recompiled under the new Absoft Fortran 13 compiler on a 64-bit Linux environment system. The results of the 32-bit and 64-bit systems are slightly different even with the same source code, but these small differences can be ignored. Level 2 WINDII data for volume emission rate, wind velocity, and Doppler temperature are selected in order to examine the differences between results using previous and new compilers.

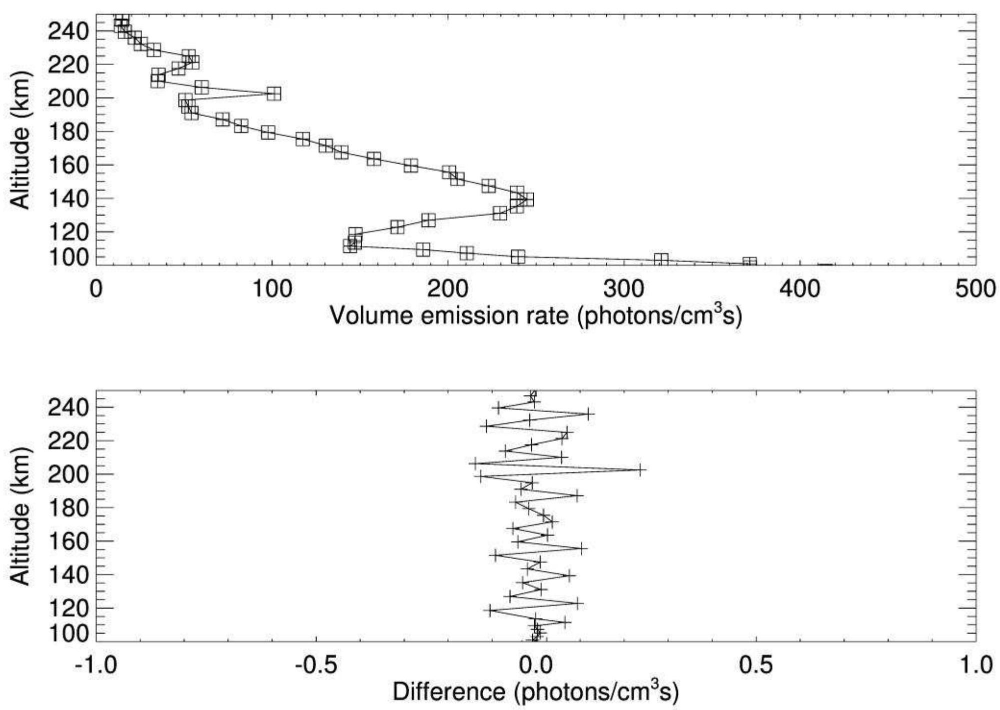

Figure 1. Upper panel: Volume emission rate profile of WINDII O(^{1}S) green line for Field Of View 1. The measurement time is 19:06:25 UT on September 15, 1995. The squares present the results using the previous compiler, and the crosses indicate the new results using the new compiler. Lower panel: The differences between results of the two different compilers.

4.1.1 Volume emission rate

Level 2 WINDII data on September 15, 1995 are selected randomly to compare the results between the previous and new compilers on the different systems. Figure 1 presents the WINDII $O(^1S)$ green line volume emission rate for Field Of View 1 (FOV 1) on UARS day 1465 (September 15, 1995). The measurement ID is 43788, and the time is 68787203 millisecond (19:06:25 UT). The local time is 09:55:09 LT. The exposure time is 1.024 sec. The mean locations for the profiles are 40.1° N and 222.5° E. The bin is 25 pixels wide by 2 pixels high, and number of altitudes is 67 with a bottom altitude of 68.3 km and a top altitude of 284.8 km, of which only a portion is shown in the figure. The upper panel shows the volume emission rate vertical profiles of the previous results using the 32-bit compiler (squares) and the 64-bit compiler (crosses); the values appear identical. The lower panel shows the difference between two results. They are not exactly the same, but the maximum difference is less than 0.3 photons cm^{-3} s^{-1}. These differences can be ignored, as they are smaller than the measurement error. For more background on the WINDII instrument, see Shepherd et al. (1993).

4.1.2 Wind

The Doppler wind vertical profile of the $O(^1S)$ green line on September 15, 1995 is shown in the upper panel of Figure 2 . The measurement time and location are same as in Figure 1. The symbols are same; the squares indicate the results using the previous system compiler, and the crosses are for the new results. The lower panel shows the differences between previous and new results, and the differences are very small. Below about 190 km altitude, the previous and new results are almost the same. The maximum difference in this case is about 0.4 m s^{-1} around 250 km altitude.

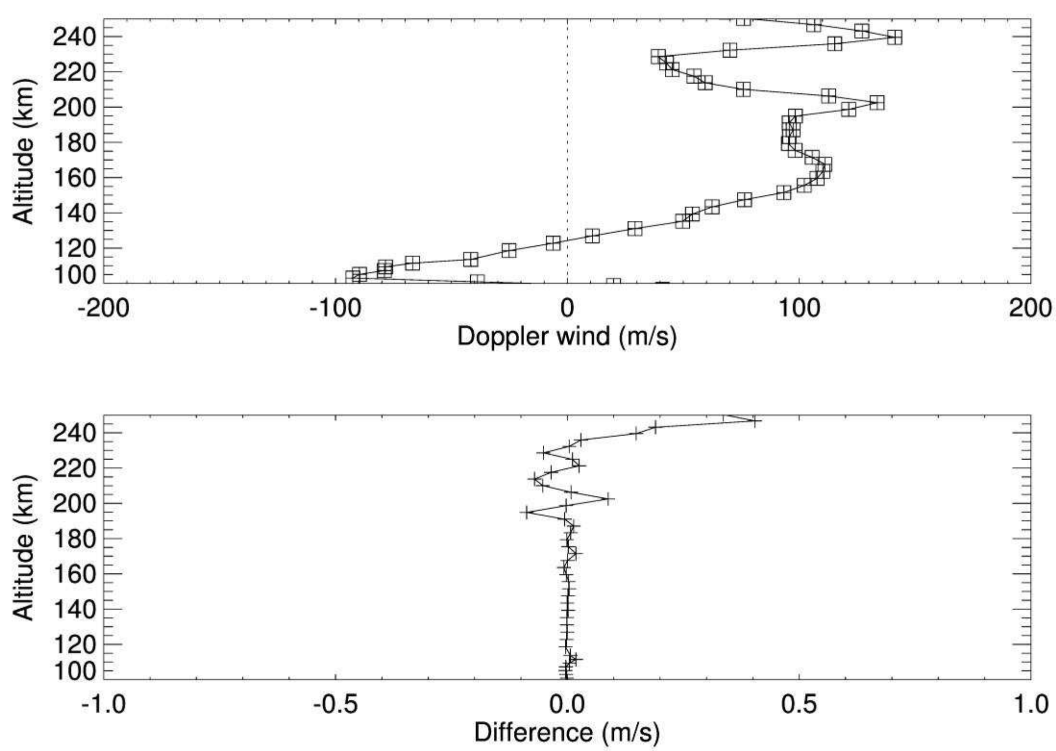

Figure 2. (Upper panel) Doppler wind for the $O(^1S)$ green line for FOV 1 on September 15, 1995. (Lower panel) The differences using the two different system compilers. The measurement time and exposure time are same as Figure 1.

4.1.3 Doppler Temperature

Figure 3 presents the Doppler temperature profile of the WINDII (O^1S) green line on September 15, 1995. The temperature in the high thermosphere is non-LTE (Local Thermodynamic Equilibrium) due to an insufficient number of collisions to thermalize the $O(^1S)$ atoms before radiation, so the observed temperature at high altitudes is higher than the true values. However, it doesn't affect this comparison. The percentage difference for each altitude between the two results using the 32-bit and 64-bit system compilers is shown in the lower panel of Figure 3; percentage because of the large temperature variation from lower to higher altitudes. The differences are larger above 180 km altitude than those at lower altitude. The maximum difference is about -0.1% (~2K) around 240 km altitude.

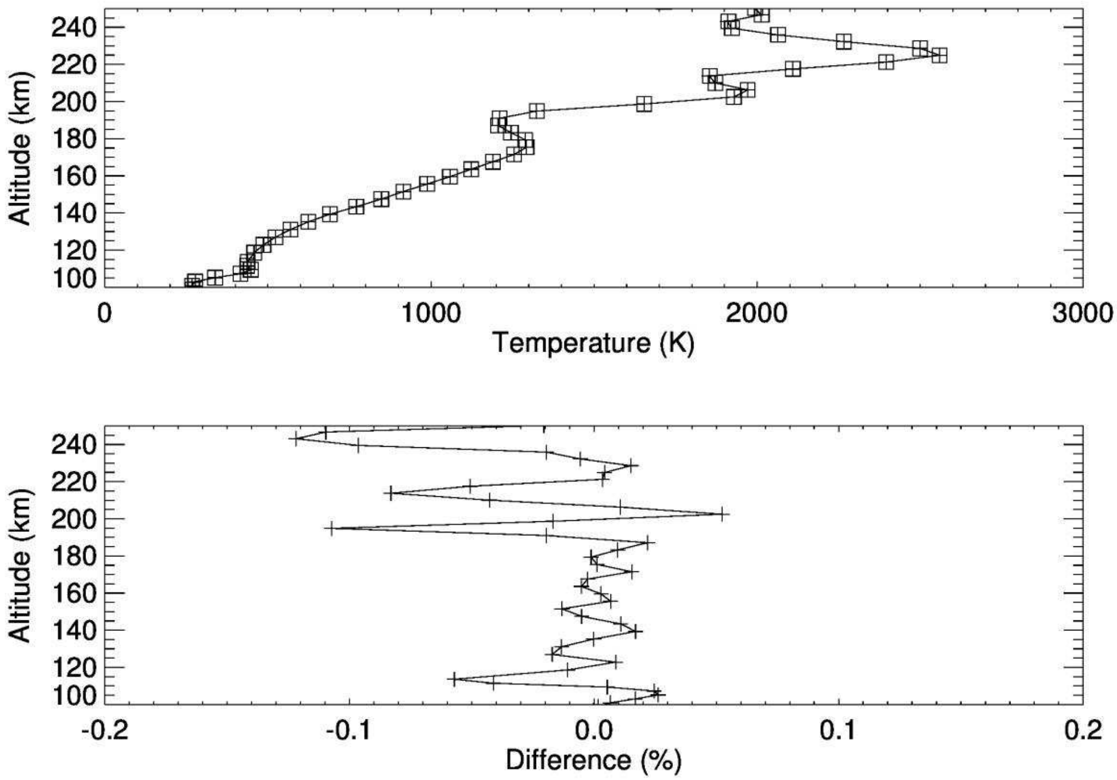

Figure 3. (Upper panel) Doppler temperature profiles for the $O(^1S)$ green line for FOV 1 on September 15, 1995. (Lower panel) The differences between the 32-bit and 64-bit system compilers. The plotting symbols and measurement time are same as for Figures 1 and 2.

4.2 Examples of newly available levels of data

After modifying the WINSLIN and OA_EXTRACT programs, the WINDII data from Level 0 through Level 2 can be fully accessed and processed with the new 64-bit Linux operating system. Graphic 2 shows the different files created during the processing. The scratch files are not saved but can be extracted if required for special studies. The WINDII Level 1 data have been reproduced and archived for the entire WINDII mission from 1992 to 2003. Also, new Level 2 data have been produced using the recompiled programs from 1997 to 2003.

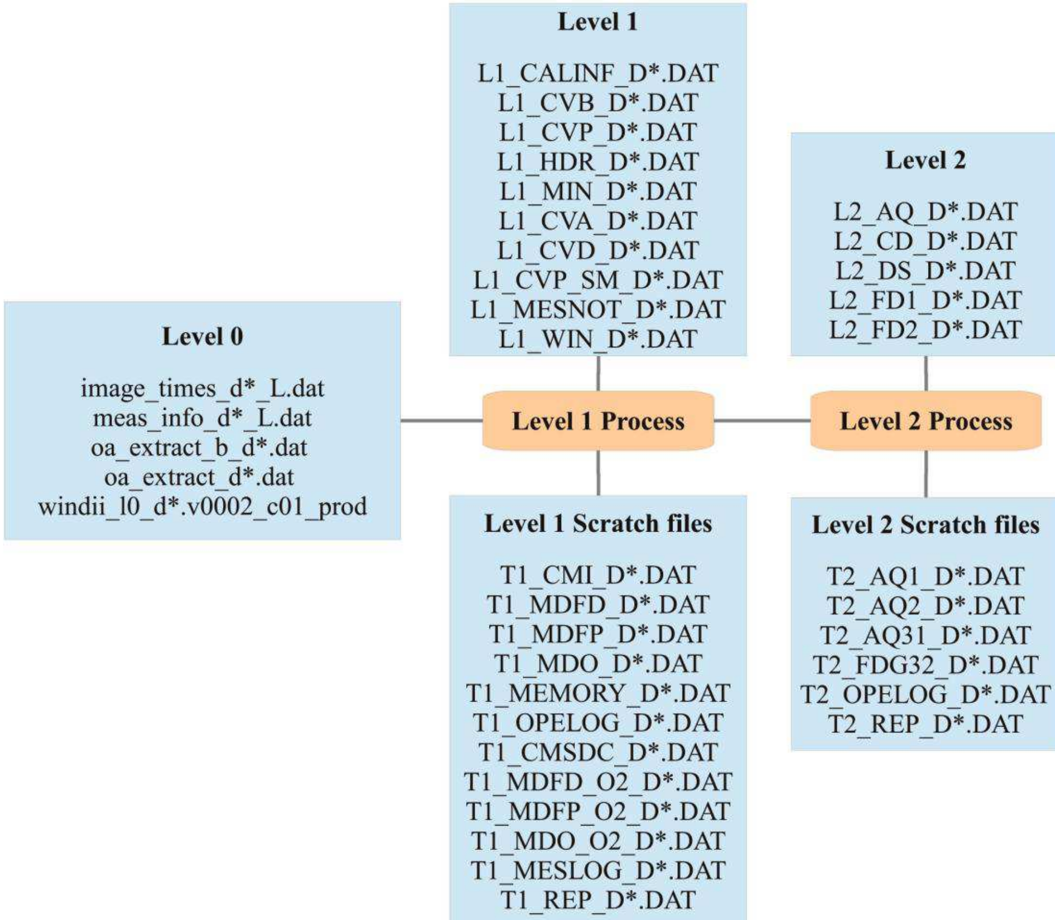

Graphic 2: Files created during the processing

4.2.1 Level 0

Accessing WINDII Level 0 data allows previous WINDII scientific applications to be further studied. One of the scientific applications using WINDII Level 0 data is Polar Mesospheric Clouds (PMC). The study of PMCs using the WINDII background channel (Filter 1: 553.1 nm) data during the 1993 ANLC campaign was demonstrated by Evans et al. (1995). Usually PMCs appear around 80 to 83 km altitude during summer time, which is then the coldest part of the atmosphere. Figure 4 is a good example of non-PMC and PMC conditions, as shown in the left and right-hand panels respectively for July 17, 1993 . The PMC observations were made at a higher resolution, of 1 x 5 pixels, yielding 30 columns in the image, as compared with normal observations of 2 x 25 pixels with 6 columns. The left panel presents an image from FOV 1 taken at an average latitude of 42° N. The Rayleigh scattered light decreases exponentially with increasing altitude as the atmospheric density decreases. The right panel shows the Filter 1 measurement at the higher latitude of 66° N. The PMC appears as a horizontal layer around 83 km altitude superimposed on the Rayleigh scattering. Using these level 0 data, occurrence frequency, short and large scale variability, and the geophysical structure of PMC can be investigated.

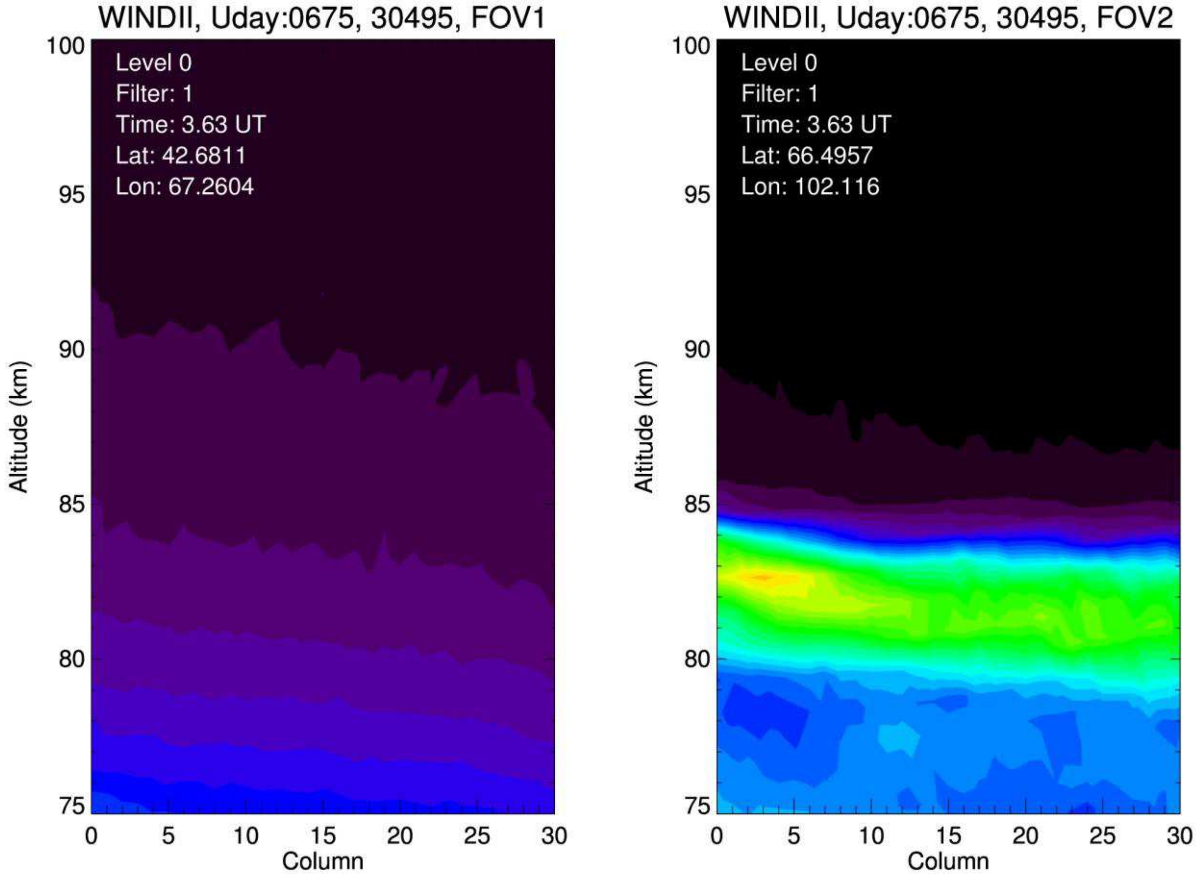

Figure 4. WINDII filter 1 image of level 0 data, windii_l0_d0675.v0002_c01_prod. It was taken on July 17, 1993 at 3.63 UT. The left panel shows FOV 1 with an average latitude of 42° N, and the right panel is for FOV 2 at 66° N latitude. The left panel is an example of normal Rayleigh scattered atmospheric background. The scattered light exponentially decreases as altitude increases. The right panel shows a typical PMC around 83 km altitude. The number 30495 is the identification number for the image.

4.2.2 Level 1

Due to the limitations on the data transfer rate imposed by the dedicated communications line between NASA Goddard and York University during the mission, only some of the WINDII Level 1 data were archived at York University. After implementation of the new WINDII data processing system, all Level 1 data for the entire WINDII operations period from 1992 to 2003 have been created and archived. Restoring Level 1 data provides the capability of modifying functions inside the data reduction software. According to a previous WINDII study (Bacsek, 1998), the Filter 4 transmission functions for the O^+ emission seem to be in error and need to be changed. Figure 5 shows a WINDII O^+ measurement from the file T1_MDO_D0406.DAT, taken on October 21, 1992 at 01:07:59 UT. The T1_MDO file (See Graphic 2) is produced by the Telemetry Depacking process and is not corrected by any calibration process. This image combines the two FOVs, columns 0 to 5 for FOV 2 and columns 6 to 11 for FOV 1. This provides both hemispheres of off-axis angles through the filter, The bright ring is created by the off-axis change of angle through the filter, and is bright in those regions of the image where the O^+ line at 732.0 nm is strongly transmitted. As suggested by Bacsek (1998), the pattern appears to be shifted from the centre axis. Preliminary work was conducted to create a new filter transmittance function that would correct this problem, but this was not completed. The O^+ emission rates can be used to derive atomic oxygen concentrations in the thermosphere, which is of great current interest.

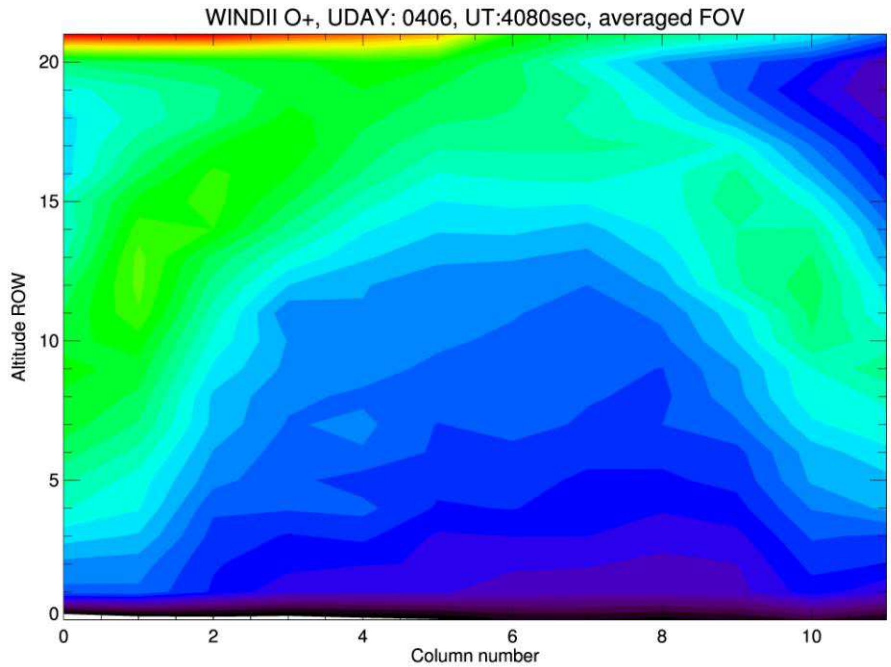

Figure 5. Combined field of view image of the WINDII O^+ channel (Filter 4) taken on October 21, 1992. The columns from 0 to 5 are for FOV 2 and columns 6 to 11 for FOV 1. Each FOV image is averaged over the 8 different mirror step images. The source image, T1_MDO_D0406.DAT, is the output of the telemetry depacking process without any calibration.

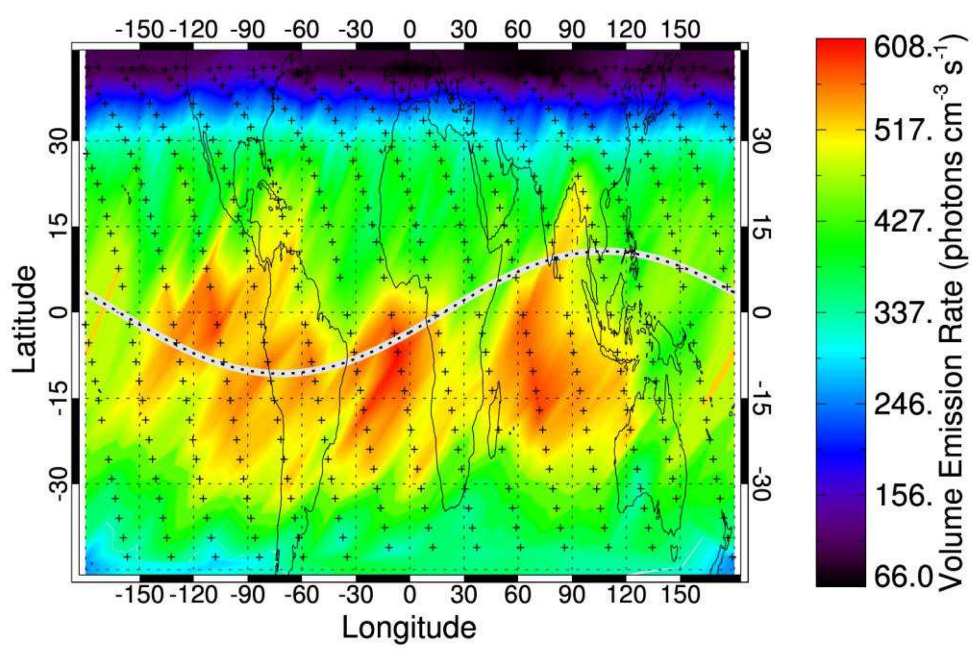

Figure 6. Global map of WINDII $O(^1S)$ volume emission rate at 100 km for 14 May 1998 (Uday 2437). Universal time proceeds from the right to the left. The magnetic equator is shown on the map as a dotted line.

4.2.3 Level 2

As the final product of the new data process, level 2 data has been produced from September 1997 to September 2003. Figure 6 shows an example of level 2 $O(^1S)$ volume emission rate data at 100 km altitude for May 14, 1998 as latitude longitude map. The range of the volume emission rate is from 66 to 608 photons/cm^3/s within the latitude band of 45° S to 45° N. The dotted line indicates the magnetic equator on the map. There is a wave number 4 pattern that is understood to be associated with the diurnal eastward propagating non-migrating tide of wavenumber 3 (DE3). The wave 4 has been studied using previous WINDII data, and this can be extended with the new data set.

5.0 Investigation of operational issues

5.1 Cold temperature operations

By 1997, the batteries in the UARS spacecraft had degraded to the point where not all instruments could be operated at the same time. Because of that, NASA requested reductions in the power requirements for individual instruments. The WINDII team agreed that WINDII could be operated without temperature control, owing to the inherent stability of the Michelson interferometer, and the frequent calibrations of phase that were made, about every 20 minutes. Without this control, the instrument temperature dropped; the filter wheel temperature fell from 21 C to about 11 C. This changed the optical path difference in the Michelson interferometer, creating a shift in the phase of the zero wind, and thus a bias in the observed winds. This state of operation was in effect from September 23, 1997 to October 29, 2002 and is referred to as “cold” operations. Without correction, this temperature change produces a wind error bias of about 200 to 400 m s^{-1}.

Figure 7 shows the temperature of the WINDII ISU (Instrument Sensor Unit), CCD detector, and filter wheel from just before the cold operation period, August 29, 1997 to December 31, 1999. These temperature data are based on the UARS engineering data. Panel (a) presents the ISU temperature changes. The crosses represent ISU temperature with WINDII turned off, and the squares indicate WINDII observation days. The normal operation temperature was about 20 C before Uday 2204 (September 23, 1997), and without temperature control the temperature was about 10 C lower, until around Uday 2600. At that time, with WINDII operating, the ISU temperature dropped suddenly to 0 C, colder than when it was turned off shortly afterwards. The WINDII data log records no special operations on that date, so it appears that some event occurred within WINDII, or on the spacecraft. From Uday 2600 onwards, the temperature is lower for both operations and non-operations, with a difference between them greater than before Uday 2600. Panel (b) shows the filter wheel temperatures during the same period. The temperature trend is very similar to the ISU temperature change. It is evident that the WINDII instrument warms from internal heat dissipation when it is turned on. The CCD cooling system has a pair of 2-stage TECs (Thermo Electric Coolers) that pump heat from the CCD to a radiator plate where it is radiated into space. The CCD temperature drops from about -50 C to -55 C during cold operations, presumably because it is controlled mainly by the radiation into space, and so is not as sensitive to the internal heat as is the filter wheel temperature.

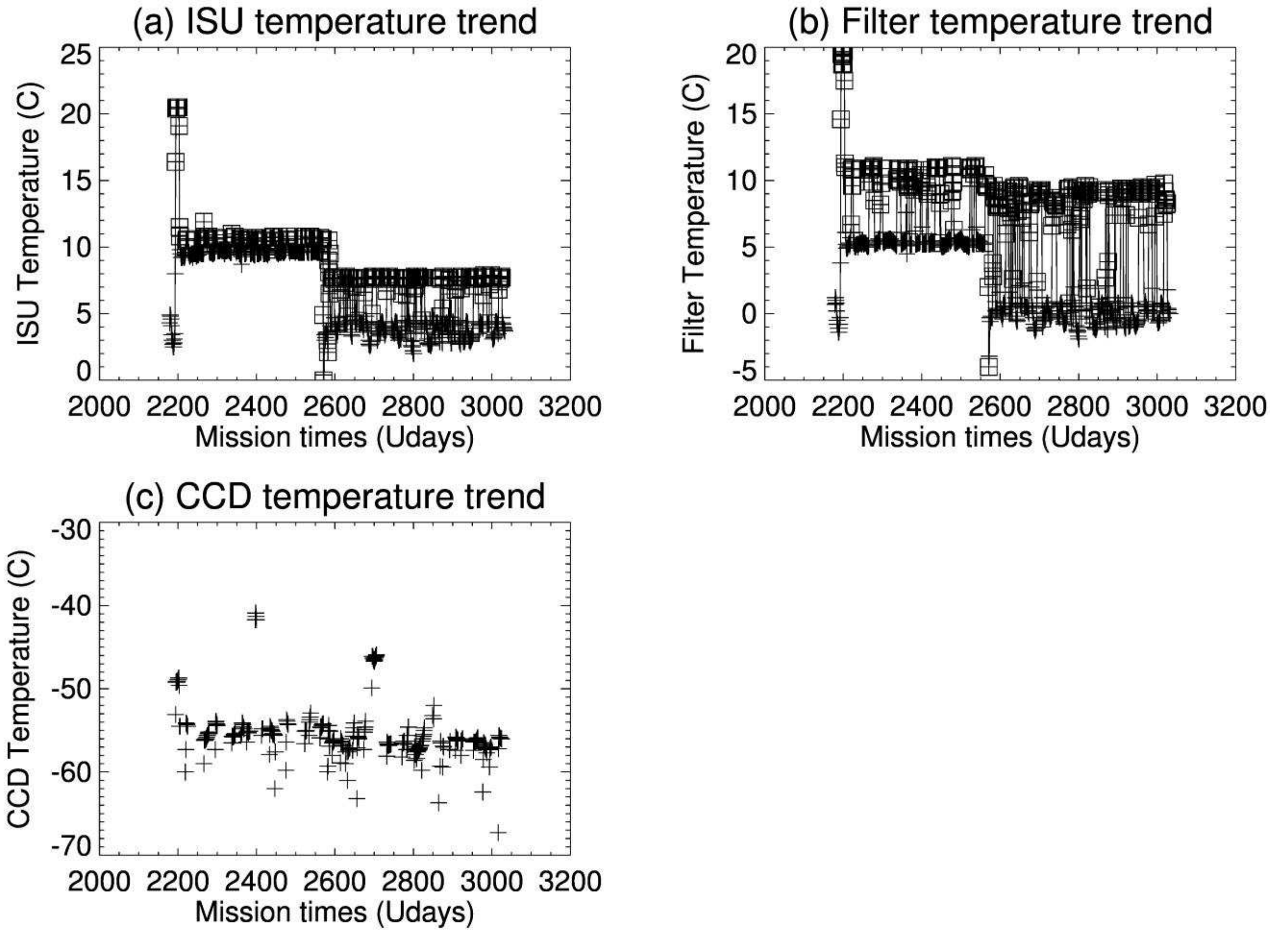

Figure 7. Temperature variations of WINDII ISU, filter wheel, and CCD detector based on the UARS engineering data from August 29, 1997 (Uday 2179) to December 31, 1999 (Uday 3033).

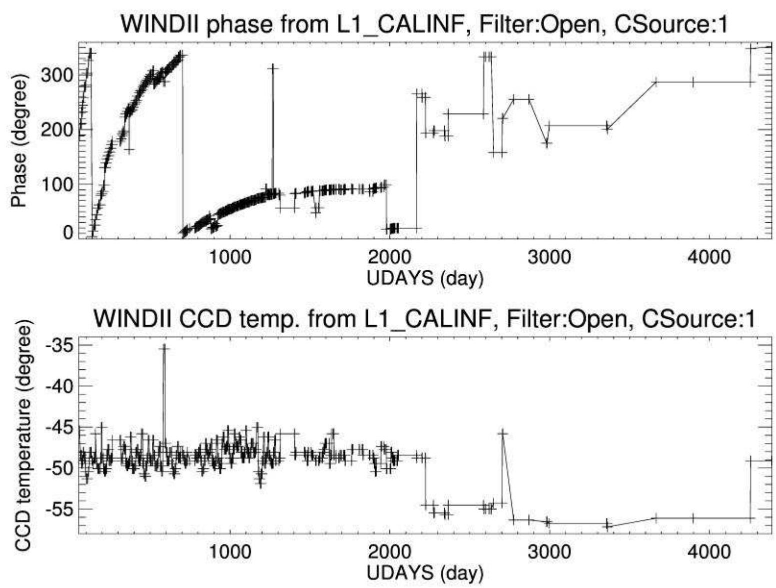

Figure 8. Phase (upper panel) and CCD temperature (lower panel) from the WINDII infrequent calibration measurements. The phase calibration light source is a 557.0 nm Kr lamp that is referenced to a He-Ne laser.

Figure 8 (upper panel) shows the instrument phase based on the WINDII infrequent calibration measurements for the entire operation period, as well as the CCD temperature contained in the WINDII data. The infrequent calibration is a rigorous calibration done about once every month, where the phase corresponding to zero wind is compared with the on-board He-Ne laser. These calibrations are stored in a Characterization Data Base (CDB) that is used to correct the frequent calibrations, which were performed about every 20 minutes, where the phase of the relevant spectral lamp is observed. The infrequent calibrations were taken even less frequently following Uday 2000, as seen in the upper panel. The zero-wind phase drifts slowly during the first 1300 days of the mission (with a 360° phase jump near day 700) and then levels off. Around Uday 2200 there is a large jump to the values that are reasonably constant during cold operations, with a jump to normal operations as NASA restored the power for temperature-controlled operations, around Uday 4250, just before WINDII was turned off for the last time. The lower panel shows a consistent CCD temperature of about -50 C during normal operations, dropping to -55 C during cold operations.

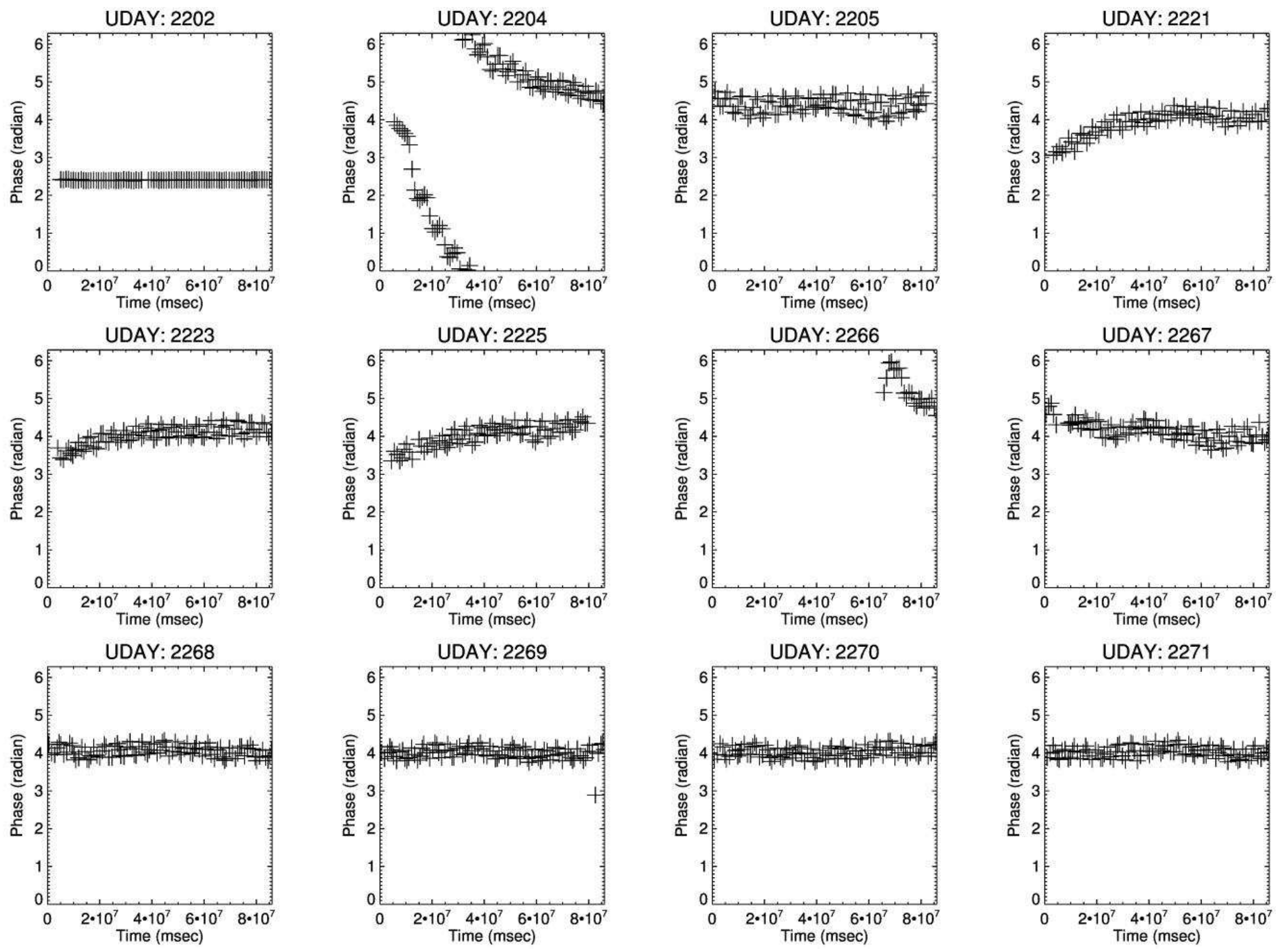

Figure 9. The WINDII instrument phases from the frequent calibration measurements with the Kr lamp based on L1_CVP data. The phase is taken from a single bin (Column: 3, Row: 10) for the field of view 1. The first date is 2202 Uday (September 21, 1997), and the last is Uday 2271 (November 29, 1997).

The same changes in instrument phase are seen in the frequent calibration for the Kr spectral lamp on a day-by-day basis shown in Figure 9 for days between Udays 2202 and 2271. These data are for a single bin in Column 3 and Row 10. For Uday 2202 (upper left, September 21, 1997) operations are normal and the phase is very constant during the day. For Udays 2204 to 2267 there are large changes during the day, while for Udays 2268 to 2271 the phase is relatively constant, but with a phase different from that on normal day 2202, with variations larger than for that day. The challenge is to determine the WINDII zero-wind phase for the cold period, and fit it to the small variations such as seen in Uday 2268.

Figure 10 shows the meridional winds derived with the previous processing for selected days between Udays 2169 and and 2225, for an altitude of 102 km disregarding the geographical location. UDays between 2168 and 2202 show relatively constant winds around zero m s^{-1}, with variations that correspond to real wind variations. For later Udays the winds are shifted by 200 to 400 m s^{-1} with variations that are partly instrument phase drift and partly real wind variations.

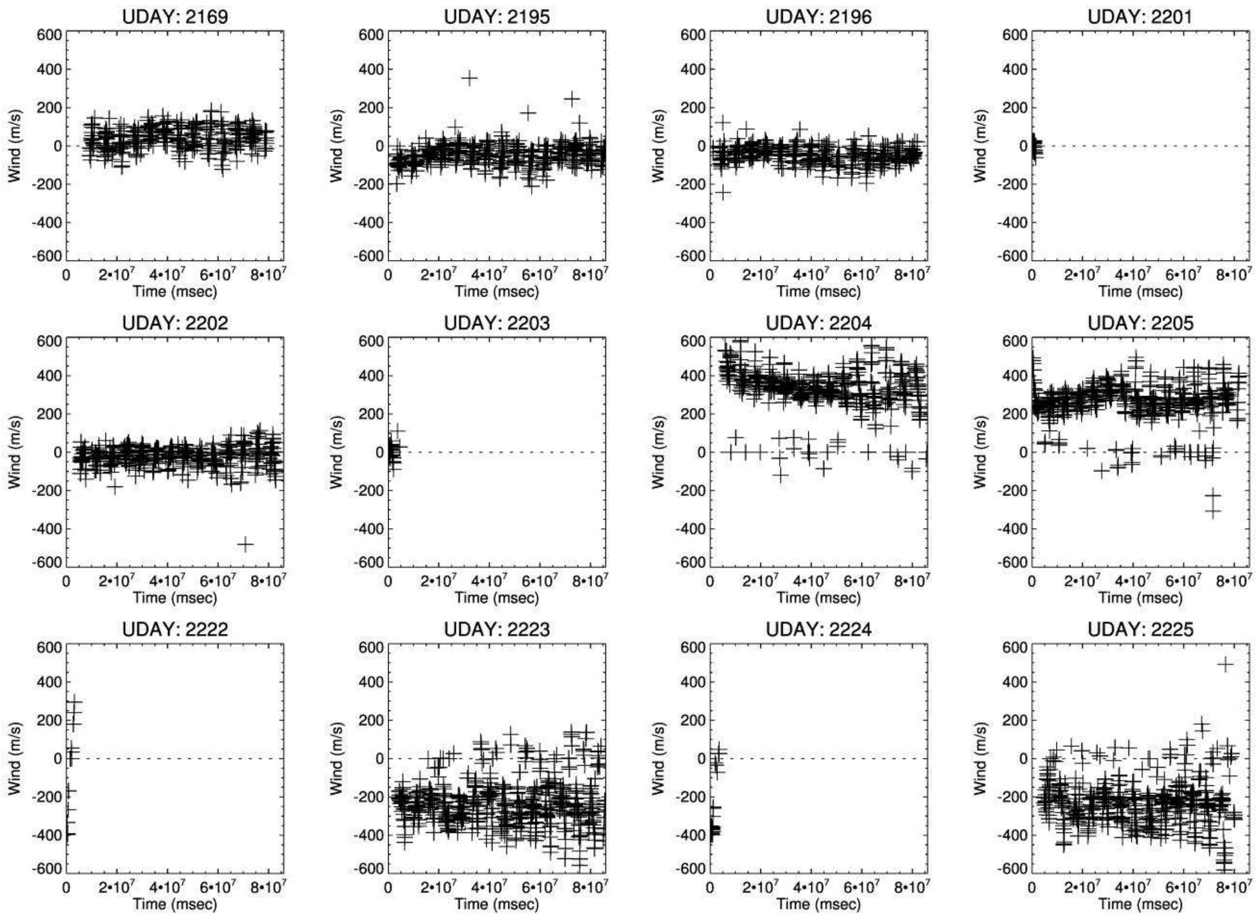

Figure 10. The meridional wind measurements of the WINDII O(^{1}S) emission line from Uday 2169 (August 19, 1997) to Uday 2225 (October 14, 1997). Each panel presents all the meridional winds measured on that day at 102 km altitude without regard for the geographical location.

5.2 New zero-wind determination for cold temperatures

The characterization data base (CDB) was created at the time of the characterization of WINDII in the David Florida Laboratory during the summer of 1991, and was updated during the mission through a process called "infrequent calibrations", carried out about once per month. This process involved viewing a tungsten source for responsivity calibration, a He-Ne laser for visibility calibration and all spectral lamps for zero-wind phase for each emission.

The existing CDB ends on Uday 2575 (September 29, 1998), the only day in the CDB occurring during the cold operation period. Figure 11 presents the CDB parameter trend for the filter 2, $O(^1S)$ green line. More infrequent calibrations exist, but the data have not been used to update the CDB. Unfortunately the IDL program required for this cannot be located, as it was not part of the SDPPS, having been written by the contractor during the characterization at the David Florida Laboratory. The problem is that for the processing just completed the last value in the CDB was used for all subsequent measurements, including those during cold operations. While this is not a problem for the responsivity and visibility, which can be seen in Figure 11 to be relatively stable, it is a problem for the zero-wind phase, which is much more sensitive. One solution to this problem is to rewrite this program from scratch, but that would take some effort.

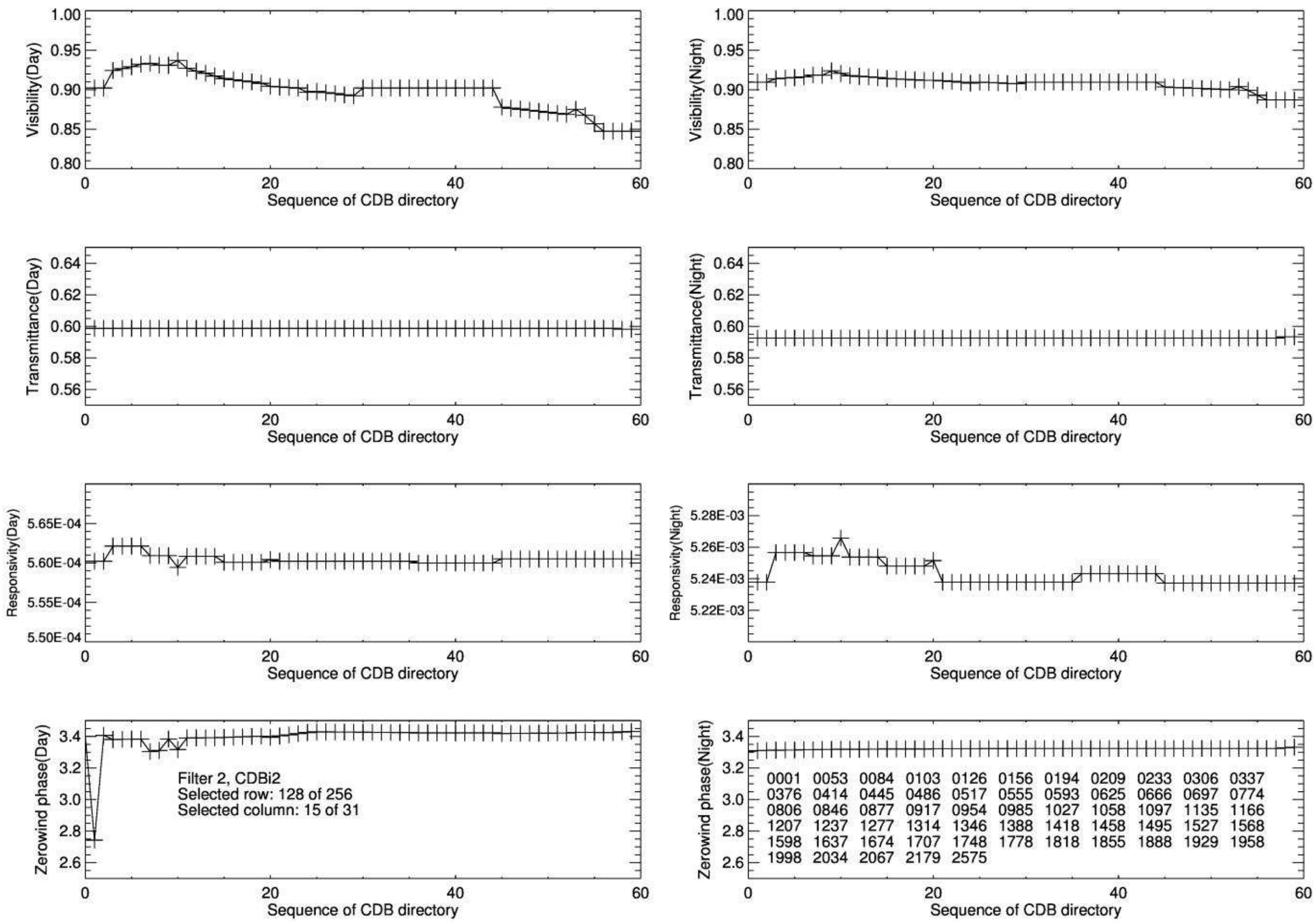

Figure 11. The trend of the WINDII CDB (Characterization Data Base) parameters; visibility, transmittance, responsivity, and zero wind phase for day (left column) and night (right column). The CDB file is for filter 2 (green line), and a single bin (column: 15, row: 128) is selected. The Udays corresponding to each CDB sequence are written in the bottom right panel. The first CDB data are from the first Uday (0001), and the last one is for Uday 2575.

A more practical and effective solution is to not use the CDB, but to work with the frequent calibrations which were made about every 20 minutes, as they have the same phase information. Unfortunately, the optimism of the team about the stability of the Michelson interferometer was not justified, as the phase drift between successive frequent calibrations is evident, owing to the day/night cycling of temperature. This can in future be solved by more complex interpolation but for the purposes of this report the validity of the frequent calibrations has been tested by looking at those WINDII wind measurements made close in time to the frequent calibrations. The results are shown in Figure 12. The lower panel shows the derived wind phase (which can be converted to wind) when the winds are corrected for measurements taken within ± 6 minutes of the frequent calibration measurement used to correct it. The values are close to zero, indicating that the bias shown in Figure 11 has been removed, and that the small variations around zero are the true winds. The upper panel shows the wind phase derived by using linear interpolation between the frequent calibration values. The larger variations seen indicate that the phase drift between frequent calibrations are too large to be corrected in this simple way. However, overall Figure 12 demonstrates that WINDII operated consistently at cold temperatures, and that valid wind measurements can be obtained.

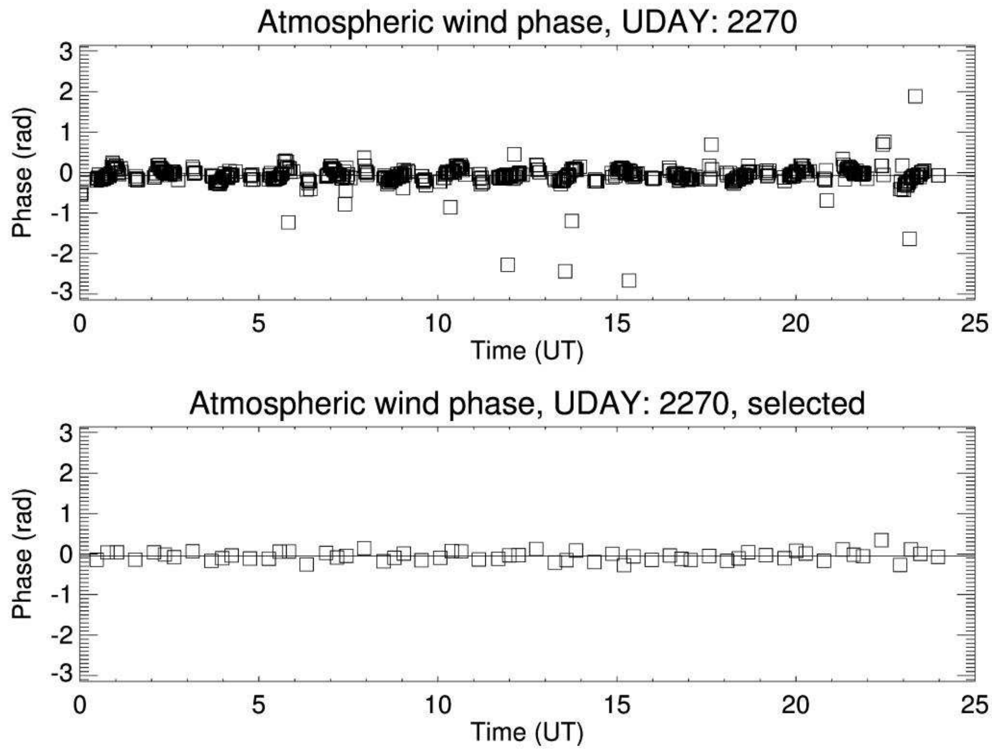

Figure 12. (Lower panel) wind phases obtained from observations made within ± 6 minutes of a frequent calibration. (Upper panel) Wind phases obtained from all observations in a day, using linear interpolation between frequent calibrations.

5.3 Impact of UARS spacecraft altitude changes

The altitude of the UARS spacecraft is affected by atmospheric drag which in turn is influenced by the space environment changes. The UARS launch was soon after a solar maximum when the spacecraft was losing one km of altitude each month. For about the first four years of the mission the spacecraft was boosted each month in order to maintain an altitude of near 585 km. Later on, the conservation of fuel became a consideration as a reserve was needed to boost the spacecraft downwards at the end of the mission, and the altitude was allowed to decline naturally as shown in Figure 13, falling to below 560 km altitude. The WINDII baffle system was designed for a fixed satellite altitude of 585 km in order to screen sunlight scattered from the cloud tops, assumed to be at 10 km altitude, from entering the instrument. The baffle scattered light is therefore expected to increase as the altitude is reduced, in fact at 540 km altitude the baffle would be seeing the hard Earth edge. To test this, three sample days, Udays 656, 3322, and 4254, are selected to evaluate the effect of altitude on the baffle scattered light.

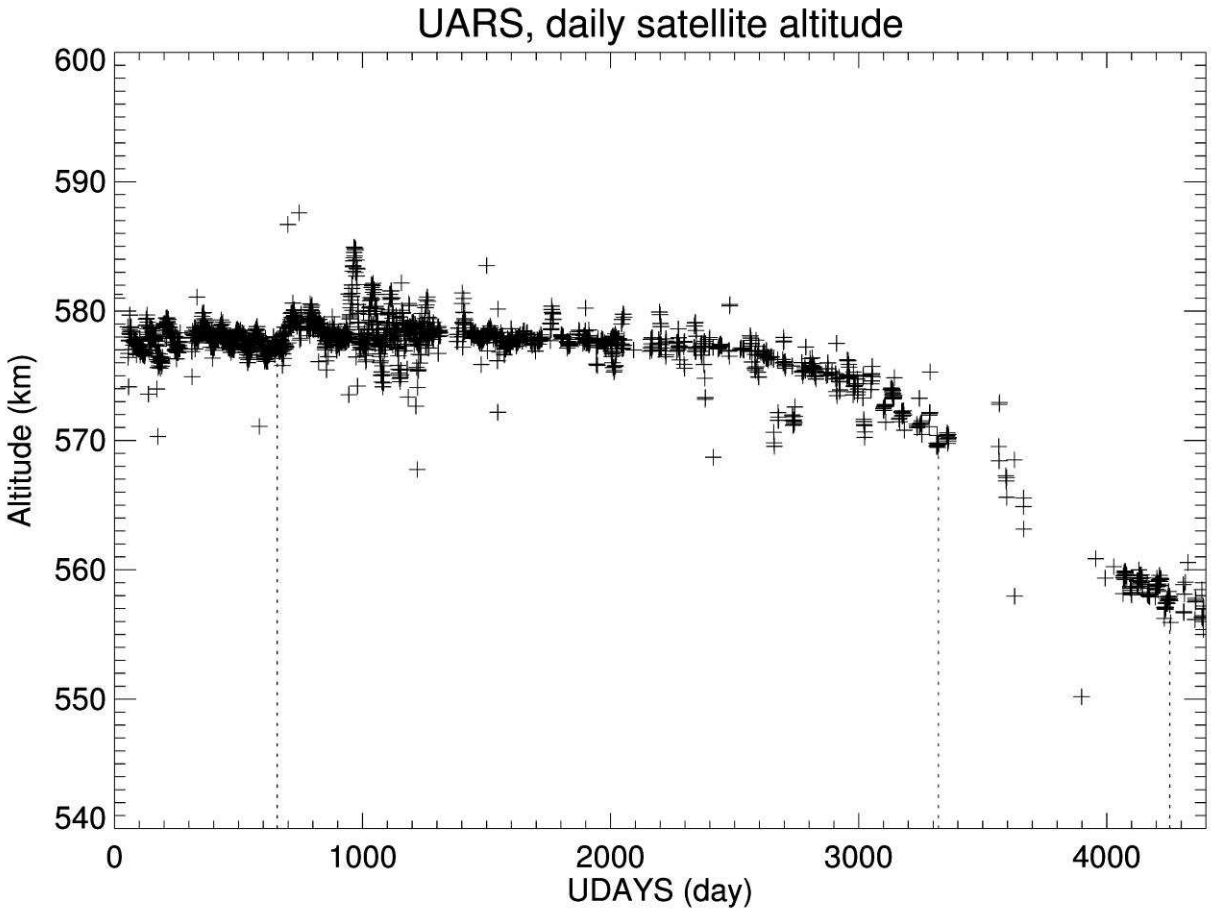

Figure 13. The daily UARS satellite altitude changes during the entire mission. It begins around 577 km altitude, and decreases to about 557 km. Dotted lines indicate the sample days for comparing lower atmosphere background light scattering during the mission.

Figure 14 shows the atmospheric background changes using the WINDII filter 1 channel. Three days, 656, 3322, and 4254, are selected for the cases of normal operation, moderate decrease of altitude, and end of mission, respectively. The sample measurements are chosen for similar solar zenith angle conditions of about 57° degree. The average and maximum signals at 150 km altitude for Udays 656 and 4254 are shown in Table 1. What is interesting is that the scattering is significantly larger for FOV 2 than for FOV 1. This was noticed earlier in the determination of temperatures from Rayleigh scattering, but had not been substantiated in this way. For some reason the two FOVs do not respond in the same way with regard to the baffle scattering.

Table 1: Average and maximum baffle scattering values at 150 km altitude

Uday	FOV 1		FOV 2	
	Average	Maximum	Average	Maximum
656	1,498	5,740	1,419	1,502
4254	1,880	8,860	15,168	24,616

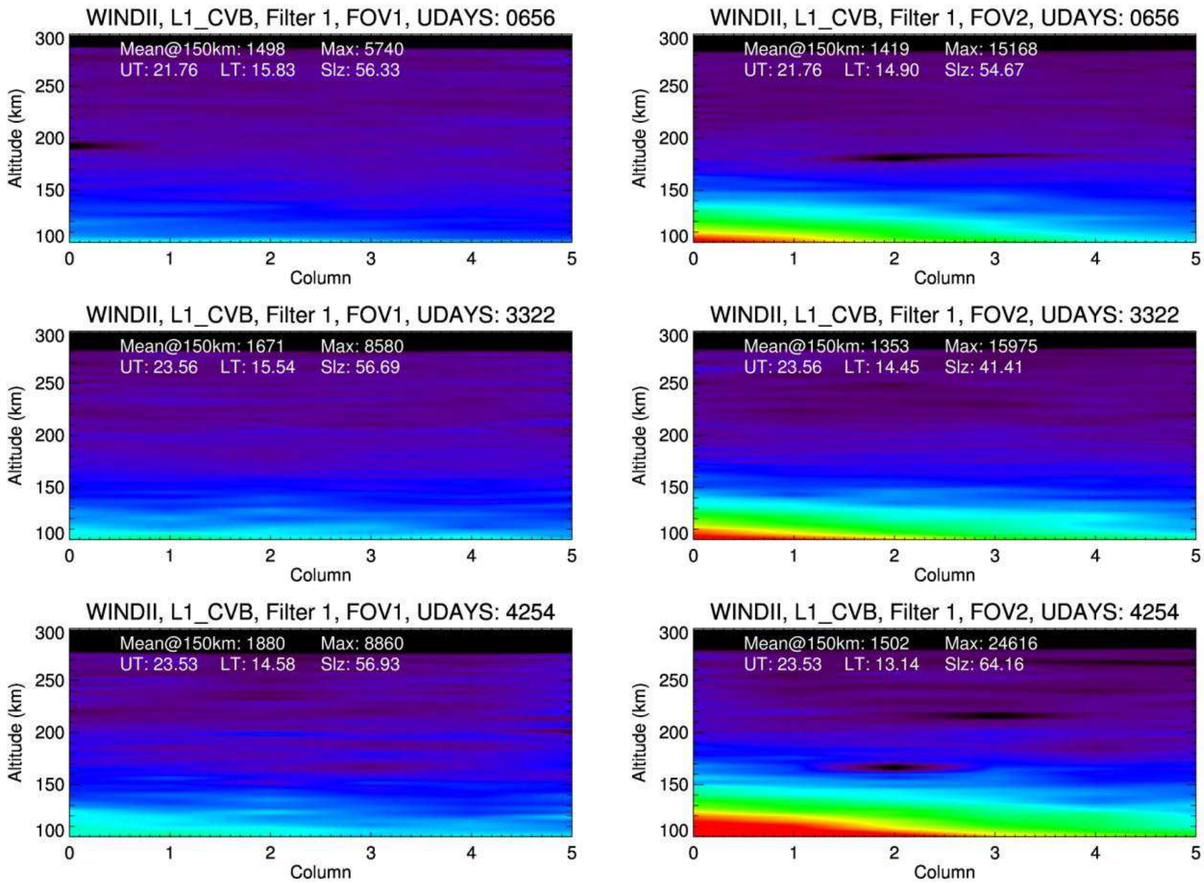

Figure 14. The WINDII background images for Udays 656, 3322, and 4254. The left panel is for FOV 1, and the right panel for the FOV 2. Similar solar zenith angle measurements are selected for the two FOVs. Note the much larger scattering for FOV 2.

6. Overview of the new WINDII dataset: Data Quality Assessment and Validation of the WINDII observations – 1991-1997 and 1997-2003

The purpose of the WINDII data quality analysis and validation is to provide means to access whether the standard retrieval as applied to the 1991 - 1997 observations of volume emission rates (VER), temperature and horizontal winds produces meaningful/correct data for the 1997 - 2003 period. The analysis concerns the observations of VER of atomic oxygen airglow $O(^1S)$, $O(^1D)$, hydroxyl OH , zonal and meridional winds, as well as Doppler temperatures derived from the $O(^1S)$ VERs. These are the data products for the observations from 1991 to 1997. The retrieval of the O^+ data has not been included in the main body of the assessed WINDII products. O^+ retrieval requires a special consideration and will be further investigated by implementing a method developed by Sheldon Bacsek (1997) instead of the original WINDII retrieval approach.

In addition to the assessment of the new dataset, the original dataset has been arranged into easily accessible data in ascii format for quick examining of climatology, global spatial and temporal coverage and trends analysis and comparisons. Graphic presentations of the data which have met the selection criterion of data quality make a catalog of these data for a quick review, in addition to the actual data files.

Validating the VERs is essential for determining the quality of the temperature retrievals in the upper mesosphere from Rayleigh scattering and the thermosphere at about 250 km height. The Doppler temperatures are provided both in actual values and residuals, normalized to the daily zonal mean values at each altitude.

1. All available WINDII observations of $O(^1S)$, $O(^1D)$ and OH airglow emissions for the period from December 1991 to March 2003 have been processes and binned according to: latitude, orbit notes (ascending/descending), for each day of observations. The most numerous dataset is that of $O(^1S)$ VER and the horizontal winds, followed by that of $O(^1D)$, OH and O_2 Atm.

2. Global variability is examined by separating daytime from nighttime observations of the VER using a selection criterion based on the solar zenith angle (SZA). The vertical profiles are examined over the altitude range from 90 to 280 km over 5 latitude bands as follows: a) Equatorial region ± 20°, Mid-latitudes ± 20° – 40°, and Mid-to-high latitudes ± 40° – 70°. Each of the data files contains the following information: Day of year, UT (hours), lat (deg), long (deg), LT (hours), SZA (deg), profile number, altitude number, altitude (km), VER (photons cm^{-3} s^{-1}), Doppler Temperature (K), or zonal and meridional components of horizontal wind (ms^{-1}).

3. The quick-look plots are produced for $O(^1S)$ and $O(^1D)$, Doppler temperature, zonal and meridional winds. These are multi-plots for each of the WINDII parameters (VER, Doppler T, zonal and meridional winds) and for each of the latitude bands from 90 to 280 km for each day of observations. A catalog of these quick-look plots has been produced for the period from 1991 to 2003.

4. Daily vertical profiles within a given latitude band and their daily zonal mean have been produced for every parameter in order to establish criterion based on standard deviation - The std is calculated at each altitude the data are considered good if the difference (observed – mean) is less than 3 std.

All available WINDII observations were processed and examined whether they meet certain quality criteria, prior to employing them in validation and dynamics analyses. The diagnostic analysis was applied to the two existing datasets. The first, called the original, encompasses the period of December, 1991 to September, 1997. The second dataset is the newly processed encompassing the period from October 1997 to March 2003. As all these data are now available assessing their quality provides means for comparison and validation of the new data.

The WINDII diagnostic analysis was applied to observations of $O(^1S)$ and $O(^1D)$ airglow (day and night time observations), OH night glow, zonal and meridional winds and Doppler temperatures derived from the $O(^1S)$ and $O(^1D)$ volume emission rates, respectively. For each of the observation days, expressed both as UARS day number and a date, the data are presented as vertical profiles of the respective parameter for latitude bands as follows: 40N-70N, 20N-40N, 20N-20S, 20S-40S, 40S-70S. All presentations are in terms of geographic coordinates. The data were processed in geomagnetic coordinates and are also available, but have not been shown within this presentation. The effect of the geomagnetic equator and the Equatorial Ionospheric Anomaly and the Equatorial Electrojet on the thermospheric airglow emissions and Doppler temperatures are most pronounced at the 20N-20S latitude band and need be considered in the dynamic analysis of the observations.

Figure 15 illustrates the quality data diagnostics applied to $O(^1S)$ daytime observations from the original dataset for UARS Day 374 (September 19, 1992) in terms of volume emission rate (photons cm^{-3} s^{-1}) (upper panel) and the corresponding Doppler temperatures (lower panel). The $O(^1S)$ VER show variation with the solar zenith angle and latitude, which is most apparent in the height and magnitude of the peak seen at ~150 km. Vertical perturbations can also be seen in the Doppler temperature. Due to baffle scattering the peak seen around 200 km in the $O(^1S)$ VER particularly at 40N-70N, 20N-40N, 20N-20S, and also apparent in the Doppler temperatures for the same latitude range are an artifact and have to ignored. Perhaps in the data analysis some provisions could be set to identify the presence of such artifacts and correct for them through interpolation of the respective profiles for the values outside the contamination range (to be explored).

Figure 15A shows an example of the same two parameters, $O(^1S)$ VER and Doppler temperature for observations on UARS Day 2649, December 12, 1998, i.e. from the newly processed dataset (1997-2003). It can be seen that the vertical distribution of the two parameters is similar to the original dataset, the quality of the observations on this particular day is better especially with respect to the lack of baffle scattering around 200 km seen at some latitudes in the earlier dataset (Figure 15). This refers also to the Doppler temperatures.

However, with time the quality of the second dataset deteriorates and although there are data for most of the days marked as providing observations, these data do not meet the selection criterion and become increasingly meaningless. Therefore the number of days with good data is drastically reduced after 2000. Figure 15B shows one of the "better" examples of such data.

Figures 16 and 16A illustrate the $O(^1S)$ nighttime observations for the period of 1991-1997 and 1998-2003, respectively. The magnitude of the nighttime $O(^1S)$ VER in both cases is of the order of few hundreds of photons cm^{-3} s^{-1}, with a peak altitude about 95 km. Some descent of the peak can be seen suggesting variation with local time and latitude. The Doppler temperatures are given here only for completeness.

There were 414 days of nighttime $O(^1S)$ VER and temperature observations which were registered during the 1991-1997 period, and 305 days of nighttime data for the 1997-2003 period. One should keep in mind that the quality of the retrieved data after September 1997 deteriorates which lead to the decrease in the good data. This has a particular effect on the wind data as will be discussed later on. Many of the observations do not cover the full altitude range for the respective emission profile and for that reason they have not been included in the validation dataset. However, for some specific case studies as the wave 4 analysis at selected altitude (e.g. 250 km) the data are still suitable as the analysis require observations only in the altitude range from about 235 to 265 km (for the temperature analysis as done by M. Shepherd).

The diagnostics for the $O(^1D)$ dayglow emission were presented in the same format as that for $O(^1S)$ and some examples are shown in Figure 17 for UARS Day 449 (December 3, 1992) and in Figure 17A – for UARS Day 1246 (February 10, 1995). Both presentations are for the original dataset with peak height varying between 200 and 230 km depending on latitude and thus on the SZA. Similar to the $O(^1S)$ Doppler temperatures are also derived from the $O(^1D)$ observations. Both $O(^1D)$ VER and Doppler temperatures are most perturbed at the 20N-20S latitudinal band likely associated with the Equatorial Ionospheric Anomaly, discussed most recently in terms of the wave4 perturbations. The $O(^1D)$ Doppler temperatures differ from the $O(^1S)$ Doppler temperatures in magnitude as there are two different approaches in the retrieval of the temperatures from the two airglow emissions. 129 days of $O(^1D)$

daytime observations were analysed for the period of 1991-1997. The nighttime $O(^1D)$ VER (SZA> 89°) were also processed (not shown here).

The OH VER are also available and examples of these for UARS Day 417 (November 1, 1992) are shown in Figure 18. The daily zonal mean profile is given in red with a peak altitude at about 86 km. The seasonal variations of the observed airglow emission with local time (solar zenith angle) is illustrated in Figure 19 by the OH VER at the equator within 10° latitude band for Dec/Jan 1992-1994 (left panel) and Mar/Apr 1992-1993 (right panel). These are composite datasets over two seasons of observations in order to provide the full range of LT coverage. The peak altitude of the OH VER varies with LT as shown.

Figure 20 shows the diagnostic panel for the zonal (upper row) and meridional (lower row) winds for UARS Day 1893 (November 16, 1996) over the altitude range from 100 to 270 km, while Figure 20A shows the zonal and meridional winds observed on UARS Day 2538 (August 21, 1998). The bias in the observed zonal and meridional winds after September 1997 is apparent in the observations shown in Figure 20A. The problem rapidly becomes greater as time progresses and toward the end of the WINDII mission no meaningful values could be obtained. Up to UARS day 2203 (September 22, 1997) the winds are acceptable, but after that there appears to be an offset by about 200-400 m sec^{-1} from the zero either for zonal (eastward or westward) or meridional (north or southward) – resulting from the instrument being operated without temperature control.

The newly processed dataset covering the period of 1997-2003 is comprised of $O(^1S)$ VER observations, which as was mentioned earlier decrease in number and quality with time, thus allowing for further comparison only till 2000. Figure 21 shows the year to year seasonal variability of the daytime $O(^1S)$ VER for 20° latitude bands from 40S to 40N, for Dec/Jan, Mar/Apr, Jun/Jul and Sep/Oct from 1997 to 2000. In this presentation are included all available data for a given season without accounting for variation in LT. From all four seasons the June/July period is the least sampled over the latitude range of interest. All composite seasonal profiles show the artifact of baffle scattering at about 190-200 km, as was already discussed. A polynomial fitting to the data outside this altitude range could provide correction of this artifact whenever possible.

Figure 22 gives the seasonal zonal mean profiles of the $O(^1S)$ nightglow over the altitude range from 90 to 110 km. The peak altitude is at 94-95 km. To examine the seasonal variability of the O(1S) nightglow VERs, the vertical profiles over the latitude range 40S-40N are shown for the period of 1992-1996 in solid line and for 1997-2000 – in dash line. For most of the seasons and latitude bands the strongest VER was observed in 1992 (black, solid), with a second strongest in 2000 (red, dashed) close to the maximum of the 22 and 23 solar cycles, while the weakest O(1S) VERs were observed in 1995-1996, near the minimum of the same, 22 solar cycle, in agreement with earlier work by Liu and Shepherd, which has examined the $O(^1S)$ airglow dependence on the solar activity and solar flux.

6.1 O(^{1}S) Airglow:

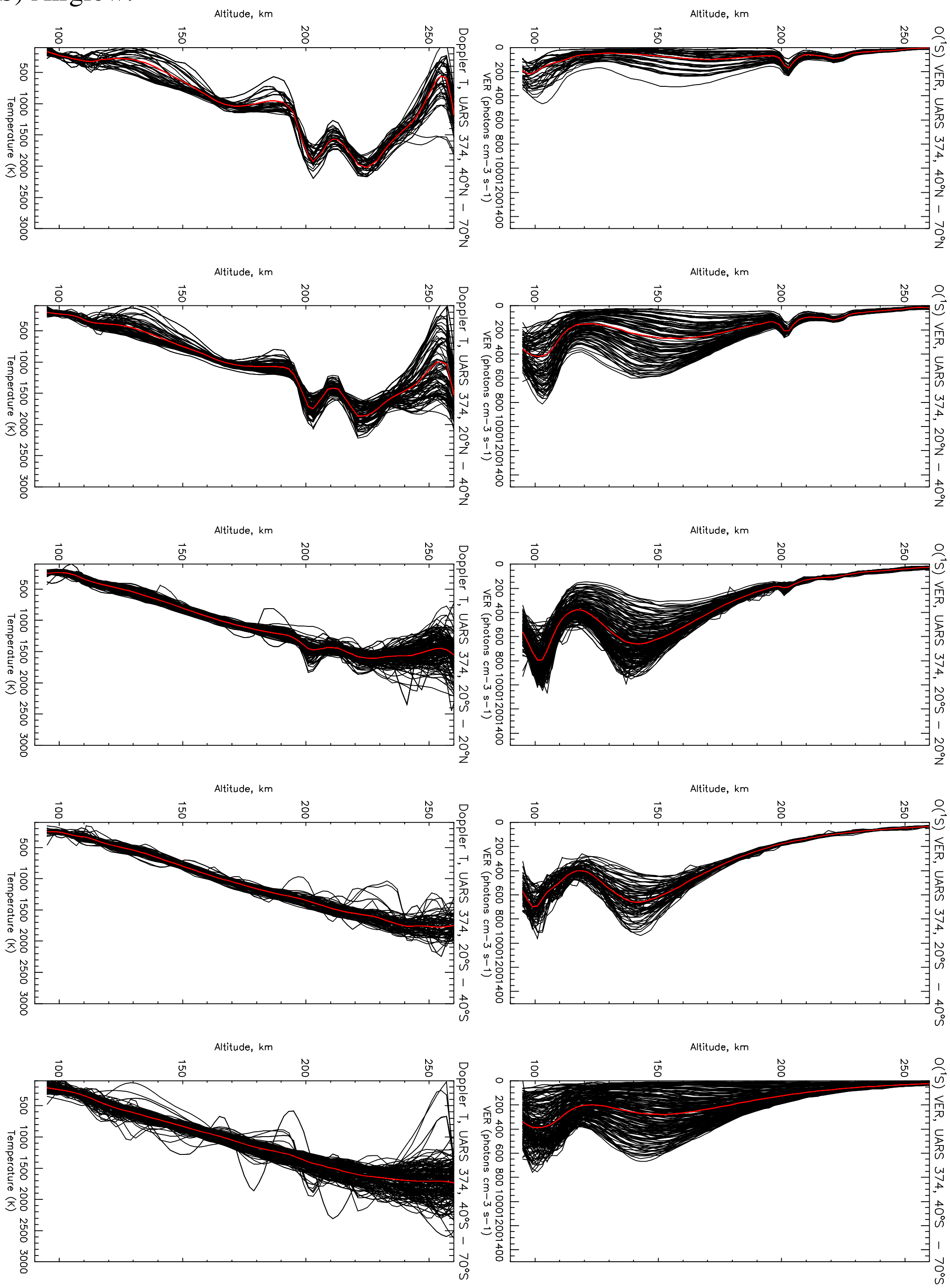

Figure 15: WINDII O(^{1}S) diagnostic panel – UARS Day 374 (September 19, 1992): Daytime Volume Emission Rates (VER - photon cm^{-3} s^{-1}) (upper/right panels) and Doppler Temperatures (left/lower panels) over the altitude range from 90 to 260 km; The original dataset, 1991-1997.

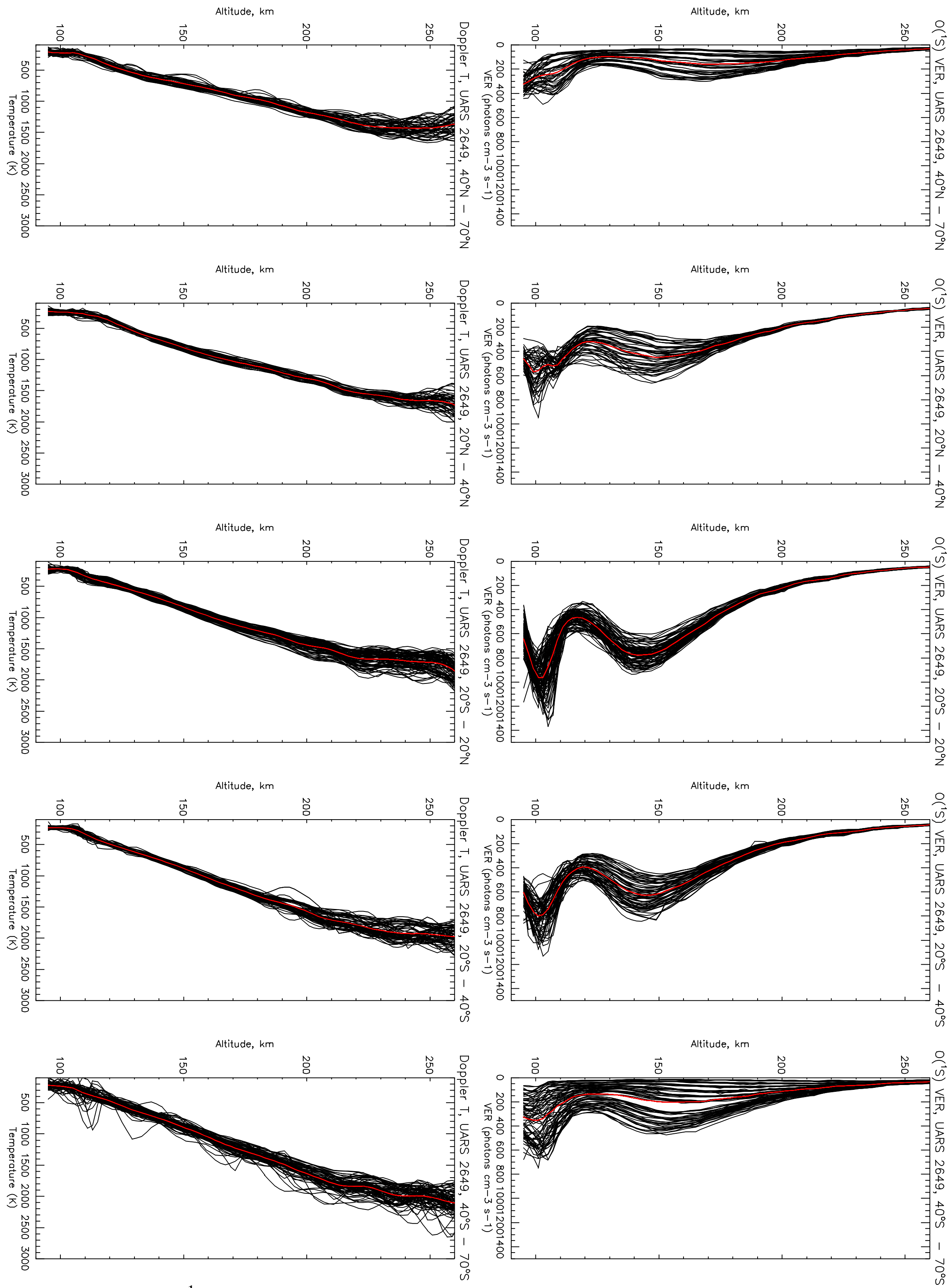

Figure 15A: WINDII $O(^1S)$ diagnostic panel – UARS Day 2649 (December 12, 1998): Daytime Volume Emission Rates (VER – photon cm^{-3} s^{-1}) (right/upper panels) and Doppler Temperatures (left/lower panels) over the altitude range from 90 to 260 km; The new dataset, 1998-2003.

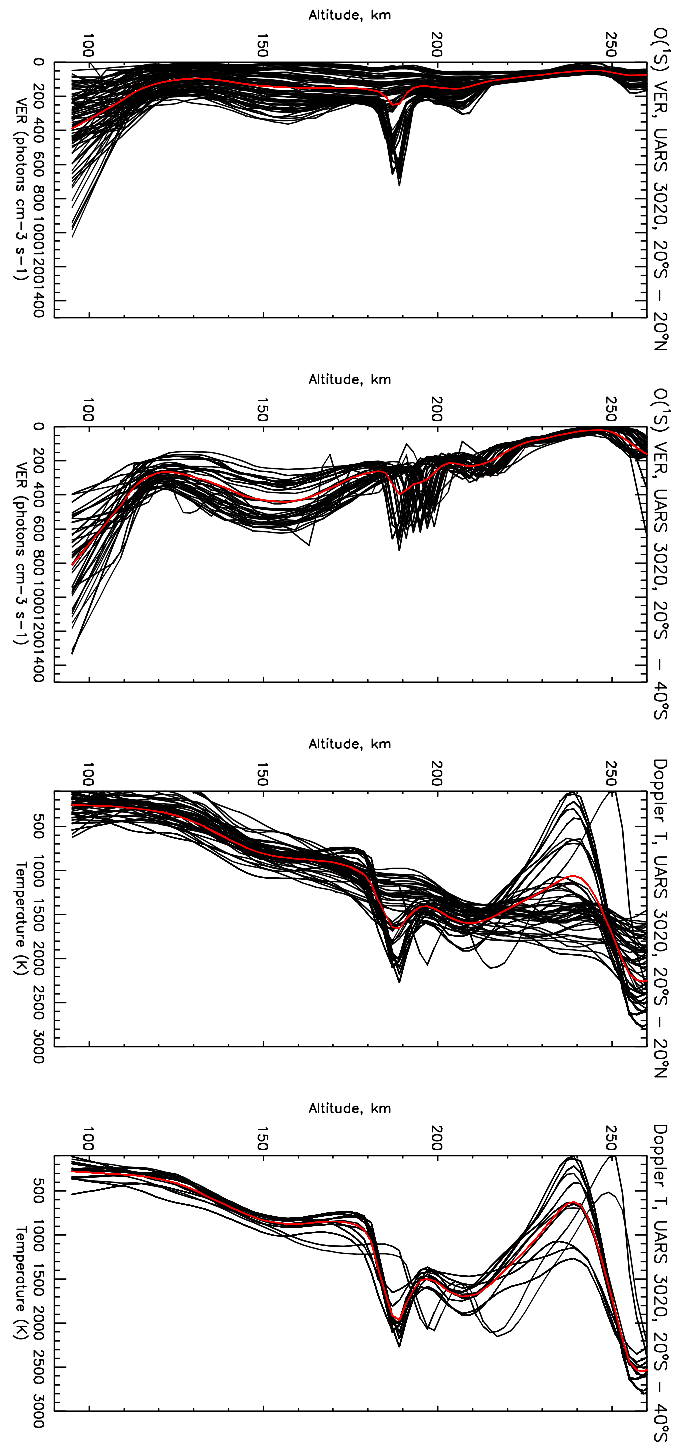

Figure 15B: WINDII O(^{1}S) diagnostic panels – UARS Day 3020 (December 17, 1999): Daytime Volume Emission Rates (VER – photon cm^{-3} s^{-1}) (upper two panels) and Doppler Temperatures (lower two panels) over the altitude range from 90 to 260 km; The new dataset, 1998-2003.

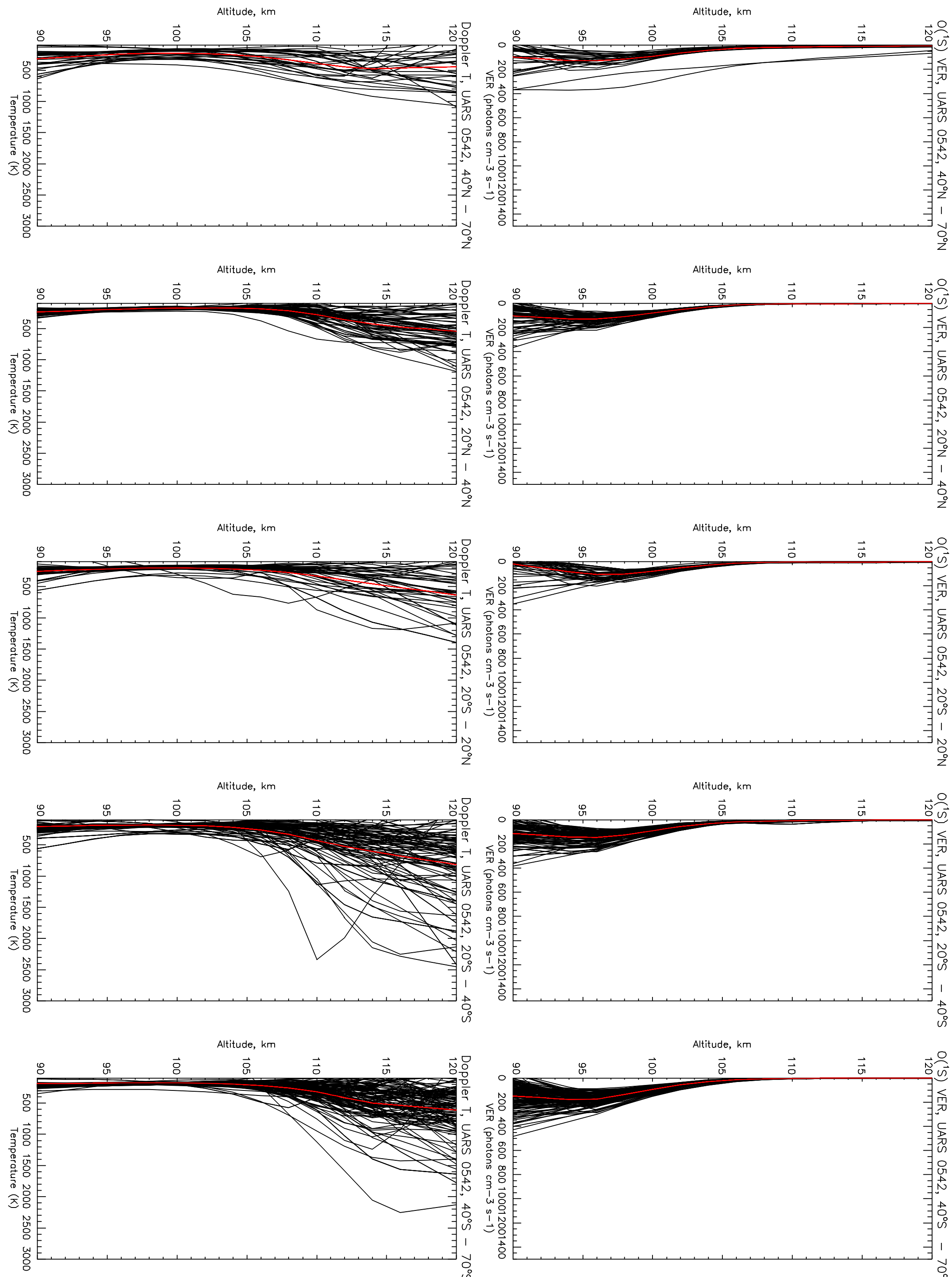

Figure 16: WINDII O(^{1}S) diagnostic panel – UARS Day 542 (March 6, 1993): Nighttime Volume Emission Rates (VER - photons cm^{-3} s^{-1}) (right/upper panels) and Doppler Temperatures (left/lower panels) over the altitude range from 90 to 120 km; the original dataset, 1991-1997.

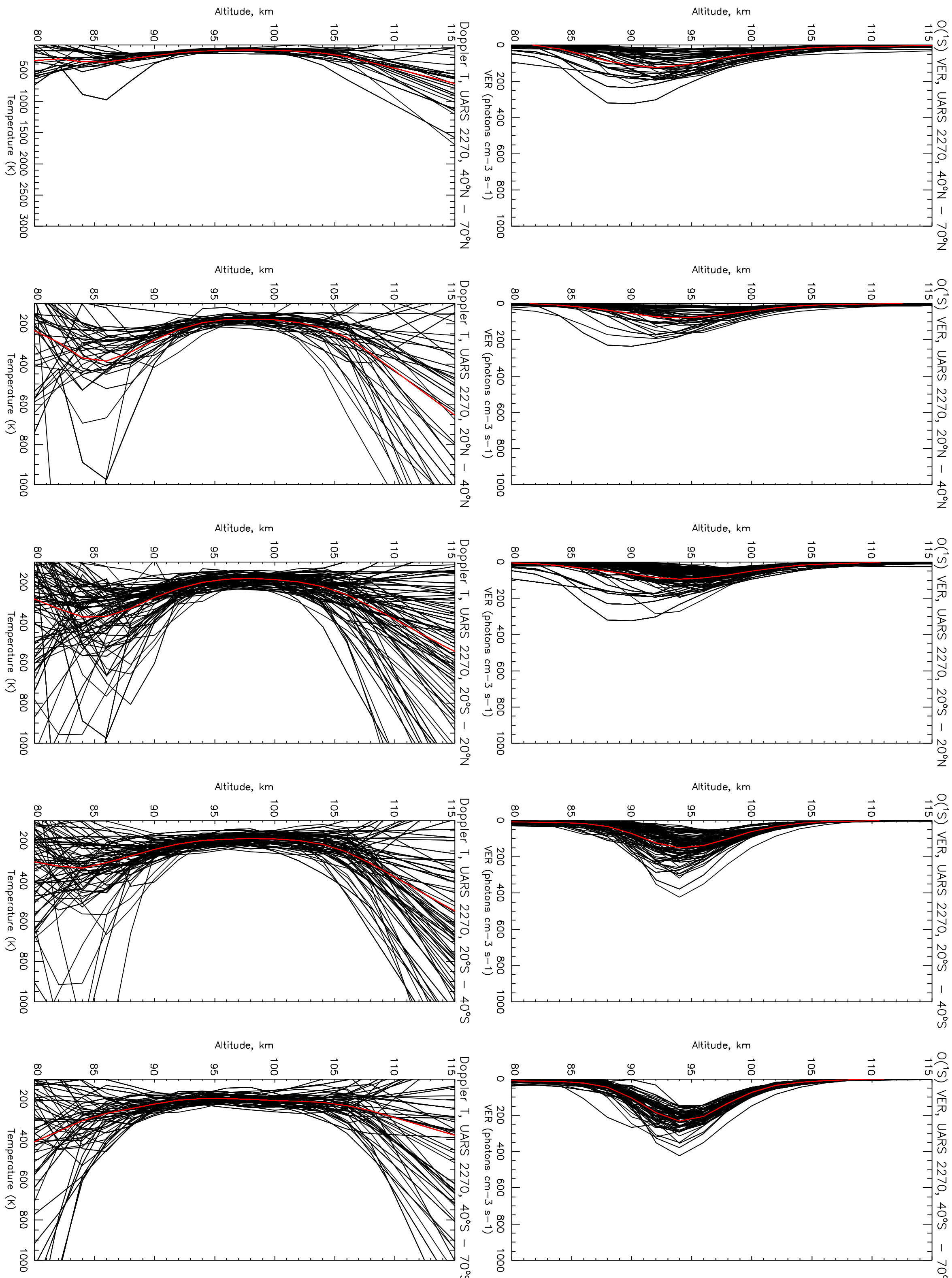

Figure 16A: WINDII O(^{1}S) diagnostic panel – UARS Day 2270 (November 28, 1997): Nighttime Volume Emission Rates (VER - photon cm^{-3} s^{-1}) (right/upper panels) and Doppler Temperatures (left/lower panels) over the altitude range from 80 to 115 km; the original dataset, 1997-2003.

6.2 $O(^1D)$ Airglow:

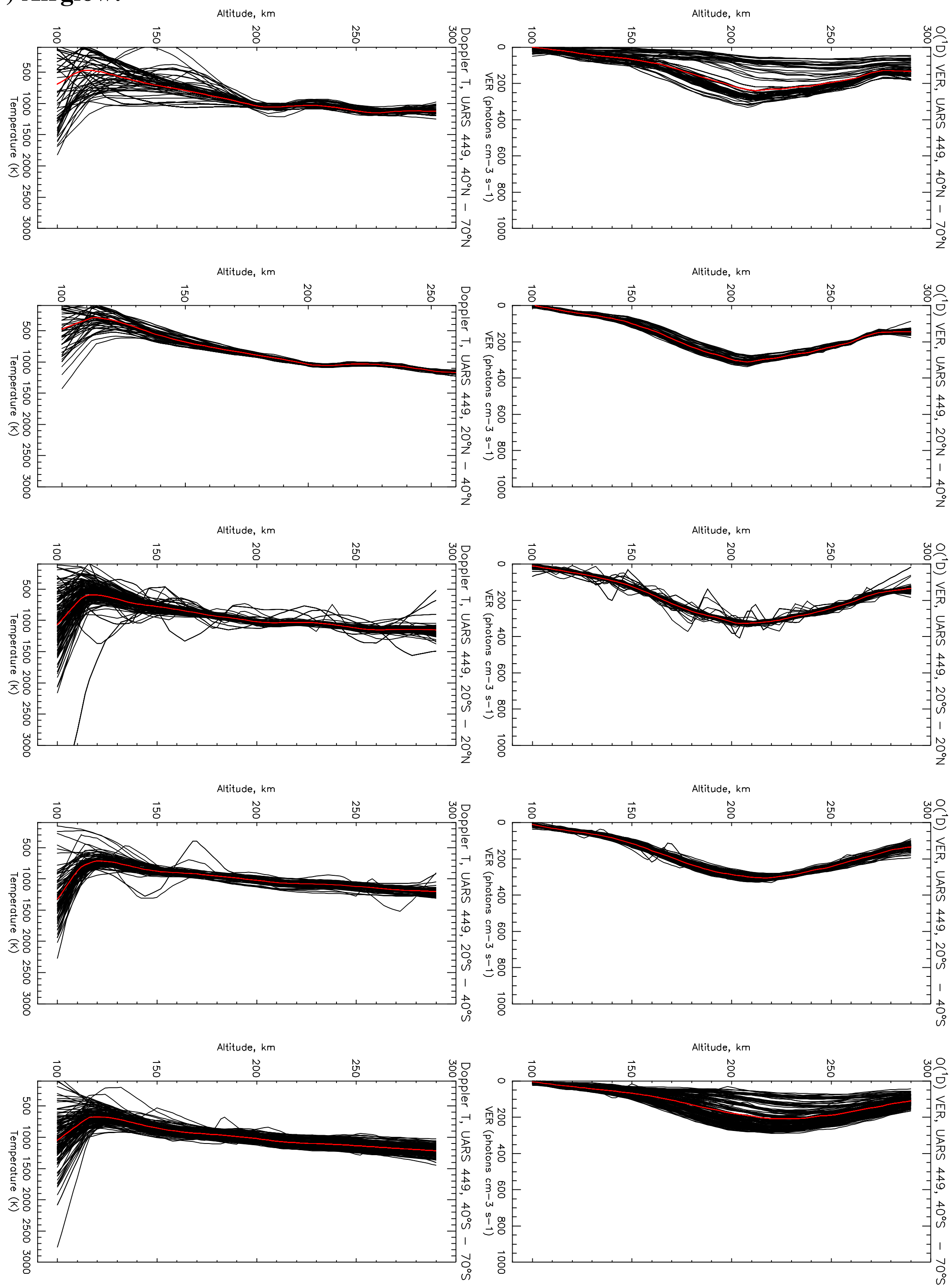

Figure 17: WINDII $O(^1D)$ diagnostic panel – UARS Day 449 (December 3, 1992): daytime Volume Emission Rates (VER - photons cm^{-3} s^{-1}) (right/upper panels) and Doppler Temperatures (left/lower panels) over the altitude range from 100 to 290 km, at 40N-70N, 20N-40N, 20N-20S, 20S-40S, 40S-70S.

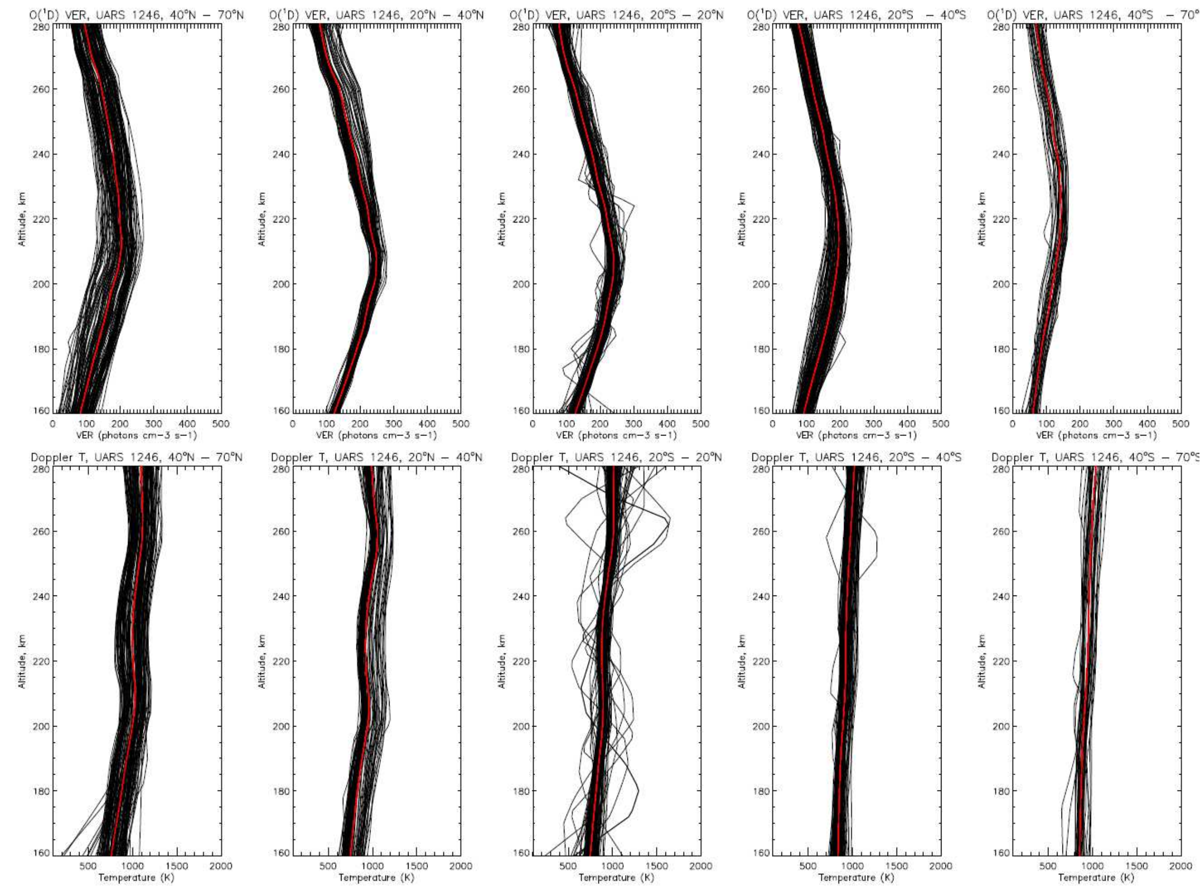

Figure 17A: WINDII O(^{1}D) diagnostic panel – UARS Day 1248 (February 10, 1995): daytime Volume Emission Rates (VER - photons cm^{-3} s^{-1}) (upper panels) and Doppler Temperatures (lower panels) over the altitude range from 160 to 300 km, at 40N-70N, 20N-40N, 20N-20S, 20S-40S, 40S-70S.

6.3 OH airglow VER

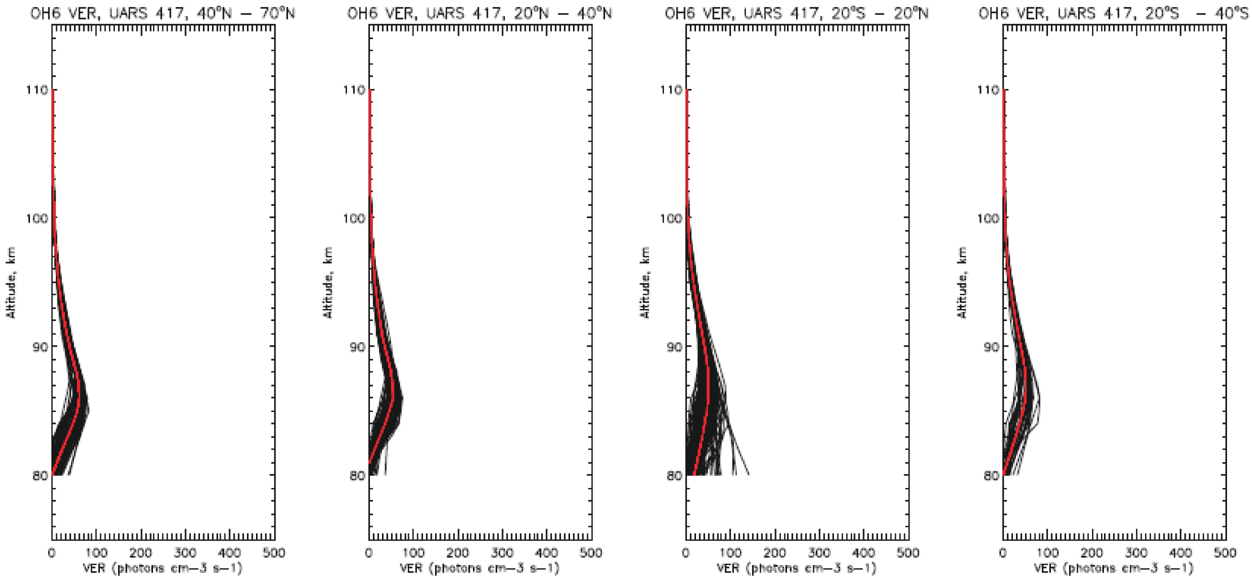

Figure 18: WINDII OH diagnostic panel – UARS Day 417 (November 1, 1992): nighttime Volume Emission Rates (VER - photons cm^{-3} s^{-1}) over the altitude range from 75 to 115 km, at 40N-70N, 20N-40N, 20N-20S, and 20S-40S. The daily zonal mean profile is given in red. The peak altitude is at ~ 86 km.

6.4 OH nightglow variability with local time (LT)

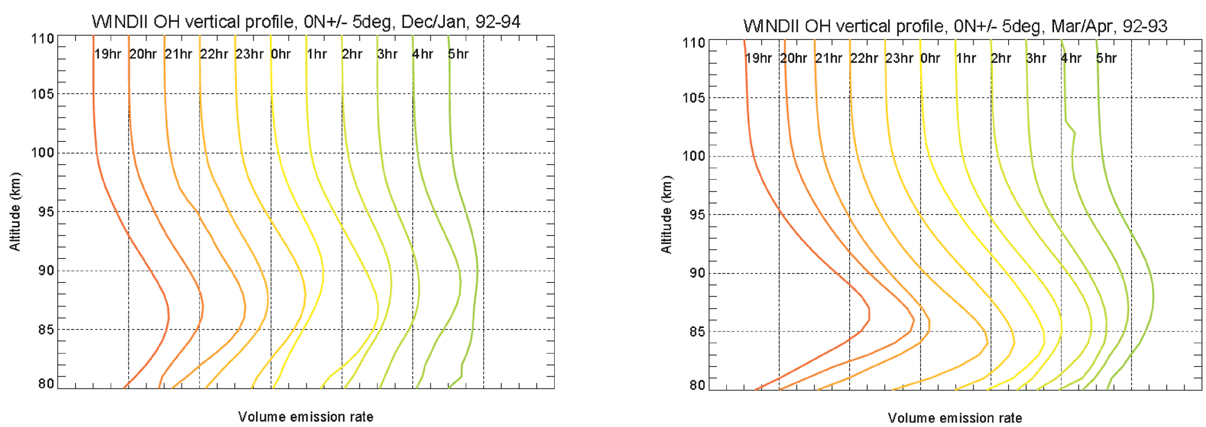

Figure 19: Composite OH night glow volume emission rate profiles as a function of local time at the Equator ± 5° for Dec/Jan 1992-1994 (left panel) and for Mar/Apr 1992-1993 (right panel).

6.5 Zonal and Meridional Winds:

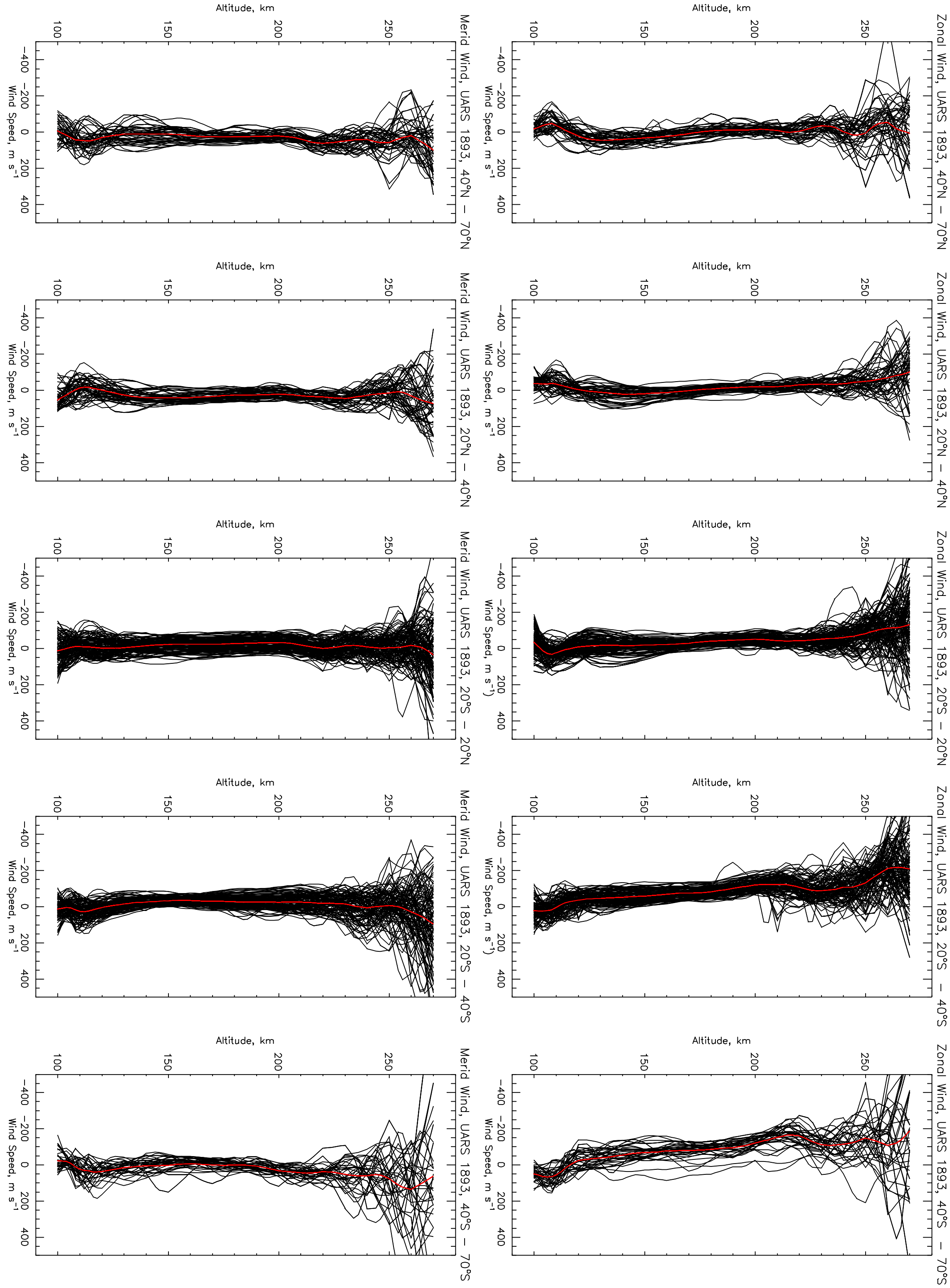

Figure 20: WINDII zonal (right/upper panels) and meridional (left/lower panels) winds from 100 to 270 km altitude for UARS Day 1893 (November 16, 1996) at 40N-70N, 20N-40N, 20N-20S, 20S-40S, 40S-70S.

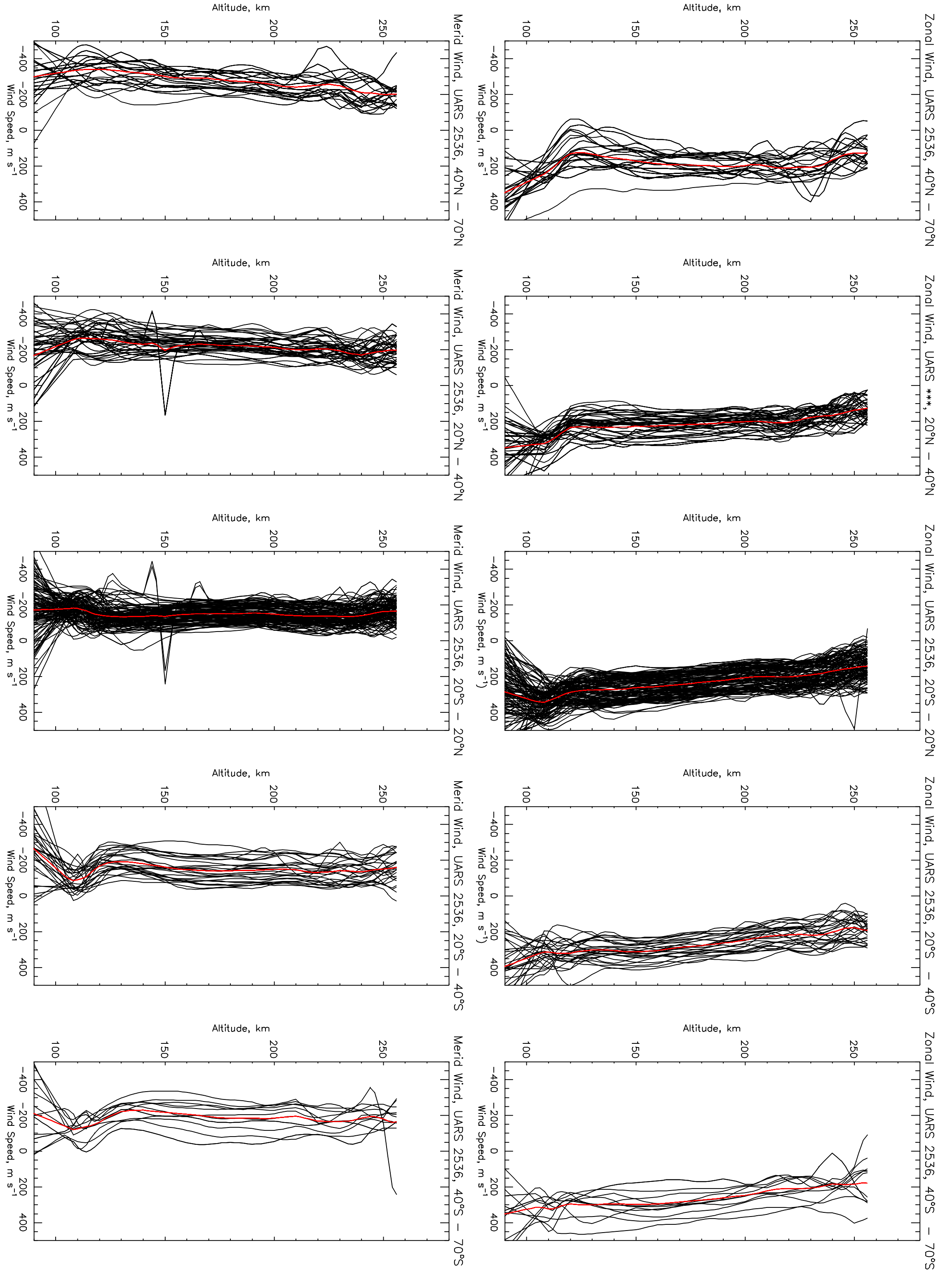

Figure 20A: WINDII zonal (right/upper panels) and meridional (left/lower panels) winds from 100 to 270 km altitude for UARS Day 2536 (August 21, 1998) at 40N-70N, 20N-40N, 20N-20S, 20S-40S, 40S-70S.The daily zonal mean profile is given in red. Observations after the cooling of the instrument and invalid zero-wind calibration.

6.6 Seasonal variability : Dec/Jan, Mar/Apr, Jun/Jul and Sep/Oct for day- and nighttime – from 1992 to 2003 – multi-plots

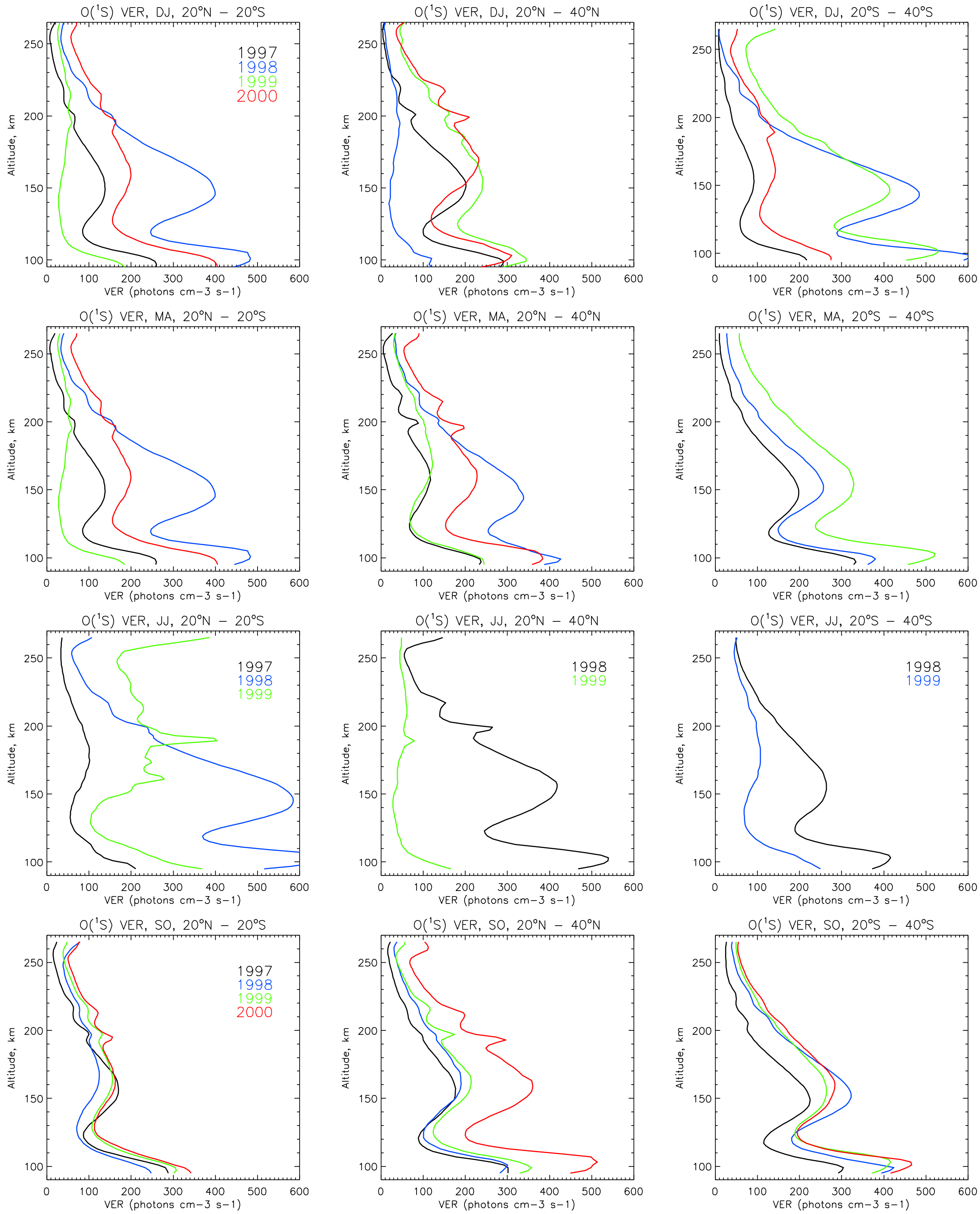

Figure 21: Seasonal variability of daytime O(^{1}S) VER from 1997 to 2000, at 20° latitudinal bands at 20N-20S, 20N-40N, and 20S-40S.

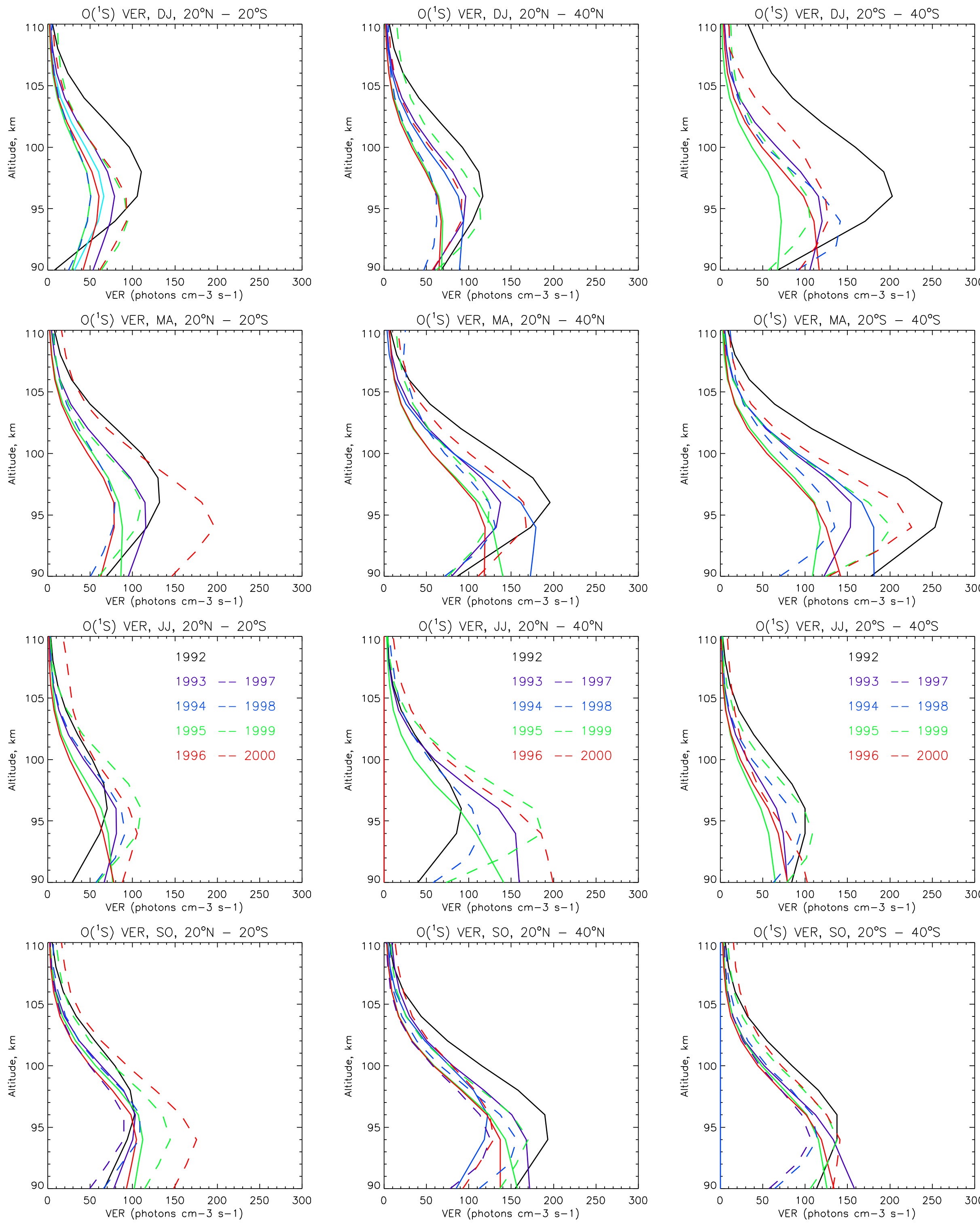

Figure 22: Seasonal variability of nighttime O(^{1}S) VER from 1991 to 2000, at 20° latitudinal bands at 20N-20S, 20N-40N, and 20S-40S. The 1992-1996 period is shown in solid line, the 1997-2000 – in dash line; colour code as shown.

6.7 Dynamical structures: Individual contour plots – illustration of the presence of dynamical signatures as the wave 4 – in $O(^1S)$ and $O(^1D)$ airglow VER, winds and Doppler temperatures

Although the Doppler temperatures are biased and their absolute values could be erroneous, they still reflect true perturbations in the atmosphere superimposed on the biased background. Therefore the daily zonal mean temperature at each altitude is subtracted from the observations producing the temperature residual profiles. The contour plots of these residual temperatures reveal the same perturbation pattern, in this case wave 4 signature, that is observed both in the $O(^1S)$ VER and the zonal wind as illustrated by the examples shown in Figures 23, 23A, 24, 24A and 25. The time when these wave 4 signatures are observed (August – September) is the time when wave 4 perturbations in the thermosphere maximizes. While these signatures are clearly seen in the original dataset, there are much fewer cases in the second dataset partly due to the limited temporal sampling and the gradual deterioration of the data quality (particularly of the wind observations).

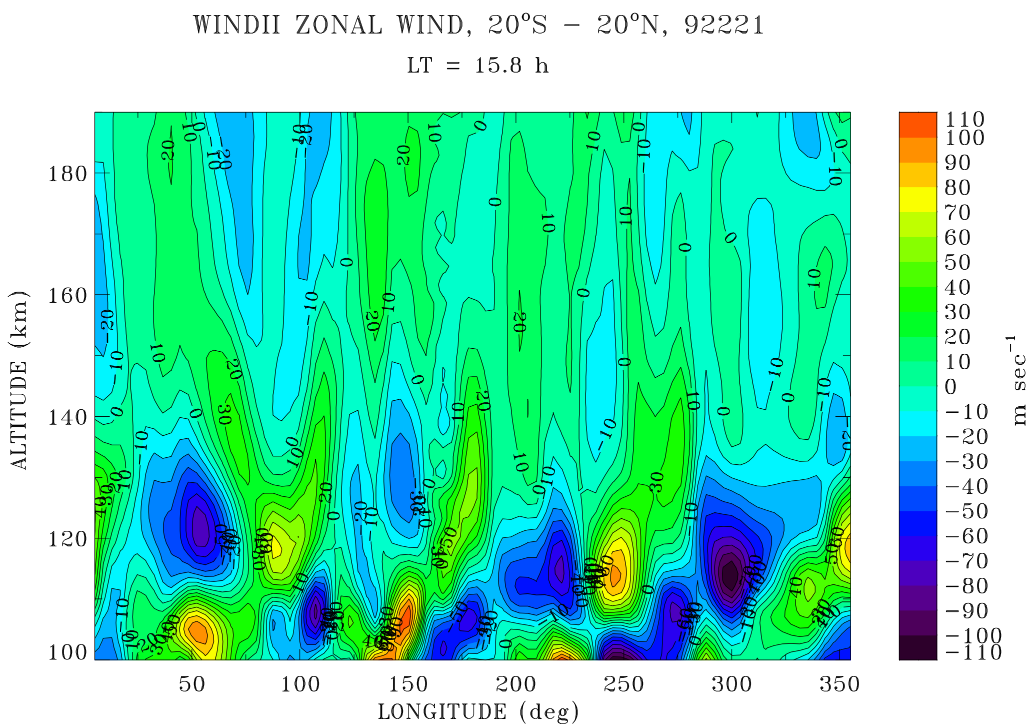

Figure 23: Zonal wind (m s^{-1}) at 20S-20N for UARS Day 332 (August 8, 1992)

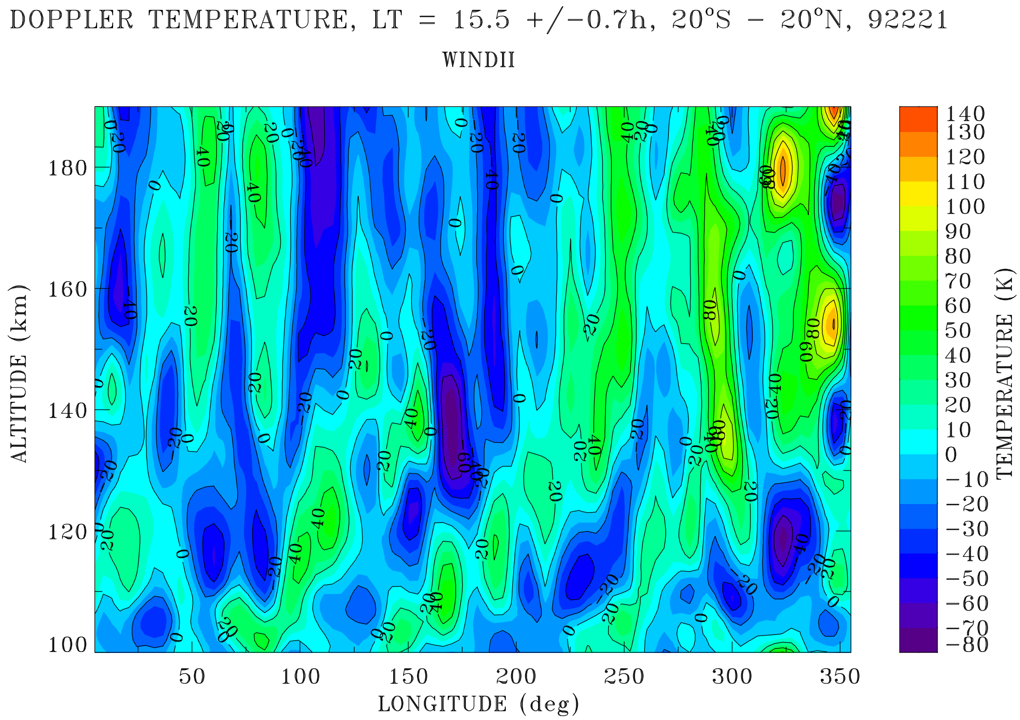

Figure 23A: Residual Doppler temperature (K) at 20S-20N for UARS Day 332 (August 8, 1992)

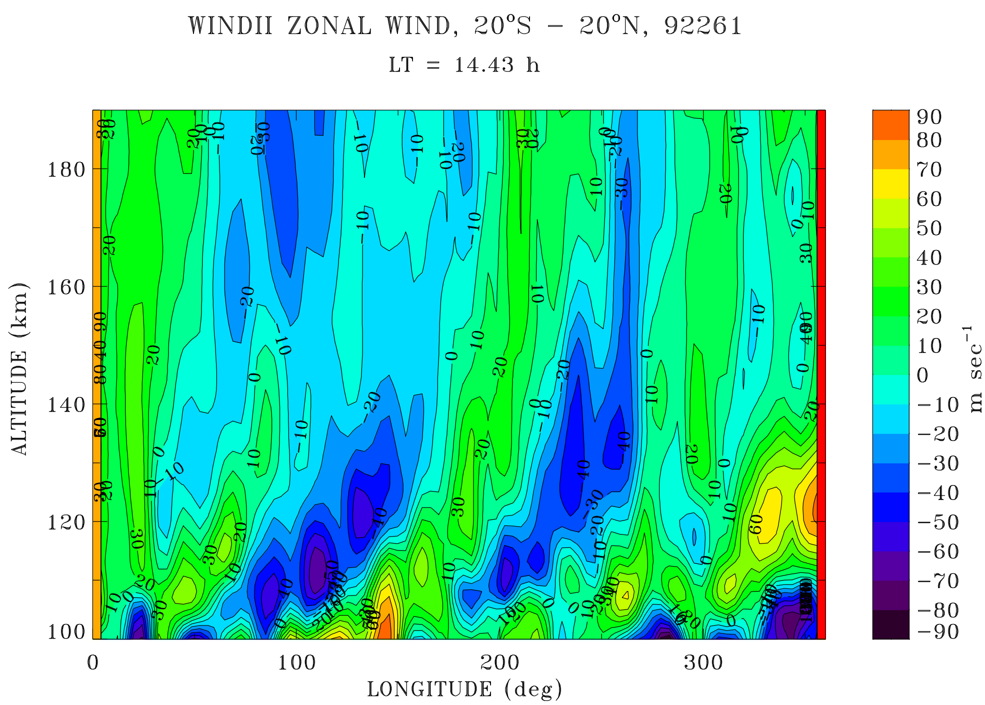

Figure 24: Zonal wind at at 20S-20N, for UARS Day 372 (September 17, 1992)

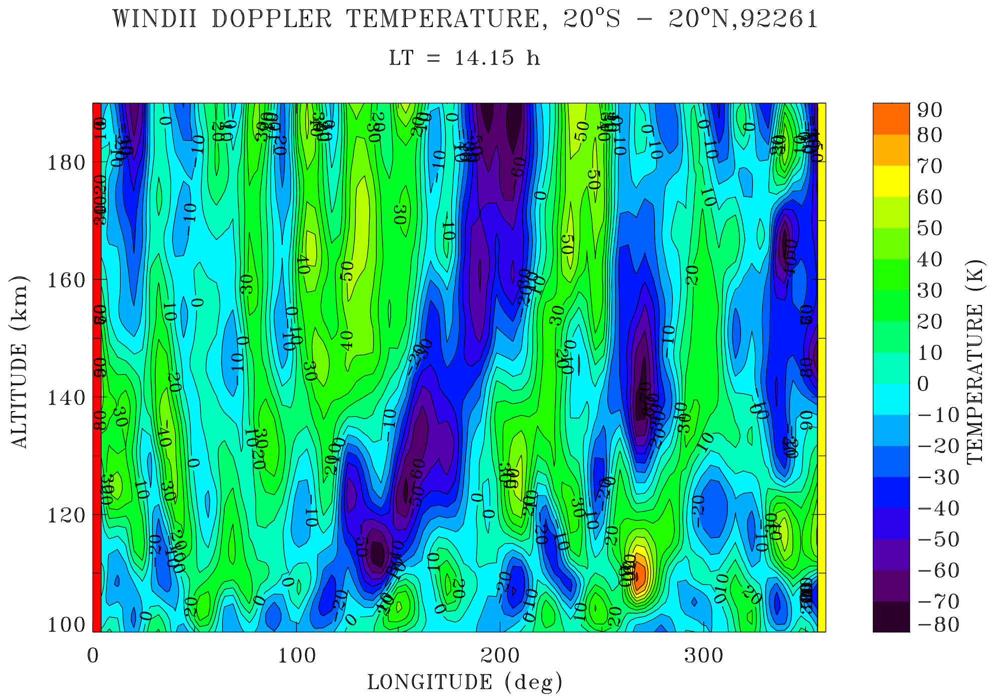

Figure 24A: Residual Doppler temperatures at 20S-20N, for UARS Day 372 (September 17, 1992)

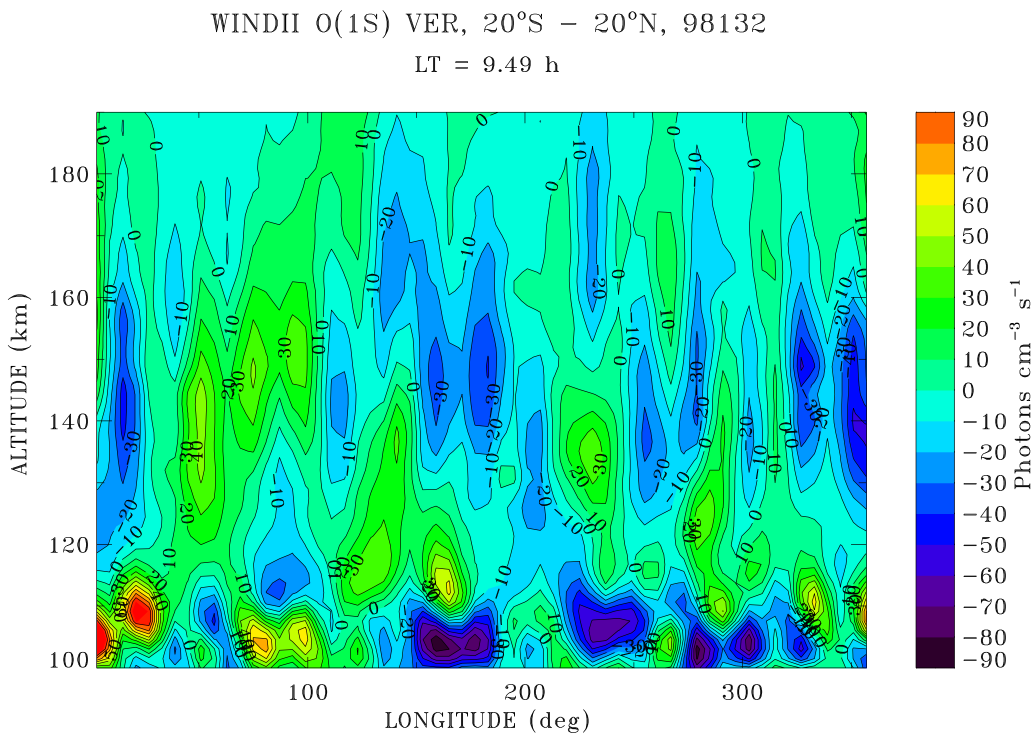

Figure 25: O(^{1}S) VER for UARS Day 2435 (May 12, 1998) at 20S-20N.

7.0 The WINDII archival dataset

The archive consists of all WINDII data processed using the new processing system, described in Section 3 of this report, as well as all FORTRAN and IDL source code. The physical archive is a Synology Disk Station DS213+ network attached storage (NAS) device with a mirrored raid disk array.This allows the archive to be directly connected to the internet and provides access to the data from a wide variety of operating systems, including Linux, UNIX, Mac and Windows computers. The DS213+ provides security and management functions to easily administer the data archive.

The data and code are archived in a simple directory tree shown in the following tables.

Table 1: **Lnx_sdppsv511_64** - top level directory for the current 64 bit Linux system and data

Sub-directories	Description
cdbv5	Calibration data organized in sub-directories labelled by UARS day number
dat_l0	Level 0 data saved in IEEE floating point format (see Graphic 2 for file types)
dat_l1	Level 1 data saved in IEEE floating point format (see Graphic 2 for file types)
dat_l2	Level 2 data saved in IEEE floating point format (see Graphic 2 for file types)
dat_scr	Level 1 and 2 scratch files saved in IEEE floating point format (see Graphic 2 for file types)
documentation	Top level documentation files describing processing, data format and summary of observations.
hdf_data	Level 2 CD, FD1 and FD2 data saved in Hierarchical Data Format
idl_sdppsv511	IDL source code for SDPPS V511 routines. Provides IDL read routines for all data files.
idl_tools	IDL source code for various data access tools.
job	Job stream command files. Text files defining input data files and processing for each UARS day.
jobit	IDL source code for job stream initialization. Interactive GUI to create job stream command files.
libU77	FORTRAN source code for various utility functions used by SDPPS V511 code.
winslin	FORTRAN source code for SDPPS V511, 64 bit Linux version, includes complied executables.
woadep	FORTRAN and IDL source code used to extract orbit and attitude data from UARS level 0 orbit and attitude files, accessible only under VAX VMS, and convert to a Linux compatible format. Processed Linux compatible OA data saved under **dat_l0** directory for all UARS days. Woadep processing is not required for current Linux version of SDPPS, but is included in the archive for completeness.

The old 32 bit Linux source code and executables are included for completeness.

Table 2: **Lnx_sdppsv511_32** – top level directory for old 32 bit Linux system

Sub-directories	Description
jobit	IDL source code for job stream initialization. Interactive GUI to create job stream command files.
libU77	FORTRAN source code for various utility functions used by SDPS V511 code.
winslin	FORTRAN source code for SDPPS V511, 32 bit Linux version, includes compiled executables.
woadep	FORTRAN and IDL source code used to extract orbit and attitude data from UARS level 0 orbit and attitude files, accessible only under VAX VMS, and convert to a Linux compatible format.

There is no database, however, all file names include the UARS day number in their name. A top level ascii text file, which is an electronic version of Annex A in this report and is located in the documentation sub-directory, provides a summary of all WINDII measurements. This file can be searched by calendar date to find the UARS day number or searched by WINDII filter number to locate dates when a particular observation type (eg, filter 7 daytime) was made. Under the dat_l0 directory, text files named meas_info_dxxxx.dat, where xxxx is the UARS day number, provide the exact time, in UARS date time format, during the given day when each measurement was taken. If, for example, a user was looking for WINDII observations taken at a given time or range of times (for correlative measurements or for an event) a search of the meas_info file for the given day would provide what WINDII observations were taken at the specified time(s). This saves reading the full data file in order to locate the desired measurement. The format and content of these files is documented in the top level documentation directory.

IDL and FORTRAN read routines are provided for each data file type. The IDL read routines are all located in the **Lnx_sdppsv511_64/idl_sdppsv511/common/src/** sub-directory and are named io_r_yyy.pro, where yyy is the name of the data file type (eg yyy = cva for the level 1 image data files). These read routines are well documented and provide the detailed description of the data formats. The file header formats are described in Annex B of this report and provide a quick summary of the content of each file type. An ascii text file copy of Annex B is included in the **documentation** sub-directory. The **Lnx_sdppsv511_64/winslin/common_for/** sub-directory contains the source code for the FORTRAN read routines, named io_r_yyy.f, using the same naming convention as for the IDL code. The **Lnx_sdppsv511_64/idl_tools/** sub-directory provides IDL source code examples of using the io_r_*.pro routines to access the WINDII data.

Given the information provided in the documentation and source code, any user should be able to access the WINDII data saved in this archive. The computer system used to develop the Linux code base will remain at York University. A full copy of the data archive will be retained on this computer, however, the DS213+ NAS is the primary archive and it should be used to make WINDII data available to the broader community.

8.0 Update on modelling capability and WINDII comparisons

8.1 Update on modelling capability

For the current project, three types of mesospheric nighttime emissions generated by the extended CMAM-SAS have been analyzed and compared with the WINDII observation. These are the O green line, the OH Meinel band and the O_2 Atmospheric Band emissions. The comparison has been carried out for all the available WINDII dataset which includes the green line emission data for 1991-2003 and OH Meinel band and O_2 Atmospheric Band emission data for 1991-1997.

A comparison of WINDII airglow data with the extended CMAM-SAS results provides a unique opportunity for validation of the model performance and analyzing atmospheric processes in the mesosphere and lower thermosphere (MLT) region. An important aspect of the validation process is the comparison of modelled and observed airglow structure, i.e., the spatial and temporal variability, with less emphasis on the absolute values. Agreement in airglow structure between the model and observations suggests that the model can capture composition changes among constituents along with temperature variations and the balance between chemistry and dynamics. Absolute emission values obtained with the model are usually smaller than those observed by up to a factor of 2-3. This disagreement between the model and observations can be attributed to 3 major reasons: (a) observation quality (e.g., instrumental calibration, presence of the solar illuminated regions after/prior sunset/sunrise, sampling issues); (b) simplified airglow model (e.g., missing or unknown mechanisms, uncertainties in rate coefficients); and (c) problems with the modelled T, O, O_3, and H fields.

8.1.1 A method used for calculation of the nighttime mesospheric emissions.

A FORTRAN subroutine for calculations of the nighttime mesospheric emissions is given in Appendix D. Chemical, kinetic and radiative processes involved in the formation of the nighttime mesospheric emissions are presented hereafter.

8.1.1.1 Hydroxyl Meinel bands.

The most complicated mesospheric nighttime airglow to model is the OH Meinel bands emission. This airglow arises as a result the reaction

$O_3 + H \rightarrow OH(v=6\text{-}9) + O_2$ (R8.1)

where the hydroxyl molecule is produced in the vibrational levels from 6 to 9. The reaction rate ($1.4\times10^{10}\times\exp(-470/T)$ cm^3s^{-1}, where T is temperature in Kelvin) is taken from Sander et al. (2002). For the nascent distribution over levels 6-9, the values of 0.08, 0.17, 0.27 and 0.48, respectively, are used (Klenerman and Smith 1987).

Due to both radiative and collisional processes the excitation energy deposited in levels v=6-9 cascades down and populates the lower vibration levels:

$OH(v1) \rightarrow OH(v2) + h\nu$, $v2<v1$ (R8.2)

$OH(v1) + O_2 \rightarrow OH(v2) + O_2$, $v2<v1$ (R8.3)

$OH(v) + N2 \rightarrow OH(v=0) + N2$ (R8.4)

The transition probabilities describing optical transitions in R8.2 are taken from Garcia-Munoz et al. (2005) and presented in Table 8.1. For collisions of the vibrationally excited hydroxyl molecule with molecular oxygen (reaction R8.3), state-to-state quenching rate constants k(v1,v2), where v2<v1, are used, whereas for OH-N_2 collisions (reaction R8.4) a so-called "sudden death" approximation, when as a results of reaction all the energy is deposited to the ground level, is utilized. Rate constants for OH-O_2 and OH- N_2 are taken from Adler-Golden (1997) and presented in Tables 8.2 and 8.3, respectively.

Table 8.1. OH Meinel bands transition probabilities A(v1,v2) (s^{-1}). Powers of 10 in parentheses. For instance, A(9,1)=2.979(-3) s^{-1} = 2.979×10^{-3} s^{-1}.

v2/v1	0	1	2	3	4	5	6	7	8
1	2.274(1)	0	0	0	0	0	0	0	0
2	1.342(1)	3.242E(1)	0	0	0	0	0	0	0
3	1.082(0)	3.860(1)	3.078(1)	0	0	0	0	0	0
4	1.327(-1)	4.082(0)	7.187(1)	2.146(1)	0	0	0	0	0
5	2.429(-2)	5.882(-1)	9.431(0)	1.083(2)	9.288(0)	0	0	0	0
6	5.689(-3)	1.212(-1)	1.529(0)	1.690(1)	1.416(2)	1.072(0)	0	0	0
7	1.498(-3)	3.111(-2)	3.510(-1)	3.237(0)	2.627(1)	1.669(2)	1.582(0)	0	0
8	4.354(-4)	9.309(-3)	9.793(-2)	7.432(-1)	5.264(0)	3.658(1)	1.815(2)	1.354(1)	0
9	1.336(-4)	2.979(-3)	3.153(-2)	2.230(-1)	1.334(0)	9.809(0)	4.460(1)	1.829(2)	3.693(1)

Chemical losses also occur with reaction of the vibrationally excited OH and atomic oxygen:

$$OH(v) + O \rightarrow H + O_2 \qquad (R8.5)$$

The rate constant for this reaction (2.5×10^{10} cm^3s^{-1}) is taken from Makhlouf et al. (1995).

The Meinel band system comprises 45 different vibrational bands. WINDII provides data for the $P_1(3)$ rotational line of the OH(8-3) band. The fraction of the $P_1(3)$ line in the total OH(8-3) emission rates decreases with temperature from 12.6% at 150 K to 10.4% at 210 K. In our calculations we approximated this fraction with 11%, a number valid for the characteristic mesosphere temperature of 200 K.

Table 8.2. State-to-state quenching rate constants for OH-O_2 collisions, k(v1,v2) in units of $10^{-13}\ cm^3s^{-1}$.

v2/v1	0	1	2	3	4	5	6	7	8
1	2								
2	0	4							
3	0	1	7						
4	0	1	2	10					
5	0	1	2	6	16				
6	1	1	3	6	11	22			
7	4	6	9	12	16	23	32		
8	4	6	8	10	14	19	25	33	
9	28	29	31	32	34	36	38	40	42

Table 8.3. Rate constants for OH(v) quenching by N_2, k(v) in units of $10^{-13}\ cm^3s^{-1}$.

V	1	2	3	4	5	6	7	8	9
k(v)	0.06	0.10	0.17	0.30	0.52	0.91	1.6	7	4.8

8.1.1.2. O_2 atmospheric bands and $O(^1S)$ green line.

In calculations of the volume emission originated from the O_2 atmospheric bands and from the $O(^1S)$ green line we followed the approach proposed by Melo et al. (2001) and McDade et al. (1986). All the reaction rate constants and empirical coefficients required for the calculations in the current study were the same as those used in Melo et al. (2001) and McDade et al. (1986).

The O_2 atmospheric band emission is the result of the atomic oxygen recombination reaction:

$$O(^3P) + O(^3P) + M \rightarrow O_2^* + M \qquad (R8.6)$$

$$O_2^* + O_2 \rightarrow O_2(b^1\Sigma_g^+) + O_2 \qquad (R8.7)$$

$$O_2(b^1\Sigma_g^+) \rightarrow O_2(X^3\Sigma_g^-) + h\nu\ (761.9\ \&\ 866nm) \qquad (R8.8)$$

The O_2 (0-0) and O_2 (0-1) atmospheric bands radiate from the excited $O_2(b^1\Sigma_g^+)$ molecules at 761.9 and 866 nm, respectively. Radiative losses occur due to different emissions of the excited molecular oxygen

O_2*. There are also collisional and chemical losses which occur upon reaction of excited molecular oxygen (O_2* and $O_2(b^1\sum_g^+)$) with N_2, O_2 and O. WINDII provides data for the O_2 (0-0) atmospheric band.

The 557.7 nm green line emission comprises the largest body of WINDII data. It radiates from the excited $O(^1S)$ atoms. Similar to the O_2 atmospheric band emission, the green line mesospheric emission is also the result of the atomic oxygen recombination reaction (R8.6) which is followed by:

$$O_2^* + O(^3P) \rightarrow O(^1S) + O_2 \qquad \text{(R8.9)}$$

$$O(^1S) \rightarrow O(^1D) + h\nu \text{ (557.7 nm)} \qquad \text{(R8.10)}$$

Collisional and chemical losses occur upon reaction of the excited molecular oxygen O_2* with N_2, O_2 and O and $O(^1S)$ with O_2. There are also radiative losses due to emissions of O_2* and branching of emission from the $O(^1S)$ level, viz. $O(^1S \rightarrow ^3P)$.

8.2. Comparison of the WINDII and CMAM climatology and variability of the O_2 Atmospheric Band data and the hydroxyl Meinel band data.

The comparison of the WINDII observations and the CMAM results for the O_2 Atmospheric Band and OH Meinel band emissions has been carried out for 1991-1997, since the new WINDII dataset covering 1998-2003 years provides information for the atomic oxygen green line emission only. The numbering system for the figures in this chapter (8.x) is different from that used in the other chapters. Vertical profiles for all three mesospheric emissions over the equator for solstice and equinox are shown in Figure 8.1. Except for the fact that the CMAM considerably, by a factor of 2-3, underestimates the volume emission rates, it can be concluded that there is a good qualitative agreement between the CMAM and WINDII data. Namely, relative values and peak locations of all the mesospheric emissions modelled by the CMAM are all in reasonable agreement with WINDII observations. As has been noticed earlier, an important aspect of the model validation is to compare the airglow structure with less emphasis on the absolute values which can differ for different reasons. It might be worth mentioning here that the emission rates obtained with the Thermosphere-Ionosphere-Mesosphere-Electrodynamics General Circulation Model (TIME-GCM), which is the only global comprehensive model used to calculate the mesospheric airglow prior to the CMAM, are also smaller by a factor of 2-4 than those obtained from WINDII (Liu, 2006). This occurs despite the fact that the TIME-GCM has the lower boundary around 30 km where the tidal and planetary wave forcing is applied, whereas the CMAM simulates this forcing in a self-consistent way.

Latitudinal variation of the vertical profiles for all three mesospheric emissions at equinox is shown in Figure 8.2. As can be seen, the WINDII profiles do not exhibit significant variations in peak locations and values of the emissions except for a slight increase of the peak location with latitude for the green line and OH emissions (note that the secondary maximum in the O_2 Atmospheric Band emission is not well understood and might be an observation artefact). The CMAM also shows an increase in peak locations with latitude for all three airglow and, unlike WINDII, provides higher values of the green line emissions at 20° and 40° N than at the equator. This likely indicates underestimation of the model atomic oxygen in tropics which may be related to a weak eddy diffusion in the tropical mesosphere. The latter can possible be fixed by using a more realistic gravity wave source with a local maximum near the equator.

The annual cycle of the OH(8-3) nighttime volume emission rates in the equatorial region averaged over 1992-1996 period is shown in Figure 8.3. As can be seen, the model is well able to capture the seasonal variability of the OH emission which shows semi-annual variations in both the emission rate (with maxima around the spring and fall equinoxes) and emission peak height. The emission rate in both the CMAM and WINDII observations maximizes and has the lowest peak height during the equinox.

Figure 8.4 shows the evolution with local time of the OH(8-3) nighttime emission for March-April near the equator and at 30°N. This nighttime evolution is mainly associated with the diurnal migrating tide generated in the troposphere, playing a major role in variability of the equatorial MLT region. Even though the observed nighttime evolution of the emission rate value and peak emission height with local time is different in the equatorial and subtropical regions, the CMAM captures quite well the observed features. In the equatorial region, the emission rate maximizes in late afternoon and decreases during the night while the emission peak height decreases during the first half of the night and increases in the second half. The pattern is quite different at 30°N: the emission rate has a minimum around the mid-night when the peak height is the highest. The ability of the CMAM to reproduce such different behaviors in the evolution of the nighttime emission suggests that the model is able to represent the atmospheric variability of the atmospheric parameters in this region in a realistic fashion.

8.3. Comparison of the WINDII and CMAM climatology and variability of the $O(^1S)$ green line emission.

The new WINDII dataset for the $O(^1S)$ green line emission covers the period from 1991 to 2003. However, the presence of large gaps in time and space in WINDII observations makes it problematic to produce a reasonable annual cycle, nighttime evolution and de-seasonalized time series of the emission rates for 1998-2003. In this case, the CMAM-WINDII comparison has been performed for the period of 1991-1997 only.

Vertical profiles of the $O(^1S)$ green line emission derived from the CMAM and WINDII observations over the equator for solstice and equinox and at different latitudes for March/April for 1991-1997 has been already presented and discussed in subsection 8.2 (see Figures 8.1 and 8.2). Figure 8.5 compares the CMAM and WINDII data for the $O(^1S)$ volume emission rate over the equator and at 20°N in March/April averaged over 1998-2003. Similar to the results for 1991-1997, it can be concluded that the model considerably underestimates the value of the emission, but reproduces well its shape and peak location. The values of the emission rates in both the CMAM and WINDII are slightly larger in 1998-2003 than in 1991-1997 which can be explained by the fact the during the period of 1998-2003, the solar activity was higher (sensitivity of the green line emission to the solar activity level will be discussed below).

The annual cycle of the $O(^1S)$ green line nighttime volume emission rates in the equatorial region is shown in Figures 8.6 and 8.7. Figure 8.6 compares the CMAM and WINDII results averaged over 1992-1997 whereas Figure 8.7 presents the CMAM results averaged over 1998-2003. Similar to the OH(8-3) emission, it can be concluded from Figure 8.6 that the model is well able to capture the seasonal variability of the emission rate. Both the model and observations show semi-annual variation in the emission rate with minima around February and September (although the CMAM cycle is shifted by about one month). Annual evolution of the emission peak height, with a prominent minimum around April, is also well reproduced by the CMAM. The CMAM results for 1998-2003 (Figure 8.7) are qualitatively quite similar to those for 1992-1997 with minima in the emission rate around February and September and with the minimal emission peak height in April.

Evolution with local time of the green line nighttime emission for March-April near the equator and around 30°N is shown in Figure 8.8 (averaged over 1992-1997 for both the CMAM and WINDII) and in Figure 8.9 (the CMAM results only, averaged over 1998-2003). And again, it can be concluded that in spite of the quite different dependence of the emission rate value and peak emission height on local time in the equatorial and subtropical regions, the CMAM is able to capture the observed emission structure, i.e. its spatial and temporal variability. The model results for 1998-2003 (Figure 8.9) are qualitatively similar to the CMAM and WINDII results for 1992-1997 (Figure 8.8).

To analyze the sensitivity of the $O(^1S)$ green line emission to the solar activity level, an approach proposed by Liu and Shepherd (2008) has been utilized. The volume emission rate has been vertically integrated and zonally averaged for four seasonal (November-January, February-April, May-July, August-October) and eight latitudinal (40-30°S, 30-20°S, 20-10°S, 10°S-0°, 0°-10°N, 10-20°N, 20-30°N, 30-40°N) bins. This averaging largely eliminates the longitudinal and local time dependence of the airglow. To eliminate the seasonal variation, the emission rates have also been de-seasonalized. That is, the mean value of all three-monthly averages over the given three-month period through all the years is subtracted from the three-month averaged emission rate for a given year. To quantify the relation of the $O(^1S)$ emission and solar activity, the de-seasonalized three-month averaged emission rates and the three-month averaged F10.7 fluxes are shown as scatter plots in Figure 8.10 for eight latitudinal bins. The superimposed straight lines are from linear regression fittings. The correlation coefficients and the fitting equations are given at the lower right corners of the each panel. Note, the CMAM results (shown on the left hand side) represent twelve years (1992-2003) of simulation, while the WINDII data represent six years (1992-1997) of observations.

For each latitude band, the emission rates are closely correlated with the F10.7 fluxes. Despite the scatter, the emission rate increases with increasing F10.7 flux along a straight line for both the CMAM and WINDII observations. The correlation coefficients obtained from the model and observations are comparable, although the CMAM coefficients are somewhat smaller. This underestimation of the solar signal may likely be explained by missing the energetic particle precipitation (EPP) effect in the current version of the extended CMAM. It is also worth noting here that the correlation and regression coefficients are generally smaller in the equatorial region for both the CMAM and WINDII data. Thus, it can be stated that the CMAM reasonably well reproduces the observed correlation between the $O(^1S)$ green line emission and solar activity.

To summarize the CMAM-WINDII comparison, it can be concluded that the model is able to capture well the vertical, latitudinal and diurnal structure of the observed nighttime mesospheric emission in the $O(^1S)$ green line and in the O_2 atmospheric and OH(8-3) Meinel bands. The model also provides a correct response of the intensity of the green line emission to variations in solar activity. All this suggests that CMAM has the ability to capture well the temporal and spatial variation of energy, chemistry and dynamical processes in the atmosphere needed for airglow analyses.

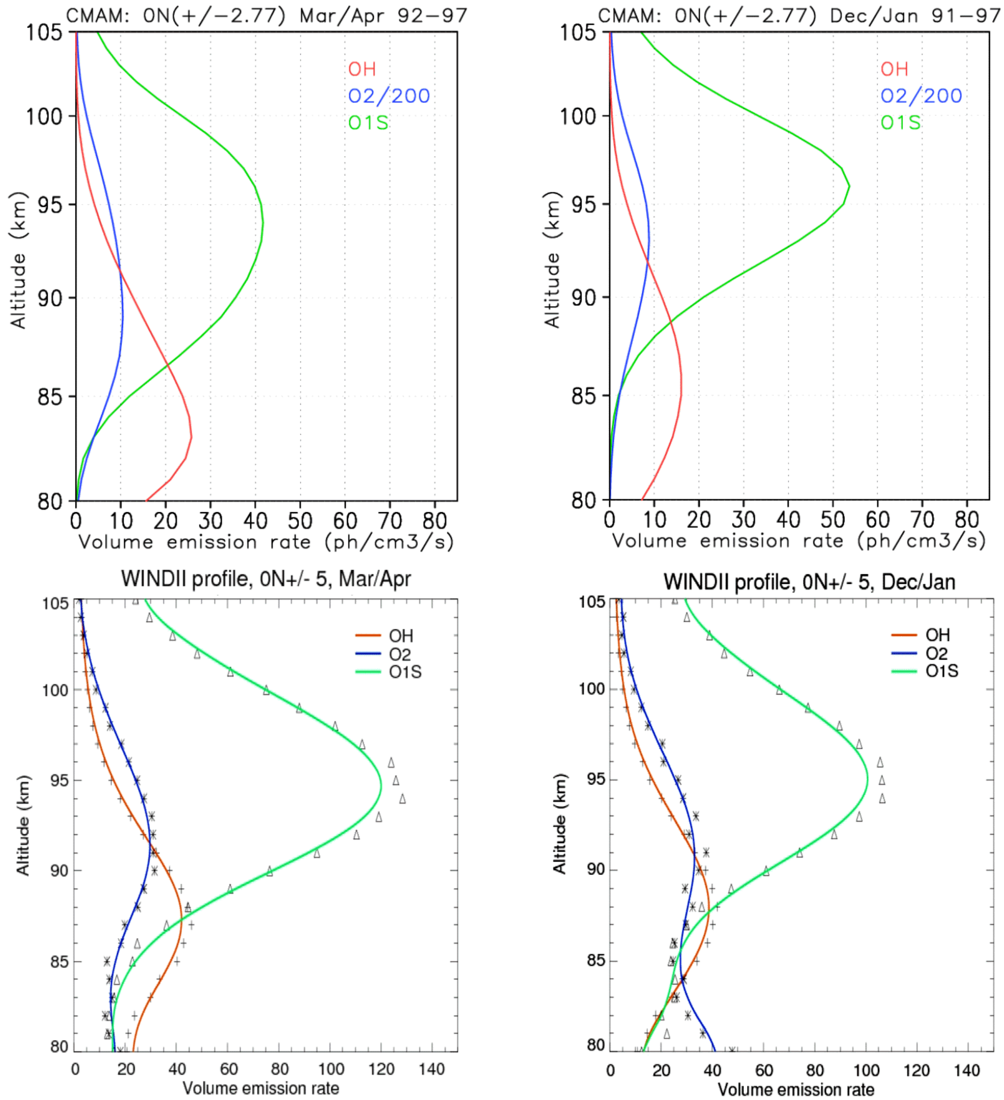

Figure 8.1. Zonally averaged volume emission rates (ph cm^{-3} s^{-1}) for 3 types of airglow over the equator in March-April (left) and December-January (right) from the CMAM (top) and WINDII (bottom). Data are for the period of January 1991 – April 1997.

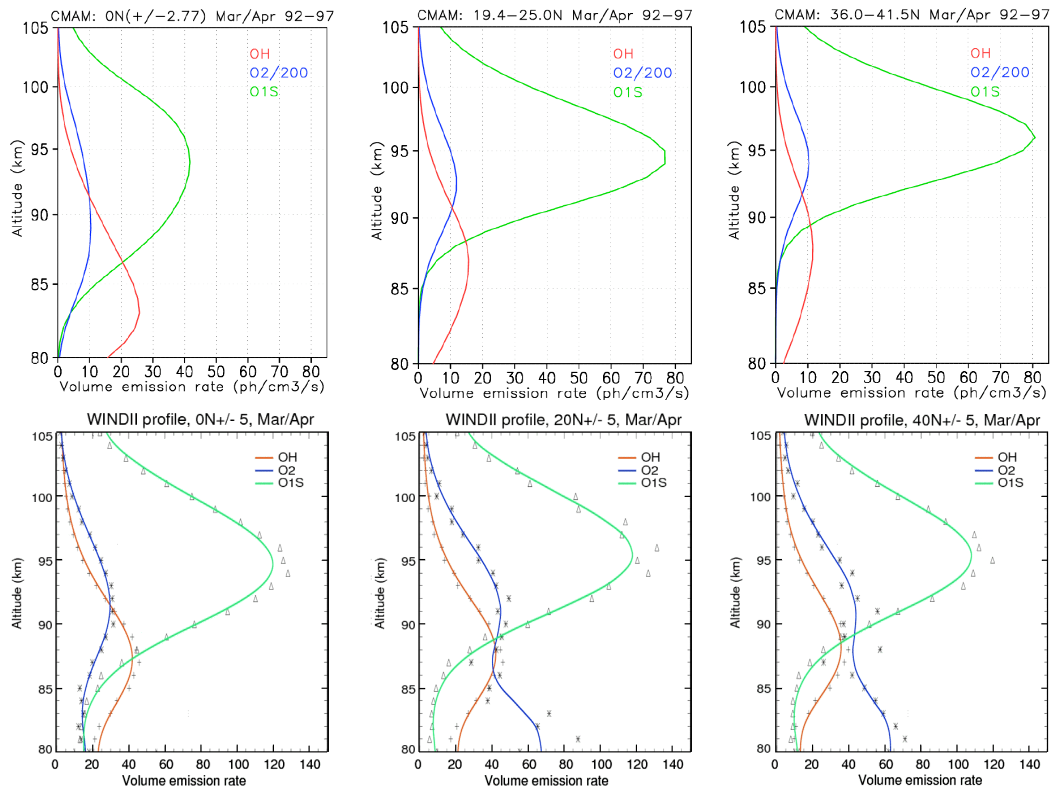

Figure 8.2. Zonally averaged volume emission rates (ph cm^{-3} s^{-1}) for 3 types of airglow over the equator (left), near 20° N (middle) and 40° N (right) in March-April from the CMAM (top) and WINDII (bottom). Data are averaged for the period of March 1991 – April 1997.

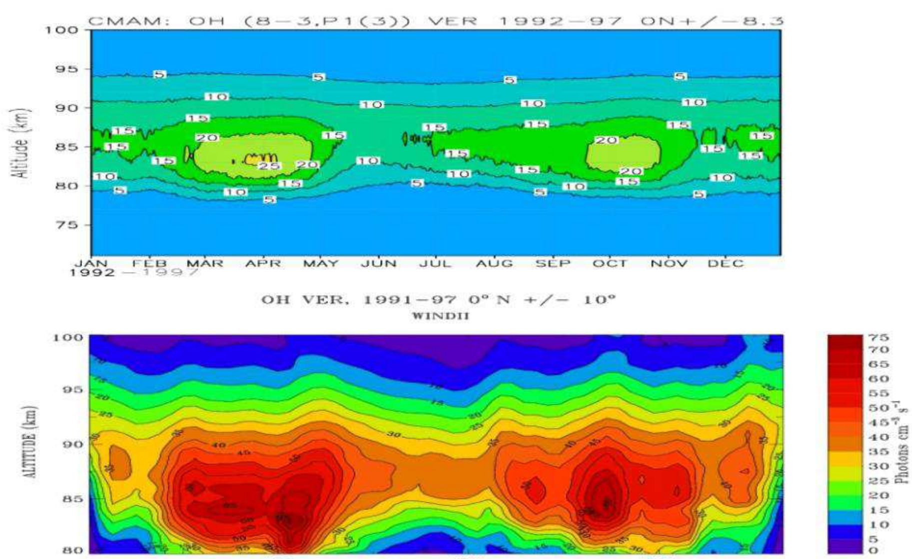

Figure 8.3. Zonally averaged annual cycle of the volume emission rate (ph cm^{-3} s^{-1}) in the $P_1(3)$ rotational line of the OH(8-3) Meinel band over the equator from the CMAM (top) and WINDII (bottom). Data are averaged over 1992 - 1997.

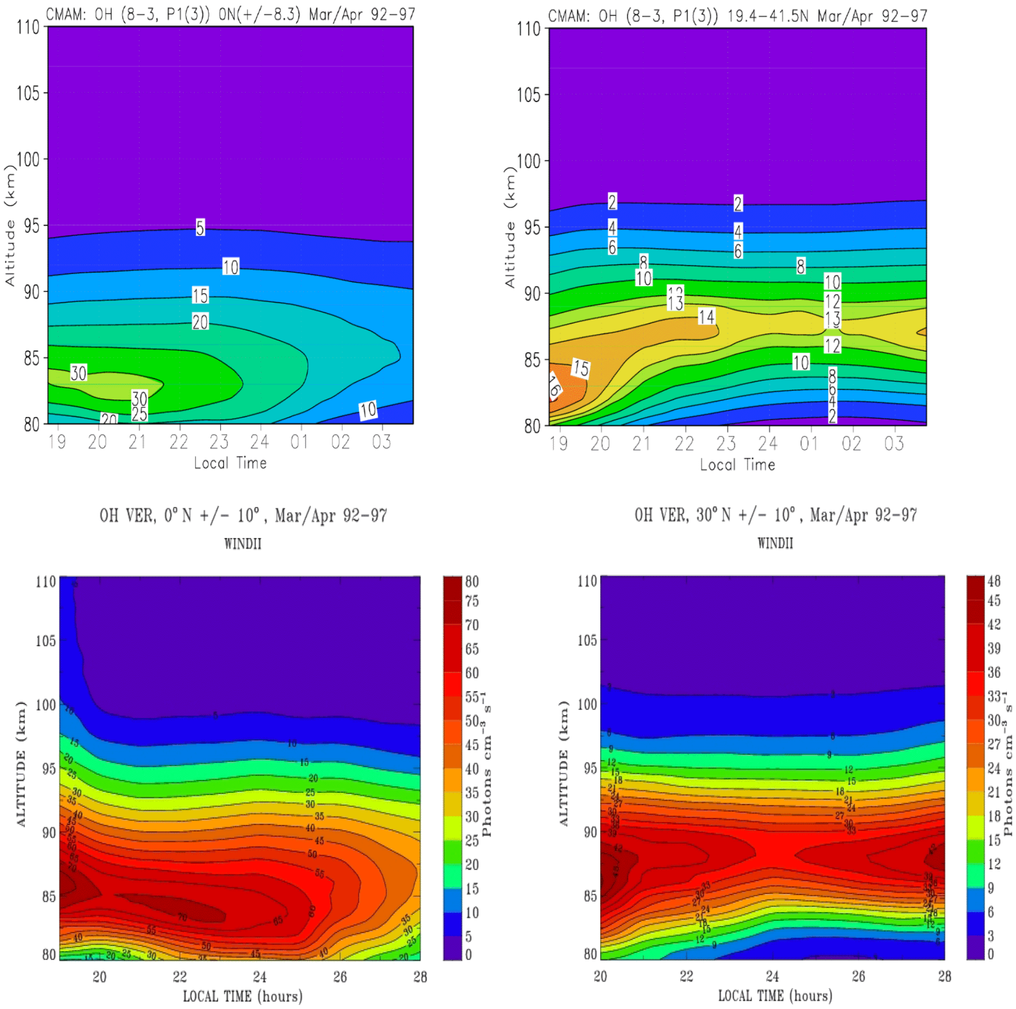

Figure 8.4. Nighttime variation with local time of the zonally averaged volume emission rate (ph cm^{-3} s^{-1}) in the $P_1(3)$ rotational line of the OH(8-3) Meinel band over the equator (left) and at 30° N (right) for March-April from the CMAM (top) and WINDII (bottom). Data are averaged over 1992 - 1997.

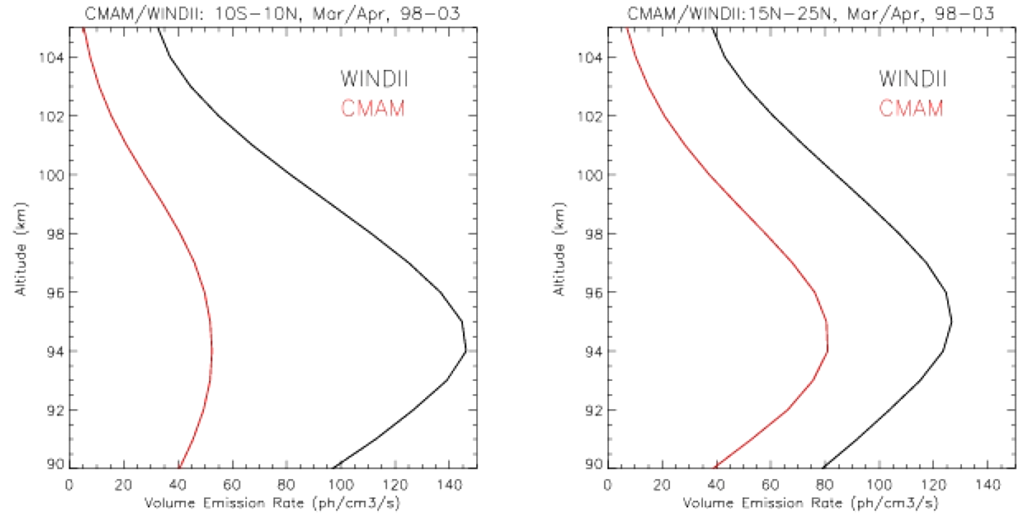

Figure 8.5. Zonally averaged $O(^1S)$ volume emission rates (ph cm^{-3} s^{-1}) over the equator (left) and near 20° N (right) in March-April from the CMAM (red) and WINDII (black). Data are averaged for the period of March 1998 - April 2003.

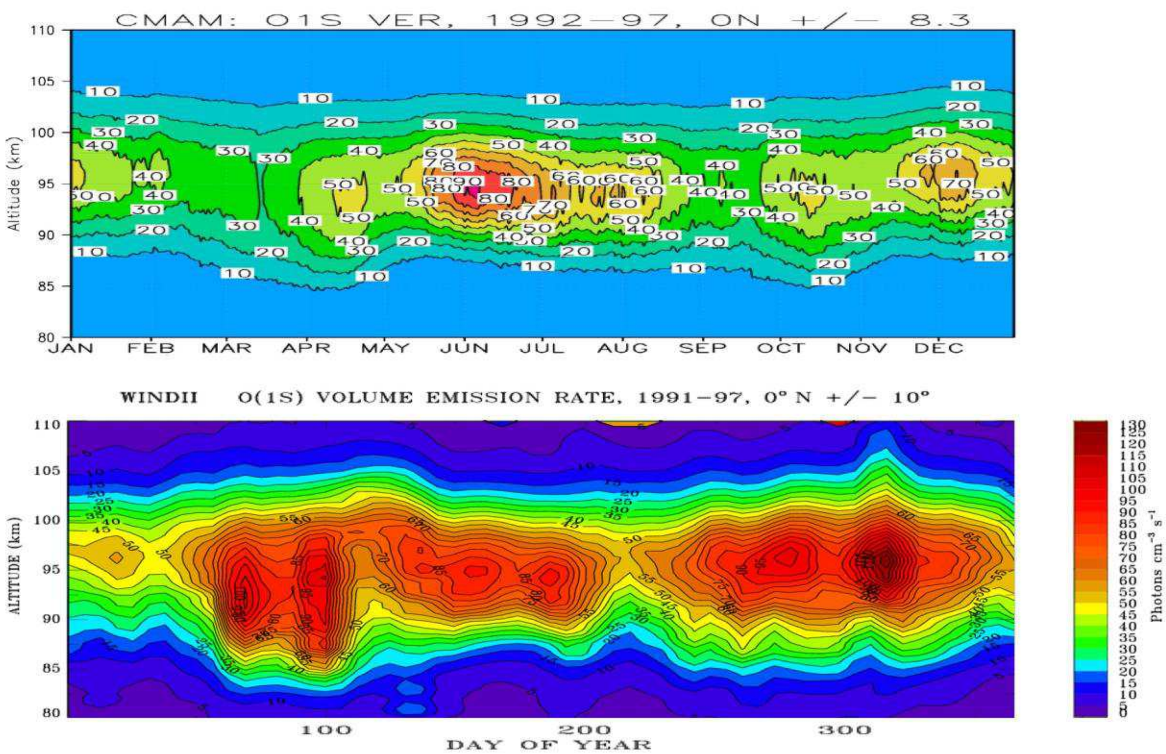

Figure 8.6. Zonally averaged annual cycle of the $O(^1S)$ volume emission rate (ph cm^{-3} s^{-1}) over the equator from the CMAM (top) and WINDII (bottom). Data are averaged over 1992 - 1997.

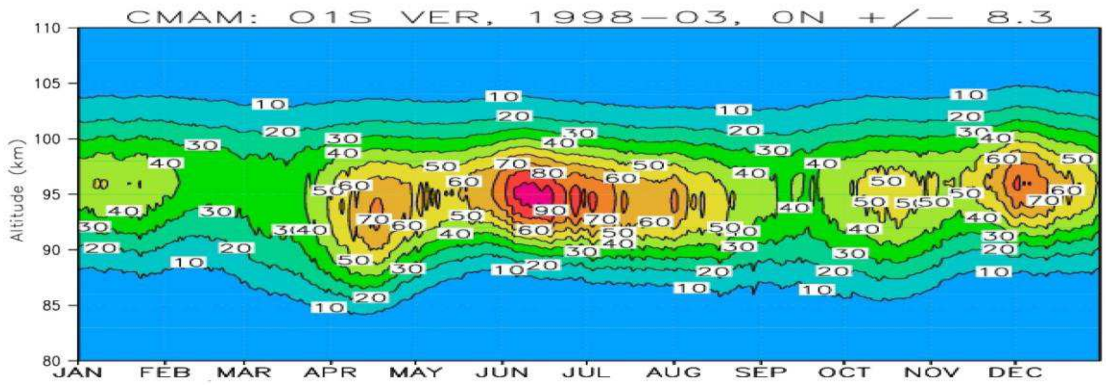

Figure 8.7. Zonally averaged annual cycle of the $O(^1S)$ volume emission rate (ph cm^{-3} s^{-1}) over the equator from the CMAM. Data are averaged over 1998 - 2003.

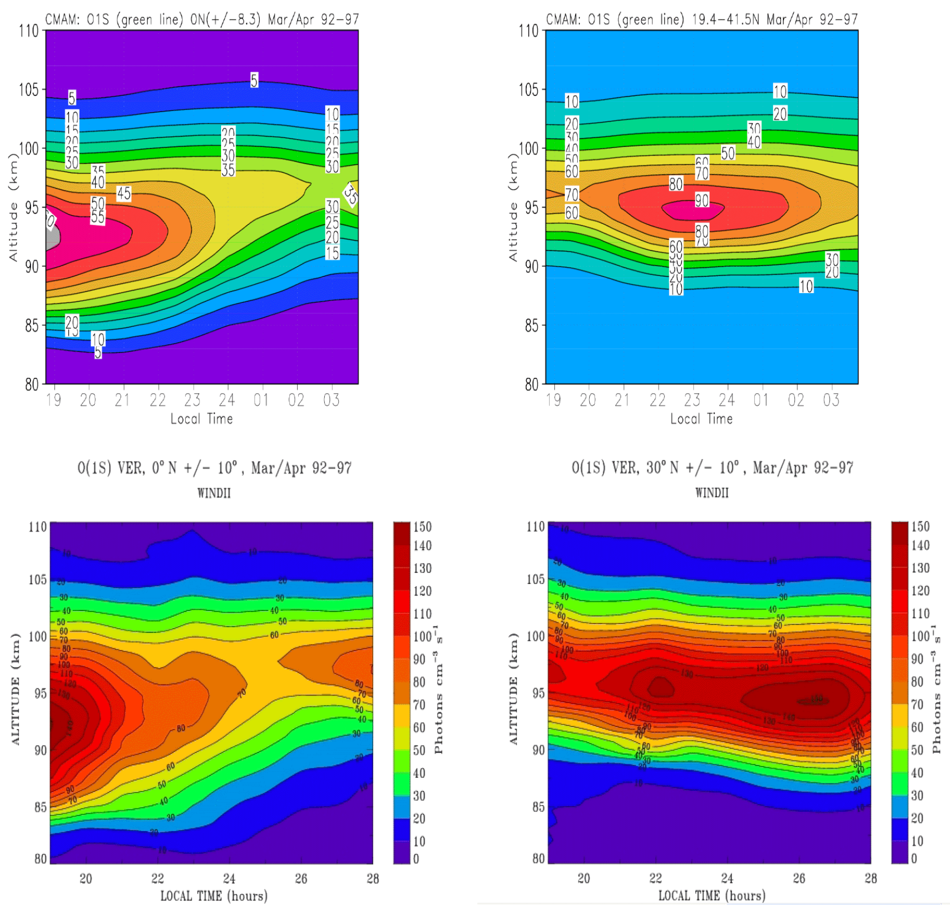

Figure 8.8. Nighttime variation with local time of the zonally averaged $O(^1S)$ volume emission rate (ph cm^{-3} s^{-1}) over the equator (left) and at 30° N (right) for March-April from the CMAM (top) and WINDII (bottom). Data are averaged over 1992 - 1997.

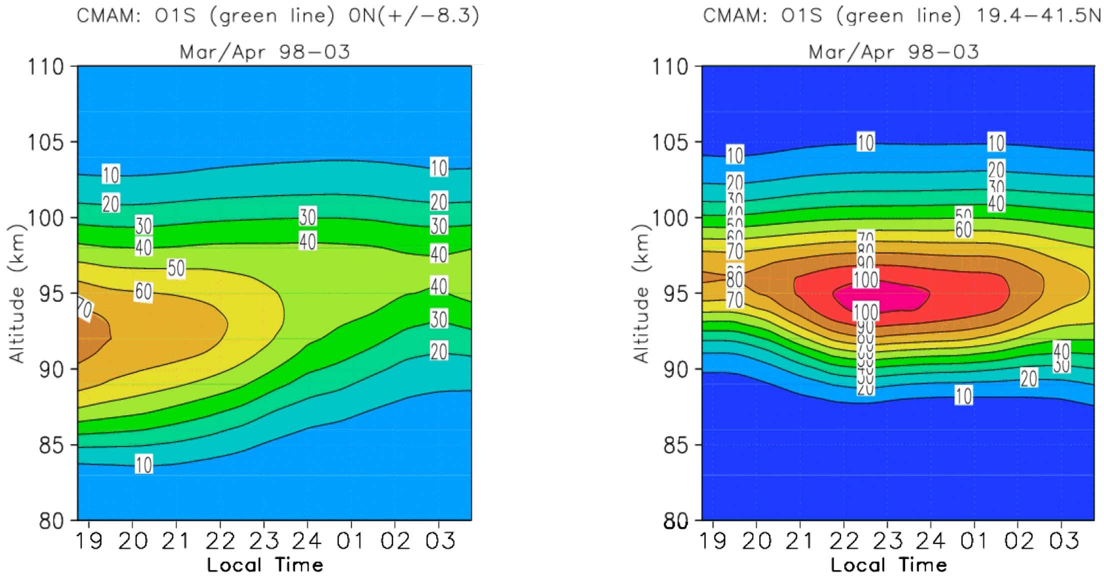

Figure 8.9. Nighttime variation with local time of the zonally averaged O(^{1}S) volume emission rate (ph cm^{-3} s^{-1}) over the equator (left) and at 30° N (right) for March-April from the CMAM. Data are averaged over 1998 - 2003.

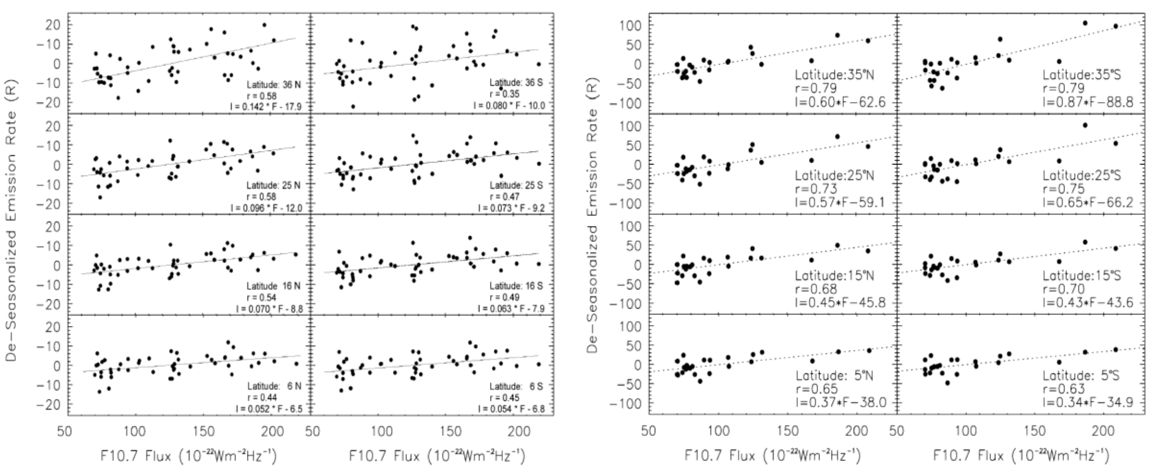

Figure 8.10. Linear relationship between the de-seasonalized three-month averaged CMAM (left) and WINDII (right) integrated emission rates and the three-month averaged solar F10.7 cm fluxes. CMAM results are based on CMAM simulations over twelve years (1992-2003), WINDII observations over six years (1992-1997).

The focus of the CMAM modelling has been the prediction of oxygen airglow emission rates and their variation over the solar cycle. The 1991 to 1997 WINDII data allowed the variation to be studied from just after the 1991 solar flux peak to the minimum that followed. The new dataset is important in allowing the subsequent increase to the peak around 2001 to be investigated. The results are shown in Figure 8.11(a, upper panel) where the 1991 to 1997 data are shown as black squares, for three-month averaged data and the 1997 to 2003 data are shown as purple squares. Three-month averages are used to remove the tidal variations, which occur slowly as the UARS orbit drifts in local time. The NRC F10.7 radio solar flux is shown as a solid black line. This panel (the upper one) shows de-seasonalized data, where the seasonal variation has been removed. The agreement is remarkable, including the depression of solar flux at the peak of the 2001 maximum. Figure 8.11(b, lower panel), shows data that have not been de-seasonalized, and the agreement is not as good, showing that removing the seasonal variation is necessary for good correlation. This suggests that there are two components of the airglow emission, one which correlates with the solar flux and one that does not. The latitude range is 0° – 10° N.

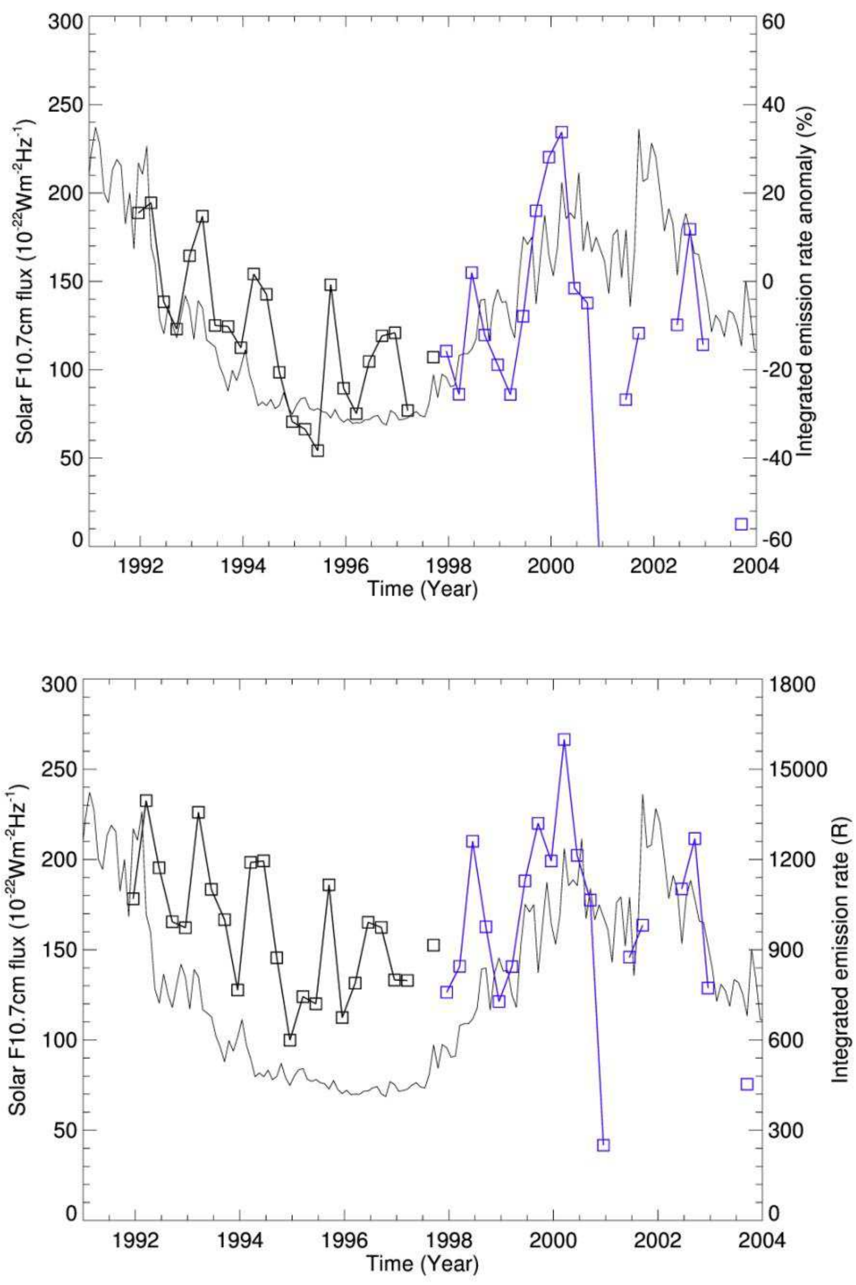

Figure 8.11 Three-month averages of WINDII O(^{1}S) integrated emission rates (squares, in Rayleigh) from 1992 to 2003 compared with the F10.7 radio solar flux solid line. For the upper panel (a) the data have been de-seasonalized while for the lower panel (b) they have not. The data from 1992 to 1997 are in black, and from 1998 to 2003 in purple. The latitude range for these data is 0° – 10° N.

9.0 Projection of future capability in data analysis and modelling

9.1 Future capability in data analysis

The re-processing of the WINDII data has been a tremendous learning experience. What required a large computer centre in 1991 can now be executed on a simple desktop computer. It took some effort, as is described herein, to convert the existing SDPPS code so that it could be compiled with current compilers in order to run on a current computer, but that has been accomplished. Once that was done, the processing itself was fairly trivial. The accomplishment of having the software under our control so that changes can easily be made is one with far reaching consequences, as this capability can be provided to any Canadian researchers that wish to take advantage of it. In the early days of the UARS mission some use was made of Level 1 data as it was available then, and not all problems with the Level 2 processing had been resolved. Once the Level 2 processing was validated, all of the scientific analysis and publications coming from WINDII were derived from Level 2. The opportunity now exists to re-visit the Level 1 data and investigate the higher degree of spatial and temporal variability than can be observed in the Level 2 data. Thus small-scale airglow structures will become a focus of future work.

At the same time, this in-depth look at the WINDII data has brought to light some unresolved problems, recognized during the mission, but without the resources to address them then. Credit must be given to the CNES contribution in writing the software, as the SDPPS has proven to be highly robust. Credit also goes to the Canadian input to the development of the SDPPS, beginning with the writing of the algorithm document, and ending with the validation and modification of the processed results. What were recognized as problems at the time have now become opportunities, since their study is still timely, perhaps more now than then. Three examples of these opportunities are described in what follows.

There is a problem with the Filter 4 data that provides O^+ emission rates at high altitudes, and OH emission rates at lower altitudes. There is evidence that the transmittance pattern of this filter as measured on the ground before launch is no longer valid, so that an adjustment is required. The O^+ data are of great potential value, as they can provide unambiguous measurements of atomic oxygen concentrations in the thermosphere. This study will be pursued through an amendment to the current grant. The solution of this problem may also provide insights into the OH situation. Good OH emission rates were obtained from Filter 6, but one has to combine the data from both filters to obtain the rotational temperatures, and this was never achieved.

The Filter 7 data, which provide airglow emission rates and winds from the O_2 Atmospheric Band Emission have never been properly evaluated. The emission rates appear to be acceptable, and results from it have been published. However, the winds are not of the quality provided by the $O(^1S)$ green line, and have been little studied. This is an excellent topic for future study as it would make available a significantly larger wind database.

The processing of the previously un-proccessed WINDII data, starting from August 9, 1997 and continuing to September 19, 2003 adds a significant body of WINDII data. It is not as large as one might think because of limitations introduced by the spacecraft towards the end of the mission, when the power levels were reduced, and also the altitude. WINDII made its contribution to power reduction by operating without thermal control from 1997 to early 2003, on the assumption that the inherent stability of the interferometer was good enough without it. We now know that this was optimistic in that some special processing is required to derive quality wind data – the airglow emission rate data are fine, as are the Doppler temperatures. As well, WINDII was turned on only part of the time, cycling it's on/off time with the other instruments. Great credit must go to the NASA/UARS team that provided a near-constant altitude for so much of the emission, maintained excellent attitude control throughout, and managed to maintain and allocate power throughout the mission.

Although the data obtained from the re-processing are not continuous they have particular value in that they overlap with the Odin and TIMED missions, launched on February 20, 2001 and December 1, 2001, respectively. The TIDI instrument on TIMED is of particular interest since it measured winds in the lower thermosphere. Migrating and non-migrating tides, as well as the different modes of non-migrating tides, can be distinguished through their propagation in local time. Satellites, which have a fixed local on a given day, cannot do this without observing for weeks or months in order for the local times to change. But WINDII and TIDI made simultaneous measurements on the same day at two different local times, which would greatly help in resolving these different tides.

In deriving winds during this period, two spacecraft related problems need to be addressed.
For a number of reasons, some understood, some not, the CDB was not maintained during the period without thermal control, and this has introduced a large wind bias. Although infrequent calibration data exist, the program to utilize them does not. It is proposed that the frequent calibration data be used instead, and this is a topic of the amendment to this grant. This current study has demonstrated that quality wind data can be achieved in this way, but more work is required for its implementation. This implementation will allow the winds from the new processing to be corrected.

Processing the data to the end of the mission has introduced data taken at lower spacecraft altitudes than that encountered before. In the current processing this has contaminated the daytime airglow to an extent not yet evaluated. On the other hand, this also provides data on the baffle scattering that did not exist before, and this knowledge can provide a better baffle scattering correction that existed previously. This will also be an area of study of future interest.

Overall, the new processing has generated a new archival dataset that provides the following. 1) Results from the complete WINDII data set that now bridge to the Odin and TIMED missions, not available before, 2) Level 1 data for the entire WINDII dataset that have not been available in their entirety before and 3) a data processing system that can be used by anyone to make changes in the processing code.

9.2 Future capability in modelling

Future capability in modelling is seen by us to be tied to the development of the whole atmosphere model extending from the surface up to and including the ionosphere. This model should include all the main physical processes governing the current state and evolution of the atmosphere and ionosphere and hence will provide a platform for the investigation of the response of, and the interaction between, the ionosphere and the neutral atmosphere to disturbances emanating from space or generated in the lower atmosphere. In particular, the model will provide an opportunity to study the impact of the lower atmosphere on the ionosphere (through waves generated in the lower atmosphere and penetrating upward) and the impact of the upper atmosphere on the mesosphere and stratosphere (through NO_X and Ox transported down from the thermosphere and created via solar extreme ultraviolet radiation (EUV) and by EPP. Understanding this coupling is important for determining how the atmosphere as a whole responds to solar and magnetic variability. It also has the potential to lead to a predictive capability for the state of the ionosphere. This is especially important in Canada where communication and power lines over large distances are important and variations in electron density in the ionosphere can cause disruptions.

Developing such a model was recently initiated in Canada under the CSA grant titled "Development of the Canadian Ionosphere and Atmosphere Model". During the course of this project the first interactive version of the model, the acronym for which is Canadian IAM or C-IAM, is targeted to be created. This model is based on the extended CMAM, which describes the neutral atmosphere and Murmansk's ionospheric model. First experiments with the C-IAM (a paper in preparation) have shown significant effects of the upward penetrating waves generating in the lower atmosphere on the ionospheric structure and resulted in reproducing the observed 4-peak longitudinal structure of ionospheric emission at 135.6 nm in the equatorial region. There are plans to use the C-IAM for comparison with the WINDII observations of the ionospheric emissions from the $O(^1D)$ red line at 630 nm and the $O(^1S)$ green line at 557.7 nm. Generally speaking, such model as the C-IAM will be a valuable tool for supporting satellite mission observing both the neutral atmosphere and ionosphere.

For the further C-IAM development processes such as photoelectron transport, EPP effects, EUV heating efficiencies and extending the magnetosphere could be addressed. In addition, we note that there will also be modelling developments within Environment Canada (EC) and we should consider how this might impact future development. We note that future plans at EC will likely include the merging of the dynamical cores of the weather forecast model and the Climate Model, the latter of which is used by the extended CMAM. The new core will be a grid point core as opposed to a spectral core. When the new EC model is in place it would be beneficially to move the C-IAM to the new dynamical frame work.

10.0 Summary and Conclusions:

This report describes the progress and convergence over the past year of two significant elements in the Canadian space science program, the WINDII dataset and the CMAM model. The "original" WINDII dataset, generated at NASA with WINDII-supplied software, was a valuable resource, but it consisted only of Level 2 data, and it was incomplete, ending in 1997. Moreover, there was no capability to process more data, or to make corrections to earlier analyses. We now have a WINDII processing system that has processed all of the WINDII data, ending in 2003, for both Levels 1 and 2, and the capability to improve the processing software as we wish.

The primary focus of the WINDII team during the mission became the $O(^1S)$ green line emission (Filter 1), as it is a single line with no nearby spectral contaminants, and it produced excellent results. The same can be said for the $O(^1D)$ red line emission (Filter 3), although fewer data were acquired because it was above the altitudes of UARS interest. Both produced excellent emission rates, winds and Doppler temperatures. Considerable effort was put on the OH emissions (Filters 4, 5 and 6) in an effort to derive rotational temperatures, but these were not successful, even though high quality emission rates were obtained. Cursory examination of the OH winds were not encouraging and these were never studied in any detail. A large body of O_2 Atmospheric Band emission (Filter 7) data was acquired, and the emission rates have been studied and published. The winds are promising, but have not been studied. Filter 4 also observes the O^+ emission at 732.0 nm at high altitudes during the daytime, as well as the OH emission at low altitudes during the night. The O^+ observations have a problem that is currently under investigation through an amendment to this grant, and can almost certainly be solved, yielding atomic concentrations in the thermosphere. Any corrections to the Filter 4 transmittances could potentially solve the problem with Filter 4 OH measurements, which could perhaps solve the problem with the rotational temperatures. In summary, the science data yield of the existing WINDII dataset could be further enhanced through detailed investigation of some problems that were recognized during the mission, but for which sufficient resources (both time and financial support) for their study were lacking at the time. In addition, as the mission progressed far beyond the original plans (11 years rather than 2.5) the support was gradually reduced at a time when the processing challenges were increasing, in terms of the reducing altitude of the spacecraft and the cessation of temperature control for the instrument. With the pressures of the mission long behind us, advantage can still be taken of the inherent value of the data for which the benefits have not yet been fully realized.

Although the simulation of airglow emission rates is only one part of the overall CMAM program, it has also made considerable progress during the past year during which detailed comparisons with the WINDII data have been made. The similar responses of the CMAM and WINDII to the solar flux variation, now observed over one entire solar cycle, is significant for de-seasonalized data, and this needs to be further understood. The emission profiles are also very similar in their altitude structure, latitude variation and seasonal variation, although the CMAM simulated values of emission rate are significantly lower than the WINDII observations. This new capability of the CMAM is very encouraging, and further study is needed.

The CMAM model has now simulated the relevant airglow emission rates for the entire length of the WINDII data record, one full solar cycle. More importantly, the newly processed WINDII data bridge into the Odin and TIMED missions, providing a data record of a little more than twenty years. Taken together, these missions, with the CMAM simulations, represent a tremendous resource for the Canadian space community in terms of trend analysis that is consistent with the extension of the CMAM model into the ionosphere, and the extensive WINDII dataset for that region.

The authors of this report thank the CSA for their perception of the value of this coordinated study of newly processed and studied WINDII data and the CMAM capability of airglow simulation. They are grateful to the CSA for making these studies possible.

<References in WINDII libraries at York University>

B.1. WINDII Flight segment to RAC ICD, September 30, 1990

SDPPS ICD(Science Data Processing Software Interface Control Document)

*Science Telemetry Format (SMAF, EMAF, SMIF, EMIF)

Flight Segment to RAC(Remote Analysis Computer) ICD

B.2. Wind Imaging Interferometer, WINDII, Algorithm Description, Issue 3.0, March 15, 1993

Part 1: Telemetry Depacking

Part 2: Data Calibration

Part 3: Data Reduction

Part 4: Production of UARS gridded data

B.3. WINDII SDPPS Interface Manual (Original Reference: WINDOC2)

Detailed description of the files for SDPPS

B.4. WINDII SDPPS User's Guide, Version 5.0, July 28, 1992

Input/Output file description, Job script example

B.5. SDPPS Design Document

Functional distribution of the constituents, the design option and retained solutions

B.6. UARS CDHF Software System (UCSS) Programmer's guide to production software support services, February, 1993

Definition of the interfaces to production software support services at the UARS CDHF (Central Data Handling Facility) and production testing services on RACs (Remote Analysis Computers)

B.7. WINDII Unix Processing Software User's Guide, Prepared by Gerry Warner, Version 1.0.0, January 1, 2005

B.8. Pro Fortran, Linux Absoft Pro Fortran User Guide, Version 13.0

< References >

Adler-Golden, S. (1997). Kinetic parameters for OH nightglow modeling consistent with recent laboratory measurements, J. Geophys. Res. 102, 19,969–19,976.

Bacsek, Sheldon, Thermospheric atomic oxygen densities and temperatures from WINDII observations of the $O^+(^2P)$ emission, M.Sc. thesis, York University, 1997

Evans, W.F.J, L.R. Laframboise, K.R. Sine, R.H. Wiens and G.G. Shepherd, Observation of polar mesospheric clouds in summer, 1993 by the WINDII instrument on UARS, Geophys. Res. Lett, 22, 2793, 1995.

Garcia-Munoz, A., J. C. McConnell, I. C. McDade, S. M. L. Melo (2005). Airglow on Mars: Some model expectations for the OH Meinel band and the O_2 IR atmospheric band, Icarus, 176, 75-95, doi: 10.1016/j.icarus.2005.01.006.

Hersom, Charles, Characterization of the WINDII instrument for determination of winds, temperature and emission rates, Ph.D. Thesis, York University, 1993

Klenerman, D., Smith I.W.M. (1987). Infrared chemiluminescence studies using a SISAM spectrometer. Reactions producing vibrationally excited OH, J. Chem. Soc., Faraday Trans. 2, 83, 229-241, Doi: 10.1039/f29878300229

Liu, G. (2006). Global variability of the oxygen airglow as observed by WINDII and predicted with the TIME-GCM, Ph. D. Thesis, York University, Toronto, Ontario, Canada, 216 pp.

Liu G., G.G. Shepherd (2008). An investigation of the solar cycle impact on the lower thermosphere $O(^1S)$ nightglow emission as observed by WINDII/UARS, Adv. Space Res. 42, 933-938.

Makhlouf, U.B., Picard, R.H., Winick, J.R. (1995). Photochemical-dynamical modeling of the measured response of airglow to gravity-waves. 1. Basic model for oh airglow, J. Geophys. Res., 100, 11289-11311, doi: 10.1029/94JD03327.

McDade, I.C., D.P. Murtagh, R.G.H. Greer, P.H.G. Dickinson, G. Witt, J. Stegman, E.J. Llewellyn, L. Thomas, D.B. Jenkins (1986). ETON-2: Quenching parameters for the proposed precursors of $O_2(b^1\Sigma_g^+)$ and $O(^1S)$ in the terrestrial nightglow, Planet. Space Sci., 34, 789-800.

Melo, S.M.L., I.C. McDade, H. Takahashi (2001). Atomic oxygen density profiles from ground-based nightglow measurements at 23°S, J. Geophys. Res., 106, 15377-15384.

Sander, S.P., Friedl, R.R., Golden, D.M., Kurylo, M.J., Huie, R.E., Orkin, V.L., Moortgat, G.K., Ravishankara, A.R., Kolb, C.E., Molina, M.J., Finlayson-Pitts, B.J. (2002). Chemical kinetics and photochemical data for use in stratospheric studies. JPL Publication 02–25.

Shepherd, G.G., G. Thuillier, W.A. Gault, B.H. Solheim, C. Hersom, J.M. Alunni, J.-F. Brun, S. Brune, P. Charlot, D.-L. Desaulniers, W.F.J. Evans, F. Girod, D. Harvie, R.H. Hum, D.J.W. Kendall, E.J. Llewellyn, R.P. Lowe, J.Ohrt, F. Pasternak, O. Peillet, I. Powell, Y. Rochon, W.E. Ward, R.H. Wiens, J. Wimperis, WINDII, the Wind Imaging Interferometer on the Upper Atmosphere Research Satellite, J. Geophys. Res., 98, 10725, 1993.

G.G. Shepherd, G. Thuillier, Y.-M. Cho, M.-L. Duboin, W.F.J. Evans, W.A. Gault, C. Hersom, D.-J.-W. Kendall, C. Lathuillère, R.P. Lowe, I.C. McDade, Y.J. Rochon, M.G. Shepherd,B.H. Solheim, D.-Y. Wang, W.E. Ward, The Wind Imaging Interferometer (WINDII) On The Upper Atmosphere Research Satellite: A Twenty-Year Perspective, Revs. Geophys. 50, RG2007, doi:10.1029/2012RG000390, 2012.

< Appendix A >

The following Appendix is in two parts, Appendix A1 and Appendix A2. Appendix contains a day-by-day list of all the WINDII data from the period of the original processing, November 4, 1991 to November 30, 1997, but compiled from the reprocessed data from that period. Appendix A2 is a list of those days recovered in the new processing, from August 9, 1997 to September 19, 2003 (note that there is some overlap between the two lists).

The measurements that were made on each day are indicated as follows. The filter(s) used for observations on a given day, e.g. 7, or 2 are indicated in the Measurement Column, and are followed by labels. The Label A indicates All day measurements (both day and night). D means day only, and N is for night only. The * Label indicates that there is no level 1 output even if there are level 0 measurements. The symbol X means that a file was created, but no measurements were taken. The background filters are not included in these lists.

Filter 2: $O(^1S)$ atomic oxygen 557.7 nm green line filter; Background Filter 1.
Filter 3: $O(^1D)$ atomic oxygen 630.0 nm red line filter; Background Filter 1
Filters 4,5,6: used in combination are employed for OH observations (night only)

- Filter 4 observes the $P_1(2)$ line at 731.63 nm in the (8,3) OH Meinel band
- Filter 6 observes the $P_1(3)$ line at 734.09 nm in the (8,3) OH Meinel band
- Filter 5 is a split filter; one half measures the total band emission rate; the other the background.

Filter 4: Daytime observations of the ionized atomic oxygen O^+ line at 732.0 nm; Background Filter 6.
Filter 7: O_2 Atmospheric band observations of lines near 763.22 nm.

<Appendix A1>

Date	Uday	Measurement	Date	Uday	Measurement
04-NOV-1991	54	3A	16-DEC-1991	96	4A, 5N, 6N
05-NOV-1991	55	4A, 5A, 6A	17-DEC-1991	97	2A
06-NOV-1991	56	4A, 5A, 6A	18-DEC-1991	98	2A
07-NOV-1991	57	2A, 7D	19-DEC-1991	99	7A
08-NOV-1991	58	2A	20-DEC-1991	100	7A
09-NOV-1991	59	4A, 5N, 6N	21-DEC-1991	101	3A
10-NOV-1991	60	4A, 5N, 6N	22-DEC-1991	102	3A
11-NOV-1991	61	7A	23-DEC-1991	103	2N
12-NOV-1991	62	7A	24-DEC-1991	104	2N
13-NOV-1991	63	4A, 5N, 6N	25-DEC-1991	105	4N, 5N, 6N
14-NOV-1991	64	4A, 5N, 6N	27-DEC-1991	107	7N
15-NOV-1991	65	7A	28-DEC-1991	108	7N
16-NOV-1991	66	7A	29-DEC-1991	109	2A, 7N
17-NOV-1991	67	4A, 5N, 6N	30-DEC-1991	110	2A
18-NOV-1991	68	4A, 5N, 6N	31-DEC-1991	111	2N, 4A, 5N, 6N
19-NOV-1991	69	3A	01-JAN-1992	112	4A, 5N, 6N
20-NOV-1991	70	3A	02-JAN-1992	113	4N, 5N, 6N, 7A
21-NOV-1991	71	3A	03-JAN-1992	114	7A
25-NOV-1991	75	2A, 4D	04-JAN-1992	115	2A, 7N
26-NOV-1991	76	2A	05-JAN-1992	116	2A
27-NOV-1991	77	2D, 4A, 5N, 6N	06-JAN-1992	117	2N, 4A, 5N, 6N
28-NOV-1991	78	4A, 5N, 6N	07-JAN-1992	118	4A, 5N, 6N
29-NOV-1991	79	4A, 5N, 6N, 7A	08-JAN-1992	119	3A
30-NOV-1991	80	7A	09-JAN-1992	120	3A
01-DEC-1991	81	4A, 5N, 6N, 7D	11-JAN-1992	122	2A
02-DEC-1991	82	4A, 5N, 6N	12-JAN-1992	123	2D, 4A, 5N, 6N
03-DEC-1991	83	2A, 4D	13-JAN-1992	124	7A
04-DEC-1991	84	2A	14-JAN-1992	125	7A
05-DEC-1991	85	2A	15-JAN-1992	126	3A, 4D
06-DEC-1991	86	2A	16-JAN-1992	127	2A
07-DEC-1991	87	2A, 4A, 5N, 6N	17-JAN-1992	128	2D, 4N, 5N, 6N
08-DEC-1991	88	4A, 5N, 6N	18-JAN-1992	129	7A
09-DEC-1991	89	2A, 4D	19-JAN-1992	130	2A
10-DEC-1991	90	2A	20-JAN-1992	131	2D, 4N, 5N, 6N
11-DEC-1991	91	2A, 4A, 5N, 6N	21-JAN-1992	132	7A
12-DEC-1991	92	4A, 5N, 6N	22-JAN-1992	133	2A, 7N
13-DEC-1991	93	3A	23-JAN-1992	134	2A, 4N, 5N, 6N
14-DEC-1991	94	3A	24-JAN-1992	135	7A
15-DEC-1991	95	3A, 4A, 5N, 6N	25-JAN-1992	136	X
			26-JAN-1992	137	X
			27-JAN-1992	138	3A, 4D
			28-JAN-1992	139	3A, 4D
			29-JAN-1992	140	7A
			30-JAN-1992	141	2A
			31-JAN-1992	142	2D, 4N, 5N, 6N

Date	Uday	Measurement
01-FEB-1992	143	7A
02-FEB-1992	144	2A, 7D
03-FEB-1992	145	2D, 4N, 5N, 6N
04-FEB-1992	146	2D, 7A
05-FEB-1992	147	2A, 7D
06-FEB-1992	148	2D, 4N, 5N, 6N
07-FEB-1992	149	7A
08-FEB-1992	150	7A
09-FEB-1992	151	2D, 4N, 5N, 6N
10-FEB-1992	152	7A
11-FEB-1992	153	2A
12-FEB-1992	154	2D, 4N, 5N, 6N
13-FEB-1992	155	3A, 4D
14-FEB-1992	156	2A, 3N
15-FEB-1992	157	7A
16-FEB-1992	158	3A, 7N
17-FEB-1992	159	3A
18-FEB-1992	160	2D, 4N, 5N, 6N
19-FEB-1992	161	2A
20-FEB-1992	162	2A
21-FEB-1992	163	4A, 5N, 6N
22-FEB-1992	164	2N, 4D
23-FEB-1992	165	7A
24-FEB-1992	166	4A, 5N, 6N
25-FEB-1992	167	4A, 5N, 6N
26-FEB-1992	168	3A, 4D
27-FEB-1992	169	2A
28-FEB-1992	170	2D, 7A
01-MAR-1992	172	7A
02-MAR-1992	173	2A
03-MAR-1992	174	7A
04-MAR-1992	175	2A
05-MAR-1992	176	2A, 4N, 5N, 6N
06-MAR-1992	177	3A, 4A
07-MAR-1992	178	2A, 3N
08-MAR-1992	179	2N, 7A
09-MAR-1992	180	2D, 4N, 5N, 6N, 7N
10-MAR-1992	181	3A
11-MAR-1992	182	2A, 3A
12-MAR-1992	183	3N, 7A
13-MAR-1992	184	4A, 5N, 6N, 7N
14-MAR-1992	185	3D, 4N, 5N, 6N
15-MAR-1992	186	3D, 7A

Date	Uday	Measurement
16-MAR-1992	187	2A, 7N
17-MAR-1992	188	2N, 7A
18-MAR-1992	189	4A, 5N, 6N
19-MAR-1992	190	3A, 4A, 5N, 6N
20-MAR-1992	191	2A
21-MAR-1992	192	2D, 7A
22-MAR-1992	193	2D, 4N, 5N, 6N, 7D
23-MAR-1992	194	2A
24-MAR-1992	195	7A
25-MAR-1992	196	2A
26-MAR-1992	197	2A, 7A
27-MAR-1992	198	2D, 4N, 5N, 6N, 7D
28-MAR-1992	199	2A
29-MAR-1992	200	2A, 7A
30-MAR-1992	201	2D, 4N, 5N, 6N, 7A
31-MAR-1992	202	2A
01-APR-1992	203	2A, 3A, 4D
02-APR-1992	204	3A, 4D, 7A
03-APR-1992	205	2D, 4N, 5N, 6N, 7N
04-APR-1992	206	2A
05-APR-1992	207	2N, 7A
06-APR-1992	208	2D, 4N, 5N, 6N, 7N
07-APR-1992	209	2A, 4N, 5N, 6N
08-APR-1992	210	2N, 3A, 4D
09-APR-1992	211	7A
10-APR-1992	212	2D, 4N, 5N, 6N, 7N
11-APR-1992	213	2A, 4N, 5N, 6N
12-APR-1992	214	2A, 7A
13-APR-1992	215	2D, 4N, 5N, 6N, 7A
14-APR-1992	216	2A, 4N, 5N, 6N
15-APR-1992	217	2A, 3A, 4D
16-APR-1992	218	3D, 4D, 7A
17-APR-1992	219	2D, 4N, 5N, 6N, 7D
18-APR-1992	220	2A
19-APR-1992	221	2D, 7A
20-APR-1992	222	2D, 4N, 5N, 6N, 7D
21-APR-1992	223	2A
22-APR-1992	224	2A, 3A, 4D
23-APR-1992	225	3A, 4D, 7A
24-APR-1992	226	2D, 4N, 5N, 6N, 7A
25-APR-1992	227	2A
26-APR-1992	228	2A, 7A
27-APR-1992	229	2D, 4N, 5N, 6N, 7A
28-APR-1992	230	2A
29-APR-1992	231	2A, 3A, 4A
30-APR-1992	232	3A, 4D, 7A

Date	Uday	Measurement
01-MAY-1992	233	2D, 4N, 5N, 6N, 7A
02-MAY-1992	234	2A
03-MAY-1992	235	2A, 7A
04-MAY-1992	236	2A, 4N, 5N, 6N, 7A
05-MAY-1992	237	2A
06-MAY-1992	238	2D, 3A, 4D
07-MAY-1992	239	3D, 4D, 7A
08-MAY-1992	240	2D, 4N, 5N, 6N, 7D
09-MAY-1992	241	2A
10-MAY-1992	242	2D, 7A
11-MAY-1992	243	2D, 4N, 5N, 6N, 7D
12-MAY-1992	244	2A
13-MAY-1992	245	2D, 3A, 4D
14-MAY-1992	246	3A, 4D, 7A
15-MAY-1992	247	2D, 4N, 5N, 6N, 7D
16-MAY-1992	248	2A
17-MAY-1992	249	2A, 7A
18-MAY-1992	250	2D, 4N, 5N, 6N, 7A
19-MAY-1992	251	2A
20-MAY-1992	252	2N, 3A, 4D
21-MAY-1992	253	3N, 7A
22-MAY-1992	254	2D, 4N, 5N, 6N, 7N
23-MAY-1992	255	2A
24-MAY-1992	256	2A, 7A
25-MAY-1992	257	2D, 4N, 5N, 6N, 7A
26-MAY-1992	258	2A
27-MAY-1992	259	2A, 3A, 4D
28-MAY-1992	260	3N, 7A
29-MAY-1992	261	2D, 4N, 5N, 6N, 7A
30-MAY-1992	262	2A
31-MAY-1992	263	2A, 7A
01-JUN-1992	264	2D, 4N, 5N, 6N, 7A
02-JUN-1992	265	2A
19-JUL-1992	312	X
21-JUL-1992	314	2A
22-JUL-1992	315	2A
23-JUL-1992	316	2A
24-JUL-1992	317	2A
25-JUL-1992	318	2A
26-JUL-1992	319	2A
27-JUL-1992	320	2A, 7A
28-JUL-1992	321	2D, 4A, 5A, 6A, 7D
29-JUL-1992	322	2A
30-JUL-1992	323	2A, 3A, 4D
31-JUL-1992	324	3N, 7A

Date	Uday	Measurement
01-AUG-1992	325	2D, 4N, 5N, 6N
02-AUG-1992	326	2A
03-AUG-1992	327	2A, 7A
04-AUG-1992	328	4N, 5N, 6N, 7D
05-AUG-1992	329	3A, 4D
06-AUG-1992	330	2N, 3A, 4D
07-AUG-1992	331	7A
08-AUG-1992	332	2D, 4N, 5N, 6N
09-AUG-1992	333	2N
10-AUG-1992	334	7A
11-AUG-1992	335	4N, 5N, 6N
12-AUG-1992	336	3A, 4D
13-AUG-1992	337	2A, 3N
14-AUG-1992	338	7A
15-AUG-1992	339	2D, 4N, 5N, 6N
16-AUG-1992	340	2A
17-AUG-1992	341	2N, 7A
18-AUG-1992	342	2D, 4N, 5N, 6N
19-AUG-1992	343	3A, 4D
20-AUG-1992	344	2A, 3N
21-AUG-1992	345	2A, 7A
22-AUG-1992	346	2D, 4N, 5N, 6N
23-AUG-1992	347	2A
24-AUG-1992	348	2A, 7A
25-AUG-1992	349	2D, 4N, 5N, 6N
26-AUG-1992	350	2D, 3A, 4D
27-AUG-1992	351	2A, 3A, 4D
28-AUG-1992	352	2A, 7A
29-AUG-1992	353	2D, 4N, 5N, 6N, 7A
30-AUG-1992	354	2A, 4N, 5N, 6N
31-AUG-1992	355	2A, 7A

Date	Uday	Measurement
01-SEP-1992	356	2D, 4N, 5N, 6N, 7N
02-SEP-1992	357	2D, 3A, 4A, 5N, 6N
03-SEP-1992	358	2A, 3A, 4D
04-SEP-1992	359	2A, 7A
05-SEP-1992	360	2D, 4N, 5N, 6N
06-SEP-1992	361	2A, 4N, 5N, 6N
07-SEP-1992	362	7A
08-SEP-1992	363	2D, 4N, 5N, 6N
09-SEP-1992	364	2D, 4A, 5A, 6A
10-SEP-1992	365	2A, 4N, 5N, 6N
11-SEP-1992	366	2D, 7A
12-SEP-1992	367	2D, 4N, 5N, 6N
13-SEP-1992	368	2A
14-SEP-1992	369	2D, 7A
15-SEP-1992	370	2D, 4N, 5N, 6N, 7D
16-SEP-1992	371	2D, 3A, 4D
17-SEP-1992	372	2A, 3D, 4D
18-SEP-1992	373	2D, 7A
19-SEP-1992	374	2D, 4N, 5N, 6N, 7D
20-SEP-1992	375	2A
21-SEP-1992	376	2D, 7A
22-SEP-1992	377	2D, 4N, 5N, 6N, 7D
23-SEP-1992	378	2D, 3A, 4D
24-SEP-1992	379	2A, 3A, 4D
25-SEP-1992	380	2A, 7A
26-SEP-1992	381	2D, 4N, 5N, 6N, 7D
27-SEP-1992	382	2A
28-SEP-1992	383	7A
29-SEP-1992	384	2D, 4N, 5N, 6N, 7D
30-SEP-1992	385	2D, 7A
01-OCT-1992	386	2A, 7D
02-OCT-1992	387	2A, 7A
03-OCT-1992	388	2D, 4N, 5N, 6N
04-OCT-1992	389	2A
05-OCT-1992	390	2A, 7A
06-OCT-1992	391	2D, 4N, 5N, 6N, 7D
07-OCT-1992	392	2D, 3A, 4A, 5N, 6N
08-OCT-1992	393	2A, 3A, 4D
09-OCT-1992	394	2A, 7A
10-OCT-1992	395	2D, 4N, 5N, 6N
11-OCT-1992	396	2A
12-OCT-1992	397	7A
13-OCT-1992	398	2D, 4N, 5N, 6N
14-OCT-1992	399	3A, 4D
15-OCT-1992	400	2A, 3N

Date	Uday	Measurement
16-OCT-1992	401	2N, 7A
17-OCT-1992	402	2D, 4N, 5N, 6N
18-OCT-1992	403	2A
19-OCT-1992	404	2N, 7A
20-OCT-1992	405	2D, 4N, 5N, 6N
21-OCT-1992	406	3A, 4D
22-OCT-1992	407	2A, 3N
23-OCT-1992	408	2N, 7A
24-OCT-1992	409	2A
25-OCT-1992	410	2A
26-OCT-1992	411	2A, 7A
27-OCT-1992	412	2A
28-OCT-1992	413	2A, 3A, 4D
29-OCT-1992	414	2D, 3A, 4A, 5N, 6N
30-OCT-1992	415	2A, 7A
31-OCT-1992	416	2A
01-NOV-1992	417	2A, 4N, 5N, 6N
02-NOV-1992	418	2A, 7A
03-NOV-1992	419	2A
04-NOV-1992	420	2A, 3A, 4D
05-NOV-1992	421	2D, 3A, 4A, 5N, 6N
06-NOV-1992	422	2D, 4N, 5N, 6N, 7A
07-NOV-1992	423	2A, 7A
08-NOV-1992	424	2A, 4N, 5N, 6N
09-NOV-1992	425	2D, 4N, 5N, 6N, 7A
10-NOV-1992	426	2A, 7A
11-NOV-1992	427	2A, 4N, 5N, 6N
12-NOV-1992	428	7A
13-NOV-1992	429	2A
14-NOV-1992	430	2D, 4A, 5A, 6A
15-NOV-1992	431	7A
16-NOV-1992	432	2A
17-NOV-1992	433	2D, 4N, 5N, 6N
18-NOV-1992	434	2D, 3A, 4D
19-NOV-1992	435	7A
20-NOV-1992	436	2A
21-NOV-1992	437	2D, 4N, 5N, 6N
22-NOV-1992	438	2D, 7A
23-NOV-1992	439	2A, 7D
24-NOV-1992	440	2D, 3A, 4D
25-NOV-1992	441	3A, 4D
26-NOV-1992	442	2A, 3D, 4D
27-NOV-1992	443	2D, 4N, 5N, 6N
28-NOV-1992	444	2D, 7A
29-NOV-1992	445	2A, 7D
30-NOV-1992	446	2D, 4N, 5N, 6N

Date	Uday	Measurement
01-DEC-1992	447	2D, 7A
02-DEC-1992	448	2D, 4N, 5N, 6N, 7D
03-DEC-1992	449	2D, 3A, 4D
04-DEC-1992	450	3A, 4D, 7A
05-DEC-1992	451	2A, 7D
06-DEC-1992	452	2A, 4N, 5N, 6N
07-DEC-1992	453	2D, 3A, 4D
08-DEC-1992	454	2A, 3A, 4D
09-DEC-1992	455	2A, 7A
10-DEC-1992	456	2D, 4N, 5N, 6N, 7D
11-DEC-1992	457	2D, 3A, 4D
12-DEC-1992	458	2A, 3A, 4D
13-DEC-1992	459	2A, 4N, 5N, 6N
14-DEC-1992	460	2D, 7A
15-DEC-1992	461	3A, 4D, 7A
16-DEC-1992	462	2A
17-DEC-1992	463	2D, 4N, 5N, 6N
18-DEC-1992	464	7N
19-DEC-1992	465	2N
20-DEC-1992	466	4N, 5N, 6N
21-DEC-1992	467	7N
22-DEC-1992	468	2N
23-DEC-1992	469	2N, 3A, 4D
24-DEC-1992	470	2D, 3N, 4N, 5N, 6N
25-DEC-1992	471	4N, 5N, 6N, 7A
26-DEC-1992	472	2A, 7N
27-DEC-1992	473	2A, 4N, 5N, 6N
28-DEC-1992	474	7A
29-DEC-1992	475	2A
30-DEC-1992	476	2N, 3A, 4D
31-DEC-1992	477	2D, 3N, 4N, 5N, 6N
01-JAN-1993	478	2D, 7A
02-JAN-1993	479	2A
03-JAN-1993	480	2A, 4N, 5N, 6N
04-JAN-1993	481	2D, 7A
05-JAN-1993	482	2A
06-JAN-1993	483	2A, 3A, 4D
07-JAN-1993	484	2D, 3A, 4A, 5N, 6N
08-JAN-1993	485	2D, 7A
09-JAN-1993	486	2A, 7D
10-JAN-1993	487	2A, 4N, 5N, 6N
11-JAN-1993	488	2D, 7A
12-JAN-1993	489	2D, 4N, 5N, 6N, 7D
13-JAN-1993	490	2D, 3A, 4A, 5N, 6N
14-JAN-1993	491	3A, 4D, 7A
15-JAN-1993	492	2D, 4N, 5N, 6N, 7A

Date	Uday	Measurement
16-JAN-1993	493	2D, 4N, 5N, 6N, 7A
17-JAN-1993	494	2D, 4N, 5N, 6N, 7A
18-JAN-1993	495	2D, 3A, 4A, 5N, 6N
19-JAN-1993	496	2D, 3A, 4A, 5N, 6N
20-JAN-1993	497	2A
21-JAN-1993	498	2A
22-JAN-1993	499	2A
23-JAN-1993	500	2A
24-JAN-1993	501	2A
25-JAN-1993	502	2A
26-JAN-1993	503	2A
27-JAN-1993	504	2A
28-JAN-1993	505	2A
29-JAN-1993	506	2A
30-JAN-1993	507	2A
31-JAN-1993	508	2D, 4N, 5N, 6N
05-FEB-1993	513	7A
06-FEB-1993	514	3A, 4D, 7D
07-FEB-1993	515	3D, 4D, 7A
08-FEB-1993	516	7A
09-FEB-1993	517	2A, 7D
10-FEB-1993	518	3A, 4D, 7D
11-FEB-1993	519	3A, 4D, 7A
12-FEB-1993	520	2A, 4N, 5N, 6N, 7D
13-FEB-1993	521	2A
14-FEB-1993	522	2A, 7A
15-FEB-1993	523	2D, 4N, 5N, 6N, 7D
16-FEB-1993	524	2A
17-FEB-1993	525	2A, 3A, 4D
18-FEB-1993	526	3A, 4D, 7A
19-FEB-1993	527	2D, 4N, 5N, 6N, 7D
20-FEB-1993	528	2A
21-FEB-1993	529	2A, 7A
22-FEB-1993	530	2D, 4N, 5N, 6N, 7D
23-FEB-1993	531	2A
24-FEB-1993	532	2D, 3A, 4D
25-FEB-1993	533	4D, 7A
26-FEB-1993	534	2D, 4N, 5N, 6N
27-FEB-1993	535	2A
28-FEB-1993	536	2D, 7A

Date	Uday	Measurement	Date	Uday	Measurement
01-MAR-1993	537	2D, 4N, 5N, 6N, 7N	16-APR-1993	583	2A, 3A
02-MAR-1993	538	2A	17-APR-1993	584	X
03-MAR-1993	539	2N, 3A, 4D	18-APR-1993	585	X
04-MAR-1993	540	3N, 7A	19-APR-1993	586	2A, 3A
05-MAR-1993	541	2D, 4N, 5N, 6N	20-APR-1993	587	2A, 3D, 7A
06-MAR-1993	542	2A	21-APR-1993	588	3A, 4D, 7D
07-MAR-1993	543	2N, 7A	22-APR-1993	589	2D, 3A, 4A, 5N, 6N
08-MAR-1993	544	2D, 4N, 5N, 6N	23-APR-1993	590	2A
09-MAR-1993	545	7A	24-APR-1993	591	2A, 7A
10-MAR-1993	546	2D, 4N, 5N, 6N	25-APR-1993	592	2D, 4N, 5N, 6N, 7D
11-MAR-1993	547	3A, 4D	26-APR-1993	593	2A
12-MAR-1993	548	2D, 3N, 4N, 5N, 6N	27-APR-1993	594	2A, 7A
13-MAR-1993	549	2D, 3A, 4D	28-APR-1993	595	3A, 4D, 7D
14-MAR-1993	550	3A, 4D	29-APR-1993	596	2D, 3A, 4A, 5N, 6N
15-MAR-1993	551	2A, 3N, 7A	30-APR-1993	597	2A
16-MAR-1993	552	3A, 4D	01-MAY-1993	598	2A, 7A
17-MAR-1993	553	2D, 3A, 4A, 5N, 6N	02-MAY-1993	599	2D, 4N, 5N, 6N, 7D
18-MAR-1993	554	2D, 3A, 4D	03-MAY-1993	600	2A
19-MAR-1993	555	2D, 3A, 4D	04-MAY-1993	601	2D, 7A
20-MAR-1993	556	2D, 3N, 7A	05-MAY-1993	602	3A, 4D, 7D
21-MAR-1993	557	2D, 4N, 5N, 6N, 7D	06-MAY-1993	603	2D, 3D, 4A, 5N, 6N
22-MAR-1993	558	2A	07-MAY-1993	604	2A
23-MAR-1993	559	2A, 7A	08-MAY-1993	605	2D, 7A
24-MAR-1993	560	2D, 3N, 7D	09-MAY-1993	606	2D, 4N, 5N, 6N, 7D
25-MAR-1993	561	2D, 3N, 4N, 5N, 6N	10-MAY-1993	607	2A
26-MAR-1993	562	2A, 4N, 5N, 6N	11-MAY-1993	608	2D, 7A
27-MAR-1993	563	2A, 7A	12-MAY-1993	609	3A, 4D, 7D
28-MAR-1993	564	2D, 4N, 5N, 6N, 7A	13-MAY-1993	610	2D, 3A, 4A, 5N, 6N
29-MAR-1993	565	2A, 4N, 5N, 6N	14-MAY-1993	611	2A
30-MAR-1993	566	2N, 7A	15-MAY-1993	612	2A, 7A
31-MAR-1993	567	3A, 4D	16-MAY-1993	613	2D, 4N, 5N, 6N, 7D
01-APR-1993	568	2D, 3N, 4N, 5N, 6N	17-MAY-1993	614	2A
02-APR-1993	569	2A, 3A	18-MAY-1993	615	2N, 3A, 4D
03-APR-1993	570	2N, 7A	19-MAY-1993	616	3N, 7A
04-APR-1993	571	2D, 4N, 5N, 6N, 7A	20-MAY-1993	617	2D, 4N, 5N, 6N
05-APR-1993	572	2A	21-MAY-1993	618	2A
06-APR-1993	573	2N, 3A, 4D	22-MAY-1993	619	2N, 7A
07-APR-1993	574	3N, 7A	23-MAY-1993	620	2D, 4N, 5N, 6N
08-APR-1993	575	2D, 4N, 5N, 6N, 7N	24-MAY-1993	621	2A
09-APR-1993	576	2A, 3A	25-MAY-1993	622	2A, 7A
10-APR-1993	577	2D, 7A	26-MAY-1993	623	3A, 4D
11-APR-1993	578	2D, 4N, 5N, 6N, 7D	27-MAY-1993	624	2D, 3N, 4A, 5N, 6N
12-APR-1993	579	2A	28-MAY-1993	625	2A
13-APR-1993	580	2D, 7A	29-MAY-1993	626	2A, 7A
14-APR-1993	581	3A, 4D, 7D			
15-APR-1993	582	2D, 3D, 4A, 5N, 6N			

Date	Uday	Measurement
01-JUN-1993	629	2A, 7A
02-JUN-1993	630	3A, 4D, 7D
03-JUN-1993	631	2D, 3A, 4A, 5N, 6N
04-JUN-1993	632	2A
05-JUN-1993	633	2A, 7A
06-JUN-1993	634	2D, 4N, 5N, 6N, 7A
07-JUN-1993	635	2A, 4N, 5N, 6N
08-JUN-1993	636	2A, 7A
09-JUN-1993	637	3A, 4D
10-JUN-1993	638	2D, 3N, 4N, 5N, 6N
11-JUN-1993	639	2A
12-JUN-1993	640	2N, 7A
13-JUN-1993	641	2D, 4N, 5N, 6N
14-JUN-1993	642	6N, 7A
15-JUN-1993	643	2A, 7N
16-JUN-1993	644	2N, 3N
17-JUN-1993	645	3N, 4N, 5N, 6N
18-JUN-1993	646	2N, 4N, 5N, 6N
19-JUN-1993	647	7N
20-JUN-1993	648	4N, 5N, 6N
21-JUN-1993	649	2A
22-JUN-1993	650	2D, 7A
23-JUN-1993	651	3A, 4D
24-JUN-1993	652	2D, 3D, 4A, 5N, 6N
25-JUN-1993	653	2A, 3A
26-JUN-1993	654	2D, 7A
27-JUN-1993	655	2D, 4N, 5N, 6N, 7D
28-JUN-1993	656	2A, 3A
29-JUN-1993	657	2D, 3A, 7A
30-JUN-1993	658	3A, 4D, 7D
01-JUL-1993	659	2D, 3A, 4A, 5N, 6N
02-JUL-1993	660	2A, 3A
03-JUL-1993	661	7A
04-JUL-1993	662	2D, 4N, 5N, 6N
05-JUL-1993	663	2A
06-JUL-1993	664	7A
07-JUL-1993	665	2A, 7D
08-JUL-1993	666	2D, 4N, 5N, 6N
09-JUL-1993	667	2A
10-JUL-1993	668	7A
11-JUL-1993	669	2D, 4N, 5N, 6N
12-JUL-1993	670	2A
13-JUL-1993	671	7A
14-JUL-1993	672	3A, 4D, 7D
15-JUL-1993	673	2D, 4N, 5N, 6N
16-JUL-1993	674	2A
17-JUL-1993	675	2D, 7A
18-JUL-1993	676	2D, 4N, 5N, 6N, 7D
19-JUL-1993	677	7A
20-JUL-1993	678	2A
21-JUL-1993	679	3A, 4D
22-JUL-1993	680	2D, 4N, 5N, 6N
23-JUL-1993	681	2A
24-JUL-1993	682	2N, 7A
25-JUL-1993	683	7A
26-JUL-1993	684	2A
27-JUL-1993	685	2N, 7A
28-JUL-1993	686	3A, 4D
29-JUL-1993	687	2D, 4N, 5N, 6N
30-JUL-1993	688	2A
01-AUG-1993	690	2D, 4N, 5N, 6N
02-AUG-1993	691	2A
03-AUG-1993	692	2D, 7A
04-AUG-1993	693	3A, 4D
05-AUG-1993	694	X
06-AUG-1993	695	X
07-AUG-1993	696	X
08-AUG-1993	697	X
09-AUG-1993	698	X
10-AUG-1993	699	X
11-AUG-1993	700	7A
12-AUG-1993	701	7A
13-AUG-1993	702	2D, 4N, 5N, 6N
14-AUG-1993	703	2A
15-AUG-1993	704	4N, 5N, 6N, 7A
16-AUG-1993	705	2D, 4N, 5N, 6N
17-AUG-1993	706	2A
18-AUG-1993	707	2N, 3A, 4D
19-AUG-1993	708	3N, 7A
20-AUG-1993	709	2D, 4N, 5N, 6N
21-AUG-1993	710	2A
22-AUG-1993	711	2N, 4N, 5N, 6N, 7A
23-AUG-1993	712	2D, 4N, 5N, 6N
24-AUG-1993	713	2A, 4N, 5N, 6N
25-AUG-1993	714	2N, 3A, 4D
26-AUG-1993	715	7A
27-AUG-1993	716	2D, 4N, 5N, 6N
28-AUG-1993	717	2A
29-AUG-1993	718	7A
30-AUG-1993	719	2D, 4N, 5N, 6N
31-AUG-1993	720	2A

Date	Uday	Measurement
01-SEP-1993	721	3A, 4D
02-SEP-1993	722	7A
03-SEP-1993	723	2D, 4N, 5N, 6N
04-SEP-1993	724	2A
05-SEP-1993	725	2A, 7A
06-SEP-1993	726	2D, 4N, 5N, 6N, 7D
07-SEP-1993	727	2A
08-SEP-1993	728	2A, 3A, 4D
09-SEP-1993	729	3A, 4D, 7A
10-SEP-1993	730	2D, 4N, 5N, 6N, 7D
11-SEP-1993	731	2A
12-SEP-1993	732	2A, 7A
13-SEP-1993	733	2D, 4N, 5N, 6N, 7D
14-SEP-1993	734	2A
15-SEP-1993	735	2A, 3A, 4D
16-SEP-1993	736	7A
17-SEP-1993	737	2D, 4N, 5N, 6N
18-SEP-1993	738	X
19-SEP-1993	739	X
20-SEP-1993	740	X
21-SEP-1993	741	X
22-SEP-1993	742	X
23-SEP-1993	743	X
24-SEP-1993	744	X
25-SEP-1993	745	7A
26-SEP-1993	746	7A
27-SEP-1993	747	2D, 4N, 5N, 6N, 7D
28-SEP-1993	748	2A
29-SEP-1993	749	2A, 3A, 4D
30-SEP-1993	750	3A, 4D, 7A
01-OCT-1993	751	2D, 4N, 5N, 6N, 7D
02-OCT-1993	752	2A
03-OCT-1993	753	X
25-OCT-1993	775	X
26-OCT-1993	776	7A
27-OCT-1993	777	3A, 4D
28-OCT-1993	778	3N, 7A
29-OCT-1993	779	2D, 4N, 5N, 6N
30-OCT-1993	780	2A
31-OCT-1993	781	2A, 4N, 5N, 6N, 7A
01-NOV-1993	782	2D, 4N, 5N, 6N, 7D
02-NOV-1993	783	2A
03-NOV-1993	784	2A, 3A, 4D
04-NOV-1993	785	3D, 4D, 7A
05-NOV-1993	786	2D, 4N, 5N, 6N, 7D
06-NOV-1993	787	2A
07-NOV-1993	788	4N, 5N, 6N, 7A
08-NOV-1993	789	2D, 4N, 5N, 6N, 7D
09-NOV-1993	790	2A
10-NOV-1993	791	2A, 3A, 4D
11-NOV-1993	792	3D, 4D, 7A
12-NOV-1993	793	2D, 4N, 5N, 6N
13-NOV-1993	794	2A
14-NOV-1993	795	7A
15-NOV-1993	796	2D, 4N, 5N, 6N
16-NOV-1993	797	2A
17-NOV-1993	798	2D, 3A, 4D
18-NOV-1993	799	7A
19-NOV-1993	800	2D, 4N, 5N, 6N
20-NOV-1993	801	2A
21-NOV-1993	802	2D, 4N, 5N, 6N, 7A
22-NOV-1993	803	4N, 5N, 6N, 7A
23-NOV-1993	804	2A, 7D
24-NOV-1993	805	2D, 3A, 4D
25-NOV-1993	806	3D, 4D, 7A
26-NOV-1993	807	2D, 4N, 5N, 6N, 7D
27-NOV-1993	808	2A
28-NOV-1993	809	2D, 4N, 5N, 6N, 7A
30-NOV-1993	811	2A, 7D
01-DEC-1993	812	2D, 3A, 4D
02-DEC-1993	813	3A, 4D, 7A
03-DEC-1993	814	2D, 4N, 5N, 6N, 7D
04-DEC-1993	815	2A
05-DEC-1993	816	2N, 7A
06-DEC-1993	817	2D, 4N, 5N, 6N
07-DEC-1993	818	2A
08-DEC-1993	819	2N, 3A, 4D
09-DEC-1993	820	7D
10-DEC-1993	821	7A
11-DEC-1993	822	2A
12-DEC-1993	823	3N, 7A
13-DEC-1993	824	4N, 5N, 6N
14-DEC-1993	825	2N
15-DEC-1993	826	2N, 7N

Date	Uday	Measurement
16-DEC-1993	827	7N
17-DEC-1993	828	4N, 5N, 6N
18-DEC-1993	829	2A
19-DEC-1993	830	2N, 7A
20-DEC-1993	831	2D, 4N, 5N, 6N
21-DEC-1993	832	2A
22-DEC-1993	833	2A, 3A
23-DEC-1993	834	2N, 7A
24-DEC-1993	835	2D, 4N, 5N, 6N
25-DEC-1993	836	2A, 6A
26-DEC-1993	837	2A, 7A
27-DEC-1993	838	7A
28-DEC-1993	839	2D, 4N, 5N, 6N
29-DEC-1993	840	2A
30-DEC-1993	841	2A, 7A
31-DEC-1993	842	2D, 4N, 5N, 6N
01-JAN-1994	843	2A
02-JAN-1994	844	2A, 3A
03-JAN-1994	845	2D, 7A
04-JAN-1994	846	2D, 4N, 5N, 6N, 7D
05-JAN-1994	847	2A
06-JAN-1994	848	2D, 7A
07-JAN-1994	849	2A, 4N, 5N, 6N
08-JAN-1994	850	2A
09-JAN-1994	851	7A
10-JAN-1994	852	2A, 4N, 5N, 6N
11-JAN-1994	853	2A
12-JAN-1994	854	7A
13-JAN-1994	855	4N, 5N, 6N, 7D
14-JAN-1994	856	2D, 4N, 5N, 6N
15-JAN-1994	857	2A
16-JAN-1994	858	2A, 4N, 5N, 6N
17-JAN-1994	859	7A
18-JAN-1994	860	2D, 4N, 5N, 6N
19-JAN-1994	861	2A
20-JAN-1994	862	4N, 5N, 6N, 7A
21-JAN-1994	863	2A, 4N, 5N, 6N
22-JAN-1994	864	2A
23-JAN-1994	865	2A, 4N, 5N, 6N
24-JAN-1994	866	2D, 7A
25-JAN-1994	867	2D, 4N, 5N, 6N
26-JAN-1994	868	2A
27-JAN-1994	869	2D, 7A
28-JAN-1994	870	2D, 4N, 5N, 6N
29-JAN-1994	871	2A
30-JAN-1994	872	2A, 4N, 5N, 6N
31-JAN-1994	873	2D, 7A

Date	Uday	Measurement
01-FEB-1994	874	2D, 4N, 5N, 6N
02-FEB-1994	875	2D, 4N, 5N, 6N, 7A
03-FEB-1994	876	2A, 7D
04-FEB-1994	877	2A, 4N, 5N, 6N, 7D
05-FEB-1994	878	2D, 4N, 5N, 6N, 7D
06-FEB-1994	879	2A
07-FEB-1994	880	2A, 4N, 5N, 6N, 7A
08-FEB-1994	881	3A, 4D
09-FEB-1994	882	2A
10-FEB-1994	883	7A
11-FEB-1994	884	2A, 4N, 5N, 6N
12-FEB-1994	885	2A
13-FEB-1994	886	2D, 4N, 5N, 6N
14-FEB-1994	887	2A, 4D
15-FEB-1994	888	7A
16-FEB-1994	889	2A, 7A
17-FEB-1994	890	2A, 7N
18-FEB-1994	891	2A, 4N, 5N, 6N
19-FEB-1994	892	2A, 4N, 5N, 6N, 7A
20-FEB-1994	893	2D, 4N, 5N, 6N
21-FEB-1994	894	2A
22-FEB-1994	895	2D, 7A
23-FEB-1994	896	2D, 4N, 5N, 6N
24-FEB-1994	897	2A
25-FEB-1994	898	2A, 4N, 5N, 6N, 7A
26-FEB-1994	899	7A
27-FEB-1994	900	2D, 7A
28-FEB-1994	901	2A

Date	Uday	Measurement
01-MAR-1994	902	2D, 3A, 4D
02-MAR-1994	903	3A, 4D
03-MAR-1994	904	2A, 3N, 7A
04-MAR-1994	905	2N, 7A
05-MAR-1994	906	2D, 4N, 5N, 6N
06-MAR-1994	907	2A
07-MAR-1994	908	2A, 4N, 5N, 6N, 7A
08-MAR-1994	909	2A, 4N, 5N, 6N
09-MAR-1994	910	2A
10-MAR-1994	911	2A, 7A
11-MAR-1994	912	2A, 4N, 5N, 6N, 7D
12-MAR-1994	913	2D, 4N, 5N, 6N
13-MAR-1994	914	2A
14-MAR-1994	915	2A, 4N, 5N, 6N, 7A
15-MAR-1994	916	2N, 4N, 5N, 6N, 7A
16-MAR-1994	917	X
17-MAR-1994	918	X
18-MAR-1994	919	2A, 3A, 7D
19-MAR-1994	920	2A, 4N, 5N, 6N, 7A
20-MAR-1994	921	7D
21-MAR-1994	922	2A, 4N, 5N, 6N, 7A
22-MAR-1994	923	2A, 3A
23-MAR-1994	924	2A, 4N, 5N, 6N, 7A
24-MAR-1994	925	2A, 4N, 5N, 6N, 7A
25-MAR-1994	926	2A, 4N, 5N, 6N, 7A
26-MAR-1994	927	2A, 3A
27-MAR-1994	928	2A, 4N, 5N, 6N, 7A
28-MAR-1994	929	3A, 4D
29-MAR-1994	930	2A, 3N, 4N, 5N, 6N
30-MAR-1994	931	2A, 3A
31-MAR-1994	932	2A, 4N, 5N, 6N, 7A
01-APR-1994	933	3A, 4D
02-APR-1994	934	3A, 4D
03-APR-1994	935	2N, 3N, 4N, 5N, 6N
04-APR-1994	936	3A, 4D
05-APR-1994	937	2N, 4N, 5N, 6N, 7A
06-APR-1994	938	3A, 4D
07-APR-1994	939	2A, 4N, 5N, 6N, 7A
08-APR-1994	940	3A, 4D
09-APR-1994	941	2A, 4N, 5N, 6N, 7A
10-APR-1994	942	3A, 4D
11-APR-1994	943	2A, 4N, 5N, 6N, 7A
12-APR-1994	944	3A, 4A, 6N
13-APR-1994	945	2N, 7N
14-APR-1994	946	2N, 3N, 4N, 5N, 6N
15-APR-1994	947	2N, 7N
16-APR-1994	948	3N, 4N, 5N, 6N
17-APR-1994	949	2N, 7N
18-APR-1994	950	2N, 3N
19-APR-1994	951	2N, 7N
20-APR-1994	952	3N, 4N, 5N, 6N
21-APR-1994	953	2N, 7N
22-APR-1994	954	3N, 4N, 5N, 6N
23-APR-1994	955	2N, 4N, 5N, 6N, 7N
24-APR-1994	956	2N, 7N
25-APR-1994	957	3N, 4N, 5N, 6N
26-APR-1994	958	2N, 7N
27-APR-1994	959	3N, 4N, 5N, 6N
28-APR-1994	960	2N, 7N
29-APR-1994	961	3N, 4N, 5N, 6N
30-APR-1994	962	2N, 7N
01-MAY-1994	963	3N, 4N, 5N, 6N
02-MAY-1994	964	2N, 7N
03-MAY-1994	965	3N
04-MAY-1994	966	3N, 7N
05-MAY-1994	967	3N, 4N, 5N, 6N
06-MAY-1994	968	2N, 7N
07-MAY-1994	969	3N, 4N, 5N, 6N
08-MAY-1994	970	3N
09-MAY-1994	971	3N, 4N, 5N, 6N
10-MAY-1994	972	7N
11-MAY-1994	973	4N, 5N, 6N
12-MAY-1994	974	2N, 7A
13-MAY-1994	975	3N, 4N, 5N, 6N
14-MAY-1994	976	2N, 7N
15-MAY-1994	977	3N, 4N, 5N, 6N
16-MAY-1994	978	2N, 7N
17-MAY-1994	979	3N, 4N, 5N, 6N
18-MAY-1994	980	7D
19-MAY-1994	981	3N, 4N, 5N, 6N
20-MAY-1994	982	2N
21-MAY-1994	983	3N, 4N, 5N, 6N
22-MAY-1994	984	2N, 7N
23-MAY-1994	985	4N, 5N, 6N, 7D
24-MAY-1994	986	2N, 4N, 5N, 6N
25-MAY-1994	987	X
26-MAY-1994	988	X
27-MAY-1994	989	7D
28-MAY-1994	990	4N, 5N, 6N, 7D
29-MAY-1994	991	7D
30-MAY-1994	992	2N, 4N, 5N, 6N
31-MAY-1994	993	2N, 7D

Date	Uday	Measurement
01-JUN-1994	994	2N, 4N, 5N, 6N, 7D
02-JUN-1994	995	2N
03-JUN-1994	996	2N, 4N, 5N, 6N, 7D
04-JUN-1994	997	2N, 7D
05-JUN-1994	998	4N, 5N, 6N, 7D
06-JUN-1994	999	2N
07-JUN-1994	1000	4N, 5N, 6N
08-JUN-1994	1001	2N
09-JUN-1994	1002	4N, 5N, 6N
10-JUN-1994	1003	2N
11-JUN-1994	1004	5N
12-JUN-1994	1005	2N
13-JUN-1994	1006	4N, 5N, 6N
14-JUN-1994	1007	4N, 5N, 6N
15-JUN-1994	1008	2N
16-JUN-1994	1009	2N, 4N, 5N, 6N
17-JUN-1994	1010	4A, 5A, 6A
18-JUN-1994	1011	4N, 5N, 6N
19-JUN-1994	1012	2N, 7A
20-JUN-1994	1013	2N, 7D
21-JUN-1994	1014	2N, 7D
22-JUN-1994	1015	4N, 5N, 6N, 7D
23-JUN-1994	1016	2N, 7D
24-JUN-1994	1017	2N, 4N, 5N, 6N, 7D
25-JUN-1994	1018	X
26-JUN-1994	1019	2N, 4N, 5N, 6N, 7D
27-JUN-1994	1020	7D
28-JUN-1994	1021	2N, 4N, 5N, 6N, 7D
29-JUN-1994	1022	X
30-JUN-1994	1023	2N, 4N, 5N, 6N, 7D
01-JUL-1994	1024	7D
02-JUL-1994	1025	2N, 4N, 5N, 6N
03-JUL-1994	1026	7N
04-JUL-1994	1027	2N, 4N, 5N, 6N, 7D
05-JUL-1994	1028	4N, 5N, 6N
06-JUL-1994	1029	2N
08-JUL-1994	1031	2N
10-JUL-1994	1033	2N
11-JUL-1994	1034	7A
12-JUL-1994	1035	4N, 5N, 6N, 7A
13-JUL-1994	1036	3N, 7A
14-JUL-1994	1037	2N, 3N, 7A
15-JUL-1994	1038	7A

Date	Uday	Measurement
16-JUL-1994	1039	4N, 5N, 6N, 7A
17-JUL-1994	1040	2N, 7A
18-JUL-1994	1041	7A
19-JUL-1994	1042	4N, 5N, 6N, 7A
20-JUL-1994	1043	2N, 7A
21-JUL-1994	1044	7A
22-JUL-1994	1045	4N, 5N, 6N, 7A
23-JUL-1994	1046	2N, 7A
24-JUL-1994	1047	7A
25-JUL-1994	1048	4N, 5N, 6N, 7D
26-JUL-1994	1049	2N, 7D
27-JUL-1994	1050	2N, 7D
28-JUL-1994	1051	7A
29-JUL-1994	1052	4N, 5N, 6N, 7D
30-JUL-1994	1053	2N, 7D
31-JUL-1994	1054	7A
01-AUG-1994	1055	4N, 5N, 6N, 7A
02-AUG-1994	1056	2N, 7A
03-AUG-1994	1057	7A
04-AUG-1994	1058	4N, 5N, 6N, 7A
05-AUG-1994	1059	2N, 7D
06-AUG-1994	1060	2N, 7A
07-AUG-1994	1061	4N, 5N, 6N, 7A
08-AUG-1994	1062	2N, 7A
09-AUG-1994	1063	7A
10-AUG-1994	1064	3N, 7D
11-AUG-1994	1065	4N, 5N, 6N, 7A
12-AUG-1994	1066	2N, 7A
13-AUG-1994	1067	7A
14-AUG-1994	1068	4N, 5N, 6N, 7A
15-AUG-1994	1069	2N, 7D
16-AUG-1994	1070	7A
17-AUG-1994	1071	4N, 5N, 6N, 7A
18-AUG-1994	1072	2N, 7A
19-AUG-1994	1073	7A
20-AUG-1994	1074	4N, 5N, 6N, 7A
21-AUG-1994	1075	2N, 7A
22-AUG-1994	1076	7A
23-AUG-1994	1077	4N, 5N, 6N, 7A
24-AUG-1994	1078	3N, 7D
25-AUG-1994	1079	2N, 3N, 7D
26-AUG-1994	1080	2N, 7A
27-AUG-1994	1081	4N, 5N, 6N, 7A
28-AUG-1994	1082	2N, 7A
29-AUG-1994	1083	2N, 7A
30-AUG-1994	1084	4N, 6N, 7A
31-AUG-1994	1085	2N, 7A

Date	Uday	Measurement
01-SEP-1994	1086	7A
02-SEP-1994	1087	4N, 5N, 6N, 7D
03-SEP-1994	1088	2N, 7A
04-SEP-1994	1089	7A
05-SEP-1994	1090	4N, 5N, 6N, 7D
06-SEP-1994	1091	2N, 7D
07-SEP-1994	1092	3N, 7D
08-SEP-1994	1093	3N, 7D
09-SEP-1994	1094	4N, 5N, 6N, 7A
10-SEP-1994	1095	2N, 7A
11-SEP-1994	1096	7A
12-SEP-1994	1097	4N, 5N, 6N, 7A
13-SEP-1994	1098	2N, 7A
14-SEP-1994	1099	7A
15-SEP-1994	1100	4N, 5N, 6N, 7A
16-SEP-1994	1101	2N, 7A
17-SEP-1994	1102	7A
18-SEP-1994	1103	4N, 5N, 6N, 7A
19-SEP-1994	1104	2N, 7A
20-SEP-1994	1105	2N, 7A
21-SEP-1994	1106	3N, 7A
22-SEP-1994	1107	3N, 4N, 5N, 6N, 7A
23-SEP-1994	1108	3A, 4D
24-SEP-1994	1109	7A
25-SEP-1994	1110	4N, 5N, 6N, 7A
26-SEP-1994	1111	2N, 7A
27-SEP-1994	1112	7A
28-SEP-1994	1113	4N, 5N, 6N, 7A
29-SEP-1994	1114	2N, 7A
30-SEP-1994	1115	7A
01-OCT-1994	1116	4N, 5N, 6N, 7A
02-OCT-1994	1117	2N, 7A
03-OCT-1994	1118	7A
04-OCT-1994	1119	4N, 5N, 6N, 7A
05-OCT-1994	1120	3N, 7A
06-OCT-1994	1121	2N, 7A
07-OCT-1994	1122	7A
08-OCT-1994	1123	4N, 5N, 6N, 7A
09-OCT-1994	1124	2N, 7A
10-OCT-1994	1125	2N, 7A
11-OCT-1994	1126	4N, 5N, 6N, 7A
12-OCT-1994	1127	2N, 7A
13-OCT-1994	1128	2N, 7A
14-OCT-1994	1129	4N, 5N, 6N, 7A
15-OCT-1994	1130	2N, 7A

Date	Uday	Measurement
16-OCT-1994	1131	7A
17-OCT-1994	1132	4N, 5N, 6N, 7A
18-OCT-1994	1133	2N, 7A
19-OCT-1994	1134	3N, 7A
20-OCT-1994	1135	7A
21-OCT-1994	1136	4N, 5N, 6N, 7D
22-OCT-1994	1137	2N, 7D
23-OCT-1994	1138	7A
24-OCT-1994	1139	4N, 5N, 6N, 7A
25-OCT-1994	1140	2N, 7D
26-OCT-1994	1141	7A
27-OCT-1994	1142	4N, 5N, 6N, 7D
28-OCT-1994	1143	2N, 7D
29-OCT-1994	1144	7A
30-OCT-1994	1145	4N, 5N, 6N, 7D
31-OCT-1994	1146	2N, 7D
01-NOV-1994	1147	7A
02-NOV-1994	1148	3N, 7D
03-NOV-1994	1149	3N, 4N, 5N, 6N, 7D
04-NOV-1994	1150	2N, 7D
05-NOV-1994	1151	7A
06-NOV-1994	1152	4N, 5N, 6N, 7A
07-NOV-1994	1153	2N, 7D
08-NOV-1994	1154	7A
09-NOV-1994	1155	4N, 5N, 6N, 7A
10-NOV-1994	1156	2N, 7A
11-NOV-1994	1157	7A
12-NOV-1994	1158	7A
13-NOV-1994	1159	7A
14-NOV-1994	1160	7A
15-NOV-1994	1161	7A
16-NOV-1994	1162	7A
17-NOV-1994	1163	7A
18-NOV-1994	1164	7A
19-NOV-1994	1165	7D
20-NOV-1994	1166	3N, 7A
21-NOV-1994	1167	3A
22-NOV-1994	1168	3N, 4D
23-NOV-1994	1169	3A, 4D
24-NOV-1994	1170	2N, 3D, 4A
25-NOV-1994	1171	3A, 4D
26-NOV-1994	1172	3N, 4D
27-NOV-1994	1173	2A, 3N, 4A, 7D
28-NOV-1994	1174	2N, 3A, 4A, 5A, 6A
29-NOV-1994	1175	3N, 4A, 5N, 6N
30-NOV-1994	1176	2N, 3A

Date	Uday	Measurement
01-DEC-1994	1177	2N, 4A
02-DEC-1994	1178	3A
03-DEC-1994	1179	3N, 4D
04-DEC-1994	1180	2A, 4N, 7D
05-DEC-1994	1181	2N, 3A
06-DEC-1994	1182	2N, 3A, 4D
07-DEC-1994	1183	3A
08-DEC-1994	1184	2N, 3D, 4A
09-DEC-1994	1185	2N, 3N, 4D
10-DEC-1994	1186	2N, 3A, 4D
11-DEC-1994	1187	3A, 7D
12-DEC-1994	1188	2N, 3A, 4D
13-DEC-1994	1189	2N, 3A
14-DEC-1994	1190	3A, 4D
15-DEC-1994	1191	2N, 3A, 4A
16-DEC-1994	1192	2N, 3A, 4D
17-DEC-1994	1193	3A, 4D
18-DEC-1994	1194	2N, 3A, 4A
19-DEC-1994	1195	2N, 3A, 4D
20-DEC-1994	1196	2N, 3A, 4D
21-DEC-1994	1197	2N, 3A, 4D
22-DEC-1994	1198	2N, 3A, 4A
23-DEC-1994	1199	2N, 3A
24-DEC-1994	1200	2N, 3A, 4D
25-DEC-1994	1201	2A, 3N, 4A, 7D
26-DEC-1994	1202	2N, 3A
27-DEC-1994	1203	2N, 3A, 4D
28-DEC-1994	1204	2N, 3A, 4D
29-DEC-1994	1205	2N, 3A, 4A
30-DEC-1994	1206	2N, 3A, 4D
31-DEC-1994	1207	2N, 3N, 4D
01-JAN-1995	1208	2A, 7D
02-JAN-1995	1209	3A
03-JAN-1995	1210	3N, 4D
04-JAN-1995	1211	3A
05-JAN-1995	1212	2N, 3N, 4D
06-JAN-1995	1213	2N, 3A
07-JAN-1995	1214	3N, 4D
08-JAN-1995	1215	2A, 3N
09-JAN-1995	1216	2N, 3A
10-JAN-1995	1217	2A, 3N
11-JAN-1995	1218	2N, 4N, 5N, 6N, 7D
12-JAN-1995	1219	7A
13-JAN-1995	1220	2A
14-JAN-1995	1221	X
15-JAN-1995	1222	7N, 8D
16-JAN-1995	1223	2A, 3A
17-JAN-1995	1224	2A
18-JAN-1995	1225	2N, 4N, 5N, 6N, 7D
19-JAN-1995	1226	3A, 4D
20-JAN-1995	1227	3N, 7A
21-JAN-1995	1228	2D, 4N, 5N, 6N
22-JAN-1995	1229	7A
23-JAN-1995	1230	2A, 3A
24-JAN-1995	1231	2A
25-JAN-1995	1232	4N, 5N, 6N, 7D
26-JAN-1995	1233	3A, 4D
27-JAN-1995	1234	3N, 7A
28-JAN-1995	1235	2A
29-JAN-1995	1236	2N, 7A
30-JAN-1995	1237	2D, 4N, 5N, 6N
31-JAN-1995	1238	2A, 3N
01-FEB-1995	1239	2N, 3A, 4D
02-FEB-1995	1240	2N, 3N, 7D
03-FEB-1995	1241	2D, 4N, 5N, 6N
04-FEB-1995	1242	2A
05-FEB-1995	1243	2N, 7D
06-FEB-1995	1244	4N, 5N, 6N, 7D
07-FEB-1995	1245	2A
08-FEB-1995	1246	2D, 3A, 4D
09-FEB-1995	1247	2N, 7D
10-FEB-1995	1248	2D, 4N, 5N, 6N
11-FEB-1995	1249	2A
12-FEB-1995	1250	2A, 7D
13-FEB-1995	1251	4N, 5N, 6N, 7D
14-FEB-1995	1252	2A
15-FEB-1995	1253	2D, 3A, 4D
16-FEB-1995	1254	2N, 3D, 4D, 7D
17-FEB-1995	1255	2A, 4N, 5N, 6N
18-FEB-1995	1256	2A
19-FEB-1995	1257	2A, 7D
20-FEB-1995	1258	2N, 4N, 5N, 6N, 7D
21-FEB-1995	1259	2A
22-FEB-1995	1260	2N, 3A, 4D
23-FEB-1995	1261	2N, 3N, 7D
24-FEB-1995	1262	2A, 4N, 5N, 6N
25-FEB-1995	1263	2A
26-FEB-1995	1264	2A, 7D
27-FEB-1995	1265	2N, 4N, 5N, 6N, 7D
28-FEB-1995	1266	2A

Date	Uday	Measurement
01-MAR-1995	1267	2A, 3A, 4D
02-MAR-1995	1268	2N, 3A, 4D, 7D
03-MAR-1995	1269	2A, 4N, 5N, 6N
04-MAR-1995	1270	2A
05-MAR-1995	1271	2A, 7D
06-MAR-1995	1272	2N, 4N, 5N, 6N, 7D
07-MAR-1995	1273	2A
08-MAR-1995	1274	3A, 4D
09-MAR-1995	1275	2N, 7D
10-MAR-1995	1276	2A, 4N, 5N, 6N
11-MAR-1995	1277	2A
12-MAR-1995	1278	2N, 7A
13-MAR-1995	1279	2A
14-MAR-1995	1280	2N, 4N, 5N, 6N, 7D
15-MAR-1995	1281	3A, 4D
16-MAR-1995	1282	3N, 7A
17-MAR-1995	1283	2D, 4N, 5N, 6N
18-MAR-1995	1284	2A
19-MAR-1995	1285	2N, 4N, 5N, 6N, 7D
20-MAR-1995	1286	2D, 4N, 5N, 6N
21-MAR-1995	1287	2A
22-MAR-1995	1288	2A, 3A, 4D
23-MAR-1995	1289	3N
07-APR-1995	1304	7D
08-APR-1995	1305	2N, 7D
09-APR-1995	1306	2N, 4N, 5N, 6N, 7D
10-APR-1995	1307	2D, 4N, 5N, 6N
11-APR-1995	1308	2A
12-APR-1995	1309	2A, 3A, 4D
13-APR-1995	1310	3N, 7A
14-APR-1995	1311	7D
15-APR-1995	1312	2A, 7D
16-APR-1995	1313	2A, 4N, 5N, 6N, 7D
17-APR-1995	1314	2D, 4N, 5N, 6N
21-JUN-1995	1379	X
22-JUN-1995	1380	7D
23-JUN-1995	1381	7D
24-JUN-1995	1382	2N, 7D
25-JUN-1995	1383	2A
26-JUN-1995	1384	7A
27-JUN-1995	1385	2D, 4N, 5N, 6N
28-JUN-1995	1386	3A, 4D
29-JUN-1995	1387	3N, 7A
13-JUL-1995	1401	4D, 5D, 6D, 7D
14-JUL-1995	1402	4A, 5A, 6A, 7D
15-JUL-1995	1403	2A

Date	Uday	Measurement
16-JUL-1995	1404	2A, 3D
17-JUL-1995	1405	2D, 4N, 5N, 6N
18-JUL-1995	1406	2A
19-JUL-1995	1407	3A, 4D
20-JUL-1995	1408	4N, 5N, 6N, 7D
21-JUL-1995	1409	7A
22-JUL-1995	1410	2D, 4N, 5N, 6N
23-JUL-1995	1411	2A
24-JUL-1995	1412	2N, 4N, 5N, 6N, 7D
25-JUL-1995	1413	7A
26-JUL-1995	1414	3A, 4D
27-JUL-1995	1415	2D, 3N, 4N, 5N, 6N
28-JUL-1995	1416	2A
16-AUG-1995	1435	7A
17-AUG-1995	1436	2A, 7D
18-AUG-1995	1437	2A
19-AUG-1995	1438	2A
20-AUG-1995	1439	2A
22-AUG-1995	1441	X
23-AUG-1995	1442	7A
24-AUG-1995	1443	2A, 7D
25-AUG-1995	1444	2A
29-AUG-1995	1448	7D
30-AUG-1995	1449	2A
31-AUG-1995	1450	2A
01-SEP-1995	1451	2A
02-SEP-1995	1452	2A
03-SEP-1995	1453	2A
04-SEP-1995	1454	2A
05-SEP-1995	1455	2A, 7D
06-SEP-1995	1456	2A
12-SEP-1995	1462	7A
13-SEP-1995	1463	2A, 7D
14-SEP-1995	1464	2A
15-SEP-1995	1465	2A
16-SEP-1995	1466	2A
17-SEP-1995	1467	2A
18-SEP-1995	1468	2A
19-SEP-1995	1469	2A
20-SEP-1995	1470	2A
21-SEP-1995	1471	2A
22-SEP-1995	1472	2A
23-SEP-1995	1473	2A
24-SEP-1995	1474	2A
27-SEP-1995	1477	7A
28-SEP-1995	1478	7A
29-SEP-1995	1479	2A
30-SEP-1995	1480	2A

Date	Uday	Measurement
01-OCT-1995	1481	2A
02-OCT-1995	1482	2A
03-OCT-1995	1483	2A
04-OCT-1995	1484	2A
05-OCT-1995	1485	2A
06-OCT-1995	1486	2A
07-OCT-1995	1487	2A
08-OCT-1995	1488	2A
09-OCT-1995	1489	2A
10-OCT-1995	1490	2A
11-OCT-1995	1491	2A
12-OCT-1995	1492	2A
20-OCT-1995	1500	X
21-OCT-1995	1501	7A
22-OCT-1995	1502	2A, 7D
23-OCT-1995	1503	7A
24-OCT-1995	1504	2A
25-OCT-1995	1505	2A
26-OCT-1995	1506	2A
27-OCT-1995	1507	2A
28-OCT-1995	1508	2A
29-OCT-1995	1509	2A
30-OCT-1995	1510	2A
31-OCT-1995	1511	2A
01-NOV-1995	1512	2A
02-NOV-1995	1513	2A
03-NOV-1995	1514	2A
04-NOV-1995	1515	2A
05-NOV-1995	1516	2A
06-NOV-1995	1517	2A
07-NOV-1995	1518	2A
08-NOV-1995	1519	2A
09-NOV-1995	1520	2A
10-NOV-1995	1521	2A
17-NOV-1995	1528	7D
18-NOV-1995	1529	2A
19-NOV-1995	1530	2A
20-NOV-1995	1531	2A
21-NOV-1995	1532	2A
22-NOV-1995	1533	2A
23-NOV-1995	1534	2A
24-NOV-1995	1535	2A
25-NOV-1995	1536	7A
26-NOV-1995	1537	2A
27-NOV-1995	1538	2A
28-NOV-1995	1539	2A
29-NOV-1995	1540	2A
30-NOV-1995	1541	2A

Date	Uday	Measurement
01-DEC-1995	1542	2D, 7A
02-DEC-1995	1543	7A
03-DEC-1995	1544	7A
04-DEC-1995	1545	7A
05-DEC-1995	1546	7N
11-DEC-1995	1552	7A
12-DEC-1995	1553	2A
13-DEC-1995	1554	2A
14-DEC-1995	1555	2A
15-DEC-1995	1556	2A
16-DEC-1995	1557	2A
17-DEC-1995	1558	2A
18-DEC-1995	1559	2A
19-DEC-1995	1560	2A
20-DEC-1995	1561	2A
21-DEC-1995	1562	2A
22-DEC-1995	1563	2A
23-DEC-1995	1564	2A
24-DEC-1995	1565	2A
29-DEC-1995	1570	7A
30-DEC-1995	1571	2A
31-DEC-1995	1572	2A
01-JAN-1996	1573	2A
02-JAN-1996	1574	2A
03-JAN-1996	1575	2A
04-JAN-1996	1576	2A
05-JAN-1996	1577	2A
06-JAN-1996	1578	2A
07-JAN-1996	1579	2A
08-JAN-1996	1580	2A
09-JAN-1996	1581	2A
10-JAN-1996	1582	2A
11-JAN-1996	1583	2A
12-JAN-1996	1584	2A
13-JAN-1996	1585	2A
14-JAN-1996	1586	2A
15-JAN-1996	1587	2A

Date	Uday	Measurement
16-JAN-1996	1588	2A
17-JAN-1996	1589	2A
18-JAN-1996	1590	2A
19-JAN-1996	1591	2A
20-JAN-1996	1592	2A
21-JAN-1996	1593	2A
22-JAN-1996	1594	2A
23-JAN-1996	1595	2A
24-JAN-1996	1596	2A
25-JAN-1996	1597	2A
26-JAN-1996	1598	2A
27-JAN-1996	1599	2A, 3A
28-JAN-1996	1600	2A, 3A
29-JAN-1996	1601	2A, 3A
30-JAN-1996	1602	2A, 3A
31-JAN-1996	1603	2A, 3A
01-FEB-1996	1604	2A, 3A
02-FEB-1996	1605	2A, 3A
14-FEB-1996	1617	7A
15-FEB-1996	1618	7A
16-FEB-1996	1619	2A, 3A
17-FEB-1996	1620	2A, 3A
18-FEB-1996	1621	2A, 3A
19-FEB-1996	1622	2A, 3A
20-FEB-1996	1623	2A, 3A
21-FEB-1996	1624	2A, 3A
22-FEB-1996	1625	2A, 3A
23-FEB-1996	1626	2A, 3A
24-FEB-1996	1627	2A, 3A
25-FEB-1996	1628	2A, 3A
26-FEB-1996	1629	2A, 3A
27-FEB-1996	1630	2A, 3A
28-FEB-1996	1631	2A, 3A
29-FEB-1996	1632	2A, 3A
01-MAR-1996	1633	2A, 3A
02-MAR-1996	1634	2A, 3A
03-MAR-1996	1635	2A, 3A
04-MAR-1996	1636	2A
05-MAR-1996	1637	X
12-MAR-1996	1644	2A, 7A
13-MAR-1996	1645	2A
14-MAR-1996	1646	2A
15-MAR-1996	1647	2A

Date	Uday	Measurement
16-MAR-1996	1648	2A
17-MAR-1996	1649	2A
18-MAR-1996	1650	2A
20-MAR-1996	1652	2A
28-MAR-1996	1660	7A
29-MAR-1996	1661	7A
30-MAR-1996	1662	2A
31-MAR-1996	1663	2A
01-APR-1996	1664	2A
02-APR-1996	1665	2A
15-APR-1996	1678	7A
16-APR-1996	1679	2A, 7D
17-APR-1996	1680	2A
18-APR-1996	1681	2A
19-APR-1996	1682	2A
20-APR-1996	1683	2A
21-APR-1996	1684	2A
22-APR-1996	1685	2A
28-APR-1996	1691	7A
29-APR-1996	1692	2A
01-MAY-1996	1694	2A
02-MAY-1996	1695	2A
03-MAY-1996	1696	2A
04-MAY-1996	1697	2A
10-MAY-1996	1703	7A
11-MAY-1996	1704	2A
12-MAY-1996	1705	2A
13-MAY-1996	1706	2A
16-MAY-1996	1709	7A
17-MAY-1996	1710	2A
18-MAY-1996	1711	2A
19-MAY-1996	1712	2A
20-MAY-1996	1713	2A
21-MAY-1996	1714	2A
22-MAY-1996	1715	2A
23-MAY-1996	1716	2A
24-MAY-1996	1717	2A
25-MAY-1996	1718	2A
26-MAY-1996	1719	2A
27-MAY-1996	1720	2A
28-MAY-1996	1721	2A
29-MAY-1996	1722	2A
30-MAY-1996	1723	2A
31-MAY-1996	1724	2A

Date	Uday	Measurement
03-JUL-1996	1757	7A
04-JUL-1996	1758	2A
05-JUL-1996	1759	2A
06-JUL-1996	1760	2A
07-JUL-1996	1761	2D, 7N
08-JUL-1996	1762	7N
09-JUL-1996	1763	7N
10-JUL-1996	1764	7N
11-JUL-1996	1765	7N
12-JUL-1996	1766	7N
13-JUL-1996	1767	7N
14-JUL-1996	1768	7N
15-JUL-1996	1769	X
15-AUG-1996	1800	7A
16-AUG-1996	1801	2A, 7D
17-AUG-1996	1802	2A
18-AUG-1996	1803	2A
19-AUG-1996	1804	2A
20-AUG-1996	1805	2A
21-AUG-1996	1806	2A
22-AUG-1996	1807	2A
23-AUG-1996	1808	2A
24-AUG-1996	1809	2A
25-AUG-1996	1810	2A
08-SEP-1996	1824	7D
09-SEP-1996	1825	2A, 7D
10-SEP-1996	1826	2A
11-SEP-1996	1827	2A
12-SEP-1996	1828	2A
13-SEP-1996	1829	2A
14-SEP-1996	1830	2A
15-SEP-1996	1831	2A
16-SEP-1996	1832	2A
17-SEP-1996	1833	2A
18-SEP-1996	1834	2A
19-SEP-1996	1835	2A
20-SEP-1996	1836	2A
21-SEP-1996	1837	2A
23-OCT-1996	1869	X
24-OCT-1996	1870	2A, 7A
25-OCT-1996	1871	2A
26-OCT-1996	1872	2A
27-OCT-1996	1873	2A
28-OCT-1996	1874	2A
29-OCT-1996	1875	2A
30-OCT-1996	1876	2A

Date	Uday	Measurement
12-NOV-1996	1889	7D
13-NOV-1996	1890	2A, 7D
14-NOV-1996	1891	2A
15-NOV-1996	1892	2A
16-NOV-1996	1893	2A
17-NOV-1996	1894	2A
18-NOV-1996	1895	4A, 5N, 6N
19-NOV-1996	1896	2A, 7N
20-NOV-1996	1897	3A
21-NOV-1996	1898	2D, 3D
22-NOV-1996	1899	2D, 3D
23-NOV-1996	1900	2A
24-NOV-1996	1901	2A
25-NOV-1996	1902	2A
26-NOV-1996	1903	2A
27-NOV-1996	1904	2A
28-NOV-1996	1905	2A
29-NOV-1996	1906	2A
30-NOV-1996	1907	2A
01-DEC-1996	1908	2N
02-DEC-1996	1909	2N, 4N, 5N, 6N
03-DEC-1996	1910	2N, 4N, 5N, 6N
04-DEC-1996	1911	2N, 4A, 5A, 6A
05-DEC-1996	1912	2A, 4N, 5N, 6N, 7N
06-DEC-1996	1913	2A, 4N, 5N, 6N
07-DEC-1996	1914	2A, 4N, 5N, 6N, 7N
08-DEC-1996	1915	2A, 7N
09-DEC-1996	1916	2A, 3A
10-DEC-1996	1917	2A, 3A
04-JAN-1997	1942	7A
05-JAN-1997	1943	7A
06-JAN-1997	1944	7D
07-JAN-1997	1945	7A
08-JAN-1997	1946	7D
09-JAN-1997	1947	7A
10-JAN-1997	1948	7D
11-JAN-1997	1949	7A
12-JAN-1997	1950	7A
25-JAN-1997	1963	7D
26-JAN-1997	1964	2A
27-JAN-1997	1965	2A
28-JAN-1997	1966	2A
29-JAN-1997	1967	2A
30-JAN-1997	1968	2A
31-JAN-1997	1969	2A

Date	Uday	Measurement
01-FEB-1997	1970	2A
02-FEB-1997	1971	2A
07-FEB-1997	1976	7A
08-FEB-1997	1977	2A
09-FEB-1997	1978	2A
10-FEB-1997	1979	2A
11-FEB-1997	1980	2A
12-FEB-1997	1981	2A
13-FEB-1997	1982	2A
14-FEB-1997	1983	2A
20-FEB-1997	1989	7A
21-FEB-1997	1990	2A
03-MAR-1997	2000	7A
04-MAR-1997	2001	2A
05-MAR-1997	2002	4N, 5N, 6N, 7D
07-MAR-1997	2004	2N, 3N, 4N, 5N, 6N
08-MAR-1997	2005	2A, 3N
09-MAR-1997	2006	2N, 3N, 4N, 5N, 6N
10-MAR-1997	2007	2A, 3N
11-MAR-1997	2008	2N, 3N, 4N, 5N, 6N
12-MAR-1997	2009	2A, 3N
13-MAR-1997	2010	2N, 3N, 4N, 5N, 6N
14-MAR-1997	2011	2A, 3N
15-MAR-1997	2012	2N, 3N, 4N, 5N, 6N
16-MAR-1997	2013	2A, 3N
17-MAR-1997	2014	2A, 3N, 4N, 5N, 6N
18-MAR-1997	2015	2A, 3N, 4N, 5N, 6N
19-MAR-1997	2016	2A, 4N, 5N, 6N, 7D
20-MAR-1997	2017	2A, 3N
21-MAR-1997	2018	2D, 4N, 5N, 6N, 7D
22-MAR-1997	2019	2A, 3N
23-MAR-1997	2020	2D, 4N, 5N, 6N, 7D
24-MAR-1997	2021	2A, 3N
25-MAR-1997	2022	2D, 4N, 5N, 6N, 7D
26-MAR-1997	2023	2A, 3N
27-MAR-1997	2024	2A, 3N, 4N, 5N, 6N
28-MAR-1997	2025	2A, 3N
29-MAR-1997	2026	2A, 3N, 4N, 5N, 6N
30-MAR-1997	2027	2A, 3N
01-APR-1997	2029	2A, 3N
02-APR-1997	2030	3N, 4N, 5N, 6N, 7D
03-APR-1997	2031	2A, 3N
04-APR-1997	2032	3N, 4N, 5N, 6N, 7D
05-APR-1997	2033	2A, 3N
14-APR-1997	2042	7D
15-APR-1997	2043	2A

Date	Uday	Measurement
16-APR-1997	2044	2D, 4N, 5N, 6N, 7D
17-APR-1997	2045	2A
18-APR-1997	2046	2D, 4N, 5N, 6N, 7D
19-APR-1997	2047	2A
20-APR-1997	2048	2D, 4N, 5N, 6N, 7D
21-APR-1997	2049	2A
22-APR-1997	2050	2A, 4N, 5N, 6N, 7D
23-APR-1997	2051	2A
24-APR-1997	2052	2A, 4N, 5N, 6N, 7D
25-APR-1997	2053	2A
26-APR-1997	2054	2A, 4N, 5N, 6N, 7D
27-APR-1997	2055	2A
04-JUN-1997	2093	7D
09-AUG-1997	2159	7A
12-AUG-1997	2162	7A
13-AUG-1997	2163	2A
14-AUG-1997	2164	2A, 3A, 4D
15-AUG-1997	2165	2A, 3A, 4D
16-AUG-1997	2166	2A, 4N, 5N, 6N, 7D
17-AUG-1997	2167	2A
18-AUG-1997	2168	2A, 4N, 5N, 6N, 7D
19-AUG-1997	2169	2A
13-SEP-1997	2194	7A
14-SEP-1997	2195	2A
15-SEP-1997	2196	2A
16-SEP-1997	2197	4N, 5N, 6N, 7D
17-SEP-1997	2198	2A
18-SEP-1997	2199	2N, 4N, 5N, 6N, 7D
19-SEP-1997	2200	2A
20-SEP-1997	2201	2A, 4N, 5N, 6N, 7D
21-SEP-1997	2202	2A
22-SEP-1997	2203	2A, 4N, 5N, 6N, 7D
23-SEP-1997	2204	2A
24-SEP-1997	2205	2A
09-OCT-1997	2220	7A
10-OCT-1997	2221	2A
11-OCT-1997	2222	2A, 4N, 5N, 6N, 7D
12-OCT-1997	2223	2A
13-OCT-1997	2224	2A, 4N, 5N, 6N, 7D
14-OCT-1997	2225	2A
24-NOV-1997	2266	2A, 7D
25-NOV-1997	2267	2A
26-NOV-1997	2268	2N
27-NOV-1997	2269	2N
28-NOV-1997	2270	2N
29-NOV-1997	2271	2N
30-NOV-1997	2272	2A

Note: Label A in the measurement column indicates All day measurement. D means day, and N for night. Label * shows there is no level 1 output even if there is level 0 measurements.

<Appendix A2>

Date	Uday	Measurement
09-AUG-1997	2159	7A
12-AUG-1997	2162	7A
13-AUG-1997	2163	2A
14-AUG-1997	2164	2A, 3A, 4D
15-AUG-1997	2165	2A, 3A, 4D
16-AUG-1997	2166	2A, 4N, 5N, 6N, 7D
17-AUG-1997	2167	2A
18-AUG-1997	2168	2A, 4N, 5N, 6N, 7D
19-AUG-1997	2169	2A
13-SEP-1997	2194	7A
14-SEP-1997	2195	2A
15-SEP-1997	2196	2A
16-SEP-1997	2197	4N, 5N, 6N, 7D
17-SEP-1997	2198	2A
18-SEP-1997	2199	2N, 4N, 5N, 6N, 7D
19-SEP-1997	2200	2A
20-SEP-1997	2201	2A, 4N, 5N, 6N, 7D
21-SEP-1997	2202	2A
22-SEP-1997	2203	2A, 4N, 5N, 6N, 7D
23-SEP-1997	2204	2A
24-SEP-1997	2205	2A
09-OCT-1997	2220	7A
10-OCT-1997	2221	2A
11-OCT-1997	2222	2A, 4N, 5N, 6N, 7D
12-OCT-1997	2223	2A
13-OCT-1997	2224	2A, 4N, 5N, 6N, 7D
14-OCT-1997	2225	2A
24-NOV-1997	2266	2A, 7D
25-NOV-1997	2267	2A
26-NOV-1997	2268	2N
27-NOV-1997	2269	2N
28-NOV-1997	2270	2N
29-NOV-1997	2271	2N
30-NOV-1997	2272	2A
01-DEC-1997	2273	4N, 5N, 6N, 7D
02-DEC-1997	2274	2A*
03-DEC-1997	2275	4N, 5N, 6N, 7D
04-DEC-1997	2276	2A*
05-DEC-1997	2277	2A*
06-DEC-1997	2278	2A*
07-DEC-1997	2279	2N, 4N, 5N, 6N, 7D
23-DEC-1997	2295	2A
24-DEC-1997	2296	2D, 4N, 5N, 6N, 7D
25-DEC-1997	2297	2A
26-DEC-1997	2298	2A, 4N, 5N, 6N, 7D
27-DEC-1997	2299	2A
03-FEB-1998	2337	2A
04-FEB-1998	2338	2A, 4N, 5N, 6N, 7D
05-FEB-1998	2339	2A, 4N, 5N, 6N
06-FEB-1998	2340	2N, 4N, 5N, 6N, 7D
07-FEB-1998	2341	2A, 4N, 5N, 6N
08-FEB-1998	2342	2A, 4N, 5N, 6N, 7D
09-FEB-1998	2343	2A, 4N, 5N, 6N
10-FEB-1998	2344	2A, 4N, 5N, 6N, 7D
11-FEB-1998	2345	2A
12-FEB-1998	2346	4N, 5N, 6N, 7D
01-MAR-1998	2363	2A
02-MAR-1998	2364	2D, 4N, 5N, 6N, 7D
03-MAR-1998	2365	2A
04-MAR-1998	2366	2A, 4N, 5N, 6N, 7D
05-MAR-1998	2367	2A
06-MAR-1998	2368	2D, 4N, 5N, 6N, 7D
13-MAR-1998	2375	2A
14-MAR-1998	2376	4N, 5N, 6N, 7D
15-MAR-1998	2377	2D
16-MAR-1998	2378	2D, 7D
17-MAR-1998	2379	2D
18-MAR-1998	2380	4N, 5N, 6N, 7D
19-MAR-1998	2381	2D
20-MAR-1998	2382	7D
21-MAR-1998	2383	2A
04-APR-1998	2397	2A
05-APR-1998	2398	2D, 4A, 5A, 6A, 7D
06-APR-1998	2399	2A
07-APR-1998	2400	2D, 4A, 5A, 6A, 7D
20-APR-1998	2413	2A
21-APR-1998	2414	2D
22-APR-1998	2415	X
23-APR-1998	2416	X
11-MAY-1998	2434	2A
12-MAY-1998	2435	2A
13-MAY-1998	2436	2A
14-MAY-1998	2437	2A
15-MAY-1998	2438	2A
16-MAY-1998	2439	2A
17-MAY-1998	2440	2A
18-MAY-1998	2441	2A
19-MAY-1998	2442	2A
20-MAY-1998	2443	2A
21-MAY-1998	2444	2A
22-MAY-1998	2445	2A
23-MAY-1998	2446	2A
24-MAY-1998	2447	X
25-MAY-1998	2448	2D

Date	Uday	Measurement	Date	Uday	Measurement
22-JUN-1998	2476	2A	21-NOV-1998	2628	2A, 7D
23-JUN-1998	2477	2A	25-NOV-1998	2632	2A
24-JUN-1998	2478	2A	26-NOV-1998	2633	2A
25-JUN-1998	2479	X	27-NOV-1998	2634	2A
26-JUN-1998	2480	2N	28-NOV-1998	2635	2A
27-JUN-1998	2481	2N	29-NOV-1998	2636	2A
28-JUN-1998	2482	X	30-NOV-1998	2637	2A
08-AUG-1998	2523	2D	08-DEC-1998	2645	2A
09-AUG-1998	2524	2D	09-DEC-1998	2646	2A
10-AUG-1998	2525	2A	10-DEC-1998	2647	2A
11-AUG-1998	2526	2A	11-DEC-1998	2648	2A
12-AUG-1998	2527	2A	12-DEC-1998	2649	2A
19-AUG-1998	2534	2A	20-DEC-1998	2657	2A
20-AUG-1998	2535	2A	21-DEC-1998	2658	2A
21-AUG-1998	2536	2A	22-DEC-1998	2659	2N
22-AUG-1998	2537	2A	23-DEC-1998	2660	2N
23-AUG-1998	2538	2A	07-JAN-1999	2675	2A
14-SEP-1998	2560	X	08-JAN-1999	2676	2N
16-SEP-1998	2562	2A	09-JAN-1999	2677	2N
17-SEP-1998	2563	2D, 4N, 5N, 6N, 7D	10-JAN-1999	2678	2N
18-SEP-1998	2564	4N, 5N, 6N, 7D	26-JAN-1999	2694	2A
19-SEP-1998	2565	4N, 5N, 6N, 7D	27-JAN-1999	2695	2A
20-SEP-1998	2566	4N, 5N, 6N, 7D	28-JAN-1999	2696	2A
21-SEP-1998	2567	4N, 5N, 6N, 7D	29-JAN-1999	2697	2A
22-SEP-1998	2568	4N, 5N, 6N, 7D	30-JAN-1999	2698	2A
23-SEP-1998	2569	4N, 5N, 6N, 7D	31-JAN-1999	2699	2N
24-SEP-1998	2570	4N, 5N, 6N, 7D	01-FEB-1999	2700	2A
25-SEP-1998	2571	X	02-FEB-1999	2701	2A
05-OCT-1998	2581	2A	03-FEB-1999	2702	2A
06-OCT-1998	2582	2D, 4N, 5N, 6N, 7D	04-FEB-1999	2703	2A
07-OCT-1998	2583	4N, 5N, 6N, 7D	05-FEB-1999	2704	2A
08-OCT-1998	2584	4N, 5N, 6N, 7D	06-FEB-1999	2705	2A
09-OCT-1998	2585	2A	07-FEB-1999	2706	2A
10-OCT-1998	2586	2A, 3D	05-MAR-1999	2732	2A
11-OCT-1998	2587	2N, 3D, 4N, 5N, 6N,	06-MAR-1999	2733	2A
17-OCT-1998	2593	2A	07-MAR-1999	2734	2A
18-OCT-1998	2594	2D, 4N, 5N, 6N, 7D	08-MAR-1999	2735	2A
19-OCT-1998	2595	2A, 4N, 5N, 6N	09-MAR-1999	2736	2A
20-OCT-1998	2596	2A, 4N, 5N, 6N, 7D	10-MAR-1999	2737	X
21-OCT-1998	2597	2A	11-MAR-1999	2738	2A
22-OCT-1998	2598	2A, 4N, 5N, 6N, 7D	12-MAR-1999	2739	2A
07-NOV-1998	2614	2A	13-MAR-1999	2740	2A
08-NOV-1998	2615	2D, 4N, 5N, 6N, 7D	14-MAR-1999	2741	2N
09-NOV-1998	2616	2A	15-MAR-1999	2742	2A
10-NOV-1998	2617	2D, 4N, 5N, 6N, 7D	16-MAR-1999	2743	2A
11-NOV-1998	2618	2A			
12-NOV-1998	2619	2D, 4N, 5N, 6N, 7D			
13-NOV-1998	2620	2A			
14-NOV-1998	2621	2D, 4N, 5N, 6N, 7D			
20-NOV-1998	2627	2A			

Date	Uday	Measurement
13-APR-1999	2771	2A
14-APR-1999	2772	2A
15-APR-1999	2773	2A
16-APR-1999	2774	2A
17-APR-1999	2775	2A
18-APR-1999	2776	2A
19-APR-1999	2777	2A
25-APR-1999	2783	2A
26-APR-1999	2784	2D*, 3A*
28-APR-1999	2786	2A*
29-APR-1999	2787	2A*
14-MAY-1999	2802	2A
15-MAY-1999	2803	2A
16-MAY-1999	2804	2D, 4N, 5N, 6N
17-MAY-1999	2805	2A
19-MAY-1999	2807	X
20-MAY-1999	2808	2D
21-MAY-1999	2809	2D
22-MAY-1999	2810	2D
23-MAY-1999	2811	2D
24-MAY-1999	2812	2A
25-MAY-1999	2813	2D, 4N, 5N, 6N
26-MAY-1999	2814	2A
27-MAY-1999	2815	2D, 4N, 5N, 6N
28-MAY-1999	2816	2A
29-MAY-1999	2817	2D, 3A
30-MAY-1999	2818	2A, 3D
02-JUN-1999	2821	2A
03-JUN-1999	2822	2D, 4N, 5N, 6N
04-JUN-1999	2823	2A
05-JUN-1999	2824	2D, 4N, 5N, 6N
06-JUN-1999	2825	2A
07-JUN-1999	2826	2D, 4N, 5N, 6N
08-JUN-1999	2827	2A
09-JUN-1999	2828	2D, 4N, 5N, 6N
19-JUL-1999	2868	2A
20-JUL-1999	2869	2A
21-JUL-1999	2870	2A
26-JUL-1999	2875	2A
27-JUL-1999	2876	2D, 4N, 5N, 6N
28-JUL-1999	2877	2A, 4N, 5N, 6N
12-AUG-1999	2892	2A
13-AUG-1999	2893	2A, 3A
14-AUG-1999	2894	X
27-AUG-1999	2907	2A
28-AUG-1999	2908	2A
29-AUG-1999	2909	2A
30-AUG-1999	2910	2D, 4N, 5N, 6N
31-AUG-1999	2911	2A

Date	Uday	Measurement
01-SEP-1999	2912	2A
02-SEP-1999	2913	2D, 4N, 5N, 6N
10-SEP-1999	2921	2A
11-SEP-1999	2922	2A
12-SEP-1999	2923	2A, 4N, 5N, 6N
13-SEP-1999	2924	2A
14-SEP-1999	2925	2A, 4N, 5N, 6N
12-OCT-1999	2953	2A
13-OCT-1999	2954	2A, 4N, 5N, 6N
14-OCT-1999	2955	2A
15-OCT-1999	2956	2A, 4N, 5N, 6N
16-OCT-1999	2957	2A
17-OCT-1999	2958	2D, 4N, 5N, 6N
18-OCT-1999	2959	2A
19-OCT-1999	2960	2D, 4N, 5N, 6N
20-OCT-1999	2961	2A
21-OCT-1999	2962	2D, 4N, 5N, 6N
22-OCT-1999	2963	2A
23-OCT-1999	2964	2A
06-NOV-1999	2978	2A
07-NOV-1999	2979	2A
08-NOV-1999	2980	2A
09-NOV-1999	2981	2D*, 4N*, 5N*, 6N*
10-NOV-1999	2982	2A*
11-NOV-1999	2983	2A, 4N, 5N, 6N
12-NOV-1999	2984	2A
13-NOV-1999	2985	2A
14-NOV-1999	2986	2A
22-NOV-1999	2994	2A
23-NOV-1999	2995	2D, 3A
24-NOV-1999	2996	2A, 3A
25-NOV-1999	2997	2A, 4N, 5N, 6N
26-NOV-1999	2998	2D, 4N, 5N, 6N
15-DEC-1999	3017	2A
16-DEC-1999	3018	2D, 3A
17-DEC-1999	3019	2D, 3N, 4N, 5N, 6N
18-DEC-1999	3020	2A
19-DEC-1999	3021	2A
20-DEC-1999	3022	2A
21-DEC-1999	3023	2A
22-DEC-1999	3024	2N
23-DEC-1999	3025	2N

Date	Uday	Measurement	Date	Uday	Measurement
18-JAN-2000	3051	2A	19-JUL-2000	3234	2A
19-JAN-2000	3052	2A	20-JUL-2000	3235	2A
20-JAN-2000	3053	2A	21-JUL-2000	3236	2A
21-JAN-2000	3054	2A	30-JUL-2000	3245	2A
22-JAN-2000	3055	2A	31-JUL-2000	3246	2A
23-JAN-2000	3056	2A	01-AUG-2000	3247	2A
06-MAR-2000	3099	2D	02-AUG-2000	3248	2A
07-MAR-2000	3100	2D	03-AUG-2000	3249	2A
08-MAR-2000	3101	2D	04-AUG-2000	3250	2A
09-MAR-2000	3102	2D	05-AUG-2000	3251	2A
10-MAR-2000	3103	2D	06-AUG-2000	3252	2A
11-MAR-2000	3104	2D	07-AUG-2000	3253	2A
12-MAR-2000	3105	2D	08-AUG-2000	3254	2A*
13-MAR-2000	3106	2D	09-AUG-2000	3255	2A
14-MAR-2000	3107	2D	07-SEP-2000	3284	2A
15-MAR-2000	3108	2D	08-SEP-2000	3285	2A
16-MAR-2000	3109	2D	09-SEP-2000	3286	2A*
06-APR-2000	3130	2D	10-SEP-2000	3287	2A*
07-APR-2000	3131	2D	11-SEP-2000	3288	2D*
08-APR-2000	3132	2D*	07-OCT-2000	3314	2A
09-APR-2000	3133	2D	08-OCT-2000	3315	2A*
10-APR-2000	3134	2D	09-OCT-2000	3316	2A
11-APR-2000	3135	2D	10-OCT-2000	3317	2A
12-APR-2000	3136	2D*	11-OCT-2000	3318	2A*
13-APR-2000	3137	2D	12-OCT-2000	3319	2A
14-APR-2000	3138	2D	13-OCT-2000	3320	2A
15-APR-2000	3139	2D	14-OCT-2000	3321	2A
16-APR-2000	3140	2D	15-OCT-2000	3322	2A
17-APR-2000	3141	2D	16-OCT-2000	3323	2A*
18-APR-2000	3142	2D	17-NOV-2000	3355	2D
19-APR-2000	3143	2D	18-NOV-2000	3356	2A
20-APR-2000	3144	2D	19-NOV-2000	3357	2A*
09-MAY-2000	3163	2D	20-NOV-2000	3358	2A
10-MAY-2000	3164	2D	21-NOV-2000	3359	2A
11-MAY-2000	3165	2D	22-NOV-2000	3360	2D, 4A, 5A, 6A
19-MAY-2000	3173	2D	23-NOV-2000	3361	2A
20-MAY-2000	3174	2D	24-NOV-2000	3362	2A
21-MAY-2000	3175	2D	25-NOV-2000	3363	2A
22-MAY-2000	3176	2D			
23-MAY-2000	3177	2D*			
24-MAY-2000	3178	2D*			
25-MAY-2000	3179	2D			
26-MAY-2000	3180	2D*			
27-MAY-2000	3181	2D			
28-MAY-2000	3182	2D			
29-MAY-2000	3183	2D			
30-MAY-2000	3184	2D			

Date	Uday	Measurement
15-JUN-2001	3565	2A
16-JUN-2001	3566	2A
17-JUN-2001	3567	2A
18-JUN-2001	3568	2A
13-JUL-2001	3593	2A*
14-JUL-2001	3594	2A
15-JUL-2001	3595	2A
16-JUL-2001	3596	2A
17-JUL-2001	3597	2A
18-JUL-2001	3598	X
19-JUL-2001	3599	X
17-AUG-2001	3628	2A
18-AUG-2001	3629	2D
19-AUG-2001	3630	X
20-AUG-2001	3631	X
21-AUG-2001	3632	X
22-AUG-2001	3633	X
23-AUG-2001	3634	X
24-AUG-2001	3635	X
25-AUG-2001	3636	X
26-AUG-2001	3637	X
22-SEP-2001	3664	2A
24-SEP-2001	3666	4N, 5N, 6N, 7D
11-MAY-2002	3895	X
12-MAY-2002	3896	X
13-MAY-2002	3897	X
14-MAY-2002	3898	X
15-MAY-2002	3899	X
31-MAY-2002	3915	X
01-JUN-2002	3916	X
02-JUN-2002	3917	X
03-JUN-2002	3918	X
04-JUN-2002	3919	X
05-JUN-2002	3920	X
06-JUN-2002	3921	X
07-JUN-2002	3922	X
08-JUN-2002	3923	X
09-JUN-2002	3924	X
10-JUN-2002	3925	X
11-JUN-2002	3926	X
13-JUN-2002	3928	X
15-JUN-2002	3930	X
07-JUL-2002	3952	X
08-JUL-2002	3953	X
09-JUL-2002	3954	X
10-JUL-2002	3955	X
11-JUL-2002	3956	2D
12-JUL-2002	3957	X
10-AUG-2002	3986	X
12-AUG-2002	3988	X
13-AUG-2002	3989	X
14-AUG-2002	3990	X
15-AUG-2002	3991	X
16-AUG-2002	3992	X
17-AUG-2002	3993	X
18-AUG-2002	3994	2A
29-OCT-2002	4066	2D*
30-OCT-2002	4067	2D
31-OCT-2002	4068	2D
01-NOV-2002	4069	2D
02-NOV-2002	4070	2A
03-NOV-2002	4071	2A
04-NOV-2002	4072	2A
05-NOV-2002	4073	2A
06-NOV-2002	4074	2A
07-NOV-2002	4075	2A
08-NOV-2002	4076	2A
09-NOV-2002	4077	2A
10-NOV-2002	4078	2A*
11-NOV-2002	4079	2A
12-NOV-2002	4080	2A
13-NOV-2002	4081	2A*
27-NOV-2002	4095	2A
28-NOV-2002	4096	2A*
30-NOV-2002	4098	2A
01-DEC-2002	4099	2A
02-DEC-2002	4100	2A
03-DEC-2002	4101	2A
24-DEC-2002	4122	2A
25-DEC-2002	4123	2A
26-DEC-2002	4124	2A*
27-DEC-2002	4125	2A*
28-DEC-2002	4126	2A*
29-DEC-2002	4127	2A
30-DEC-2002	4128	2A
31-DEC-2002	4129	2A

Date	Uday	Measurement
01-JAN-2003	4130	2A
02-JAN-2003	4131	2A
03-JAN-2003	4132	2A
04-JAN-2003	4133	2A
05-JAN-2003	4134	2A
06-JAN-2003	4135	2A
07-JAN-2003	4136	2A
08-JAN-2003	4137	2A*
09-JAN-2003	4138	2A
10-JAN-2003	4139	2A
14-JAN-2003	4143	2A*
15-JAN-2003	4144	2A*
03-FEB-2003	4163	2A
04-FEB-2003	4164	2A
05-FEB-2003	4165	2A
06-FEB-2003	4166	2A
07-FEB-2003	4167	2A*
08-FEB-2003	4168	2A
09-FEB-2003	4169	2A
10-FEB-2003	4170	2A*
11-FEB-2003	4171	2A
13-FEB-2003	4173	2A
08-MAR-2003	4196	2A
09-MAR-2003	4197	2A
10-MAR-2003	4198	2A
11-MAR-2003	4199	2A*
12-MAR-2003	4200	2A
13-MAR-2003	4201	2A*
14-MAR-2003	4202	2A
15-MAR-2003	4203	2A*
16-MAR-2003	4204	2A
17-MAR-2003	4205	2A*
18-MAR-2003	4206	2A
19-MAR-2003	4207	2A
20-MAR-2003	4208	2A
21-MAR-2003	4209	2A
22-MAR-2003	4210	2A
23-MAR-2003	4211	2A
24-MAR-2003	4212	2A
25-MAR-2003	4213	2A*
26-MAR-2003	4214	2A
27-MAR-2003	4215	2A
29-MAR-2003	4217	2A
30-MAR-2003	4218	4N, 5N, 6N, 7D
31-MAR-2003	4219	2A
13-APR-2003	4232	2A
14-APR-2003	4233	2A
15-APR-2003	4234	2A
16-APR-2003	4235	2A
17-APR-2003	4236	2A
18-APR-2003	4237	2A
19-APR-2003	4238	2A
20-APR-2003	4239	2A
21-APR-2003	4240	2A
22-APR-2003	4241	2A
23-APR-2003	4242	2A*
24-APR-2003	4243	2A
25-APR-2003	4244	2A
26-APR-2003	4245	2A*
27-APR-2003	4246	2A
28-APR-2003	4247	2A
30-APR-2003	4249	2A
01-MAY-2003	4250	2A
02-MAY-2003	4251	2A*
04-MAY-2003	4253	2A
05-MAY-2003	4254	2A
06-MAY-2003	4255	2A
07-MAY-2003	4256	2A
08-MAY-2003	4257	4N, 5N, 6N, 7D
29-JUN-2003	4309	2A
30-JUN-2003	4310	2A*
01-JUL-2003	4311	2A
02-JUL-2003	4312	2A
03-JUL-2003	4313	2N
07-JUL-2003	4317	2D
17-JUL-2003	4327	2D
15-AUG-2003	4356	2A
16-AUG-2003	4357	2A
17-AUG-2003	4358	2A
18-AUG-2003	4359	2A
11-SEP-2003	4383	2D
12-SEP-2003	4384	2A
13-SEP-2003	4385	2A
14-SEP-2003	4386	2A
15-SEP-2003	4387	2A
16-SEP-2003	4388	2A
17-SEP-2003	4389	2A
18-SEP-2003	4390	4N, 5N, 6N, 7D
19-SEP-2003	4391	2A

Note: Label A in the measurement column indicates All day measurement. D means day, and N for night. Label * shows there is no level 1 output even if there are level 0 measurements.

<Appendix B>

This appendix contains the header information contained in the WINDII SDPPS output files

[windii_l0]

Measurement header data

DATAID	BYTE	204
UT	LONG	Array[2]
ORBIT	BYTE	2
ORBSEQ	BYTE	0
FWDREV	BYTE	1
CYCLE	BYTE	9
CYCLERPT	BYTE	8
FILTGR	BYTE	27
START_TIME	FLOAT	912.256
MSRFLTR	BYTE	1
OBSCAT	BYTE	1
SOBSID	BYTE	1
NBRIMG	BYTE	1
HBIN	BYTE	5
NBRRPT	BYTE	0
VBIN	BYTE	1
HIGH	BYTE	33
VOFFSET	BYTE	0
WIDE	BYTE	31
HOFFSET	BYTE	2
SEPARAT	BYTE	0
NTOP	INT	224
WT	LONG	6
MSRID	LONG	30495
APRT_STAT	BYTE	0
FWPOS_STAT	BYTE	1
EXPTIME	FLOAT	3.96800
FOV1OBL	FLOAT	67.5000
FOV2OBL	FLOAT	75.0000
EMAFTT	FLOAT	48.8960

Measurement profile data

DATAID	BYTE	170
UTMS	LONG	13071447
MSRNBR	BYTE	1
IMGNBR	BYTE	1
MIRPOS	INT	-230
EMAFTT	FLOAT	48.8960
CCDTEMP	FLOAT	-49.1045
DCMON	INT	Array[4]
DATA	INT	Array[WIDE, HIGH, FOV]

[T1_MDO]

Measurement header data

ID	LONG	44363
UT	LONG	Array[2]
UTR	LONG	Array[2]
OBSCAT	LONG	2
SPOBS	LONG	1
FWDREV	LONG	1
WT	LONG	4
FILGR	LONG	7
FILT	LONG	2
NBIMA	LONG	8
REPT	LONG	0
NVB	LONG	2
NHB	LONG	25
NI	LONG	25
NJ	LONG	6
NTOP	LONG	205
NHO	LONG	7
APST	LONG	Array[2]
EXPTIM	LONG	1024
QUALY	LONG	0
QUALYR	LONG	0

Measurement profile data

I_M	LONG	Array[NJ, NI, FOV, NBIMA]
DCM	LONG	Array[4, NBIMA]
IMANB	LONG	1
IMAQUAL	LONG	0
IMATIME	LONG	22712
T_CCD	FLOAT	-49.4370

[T1_CMI]

Measurement header data

ID	LONG	46193
UT	LONG	Array[2]
UTR	LONG	Array[2]
OBSCAT	LONG	2
SPOBS	LONG	1
FWDREV	LONG	1
WT	LONG	2
FILGR	LONG	7
FILT	LONG	2
NBIMA	LONG	8
REPT	LONG	0
NVB	LONG	2

```
   NHB              LONG                   25
   NI               LONG                   22
   NJ               LONG                    6
   NTOP             LONG                  213
   NHO              LONG                    7
   APST             LONG      Array[2]
   EXPTIM           LONG                 1024
   QUALY            LONG      Array[2]
   QUALYR           LONG      Array[2]
   T_CCD            FLOAT          -48.6365
```

Measurement profile data

```
   DCM_CR           FLOAT           250.750
   IMANB            LONG                    1
   IMATIME          LONG             86384596
   I_CR             FLOAT     Array[NJ, NI, FOV, NBIMA]
   SIGMA_CR         FLOAT     Array[NJ, NI, FOV, NBIMA]
   FLAGS            BYTE      Array[NJ, NI, FOV, NBIMA]
```

[L1_CVA]

Measurement header data

Mhead1

```
   ID               LONG                44780
   UT               LONG      Array[2]
   LTIME            FLOAT     Array[2]
   UTR              LONG      Array[2]
   LTIMER           FLOAT     Array[2]
   OBSCAT           LONG                    2
   SPOBS            LONG                    1
   FWDREV           LONG                    1
   WT               LONG                    2
   FILGR            LONG                    7
   FILT             LONG                    2
   NBIMA            LONG                    8
   REPT             LONG                    0
   NVB              LONG                    2
   NHB              LONG                   25
   NI               LONG                   23
   NJ               LONG                    6
   NTOP             LONG                  211
   NHO              LONG                    7
   APST             LONG      Array[2]
   EXPTIM           LONG                 1024
   ZS               FLOAT           580.897
   QUALY            LONG      Array[2]
   QUALYR           LONG      Array[2]
```

Mhead2

ZR	FLOAT	Array[23, 2]
LATR	FLOAT	Array[23, 2]
LONGR	FLOAT	Array[23, 2]
LOOKR	FLOAT	Array[23, 2]
DELTA_ZR	FLOAT	Array[2]
DELTA_LAT	FLOAT	Array[2]
DELTA_LONG	FLOAT	Array[2]
DEL_C_LAMB	FLOAT	4.64733e+07
T_CCD	FLOAT	-49.1045

Measurement profile data

Mdata1

I_CR	FLOAT	Array[6, 23, 2]
SIGMA_CR	FLOAT	Array[6, 23, 2]
Z	FLOAT	Array[6, 23, 2]
FLAGS	BYTE	Array[6, 23, 2]
IMANB	LONG	1

Mdata2

I_R	FLOAT	Array[6, 23, 2]
SIGMA_R	FLOAT	Array[6, 23, 2]

Mdata3

PHI_VO	FLOAT	Array[6, 23, 2]
DCM_CR	FLOAT	319.625
ZR3	FLOAT	Array[23, 2]
LATR3	FLOAT	Array[23, 2]
LONGR3	FLOAT	Array[23, 2]
LOOKR3	FLOAT	Array[23, 2]
DELTA_ZR3	FLOAT	Array[2]
DELTA_LATR3	FLOAT	Array[2]
DELTA_LONGR3	FLOAT	Array[2]

[L1_CVB]

Measurement header data

Mhead1

ID	LONG	35458
UT	LONG	Array[2]
LTIME	FLOAT	Array[2]
UTR	LONG	Array[2]
LTIMER	FLOAT	Array[2]
OBSCAT	LONG	2

```
   SPOBS           LONG                 1
   FWDREV          LONG                 0
   WT              LONG                 3
   FILGR           LONG                12
   FILT            LONG                 1
   NBIMA           LONG                 1
   REPT            LONG                 0
   NVB             LONG                 6
   NHB             LONG                25
   NI              LONG                34
   NJ              LONG                 6
   NTOP            LONG                17
   NHO             LONG                 7
   APST            LONG      Array[2]
   EXPTIM          LONG              1536
   ZS              FLOAT          576.798
   QUALY           LONG      Array[2]
   QUALYR          LONG      Array[2]


Mhead2

   ZR              FLOAT     Array[34, 2]
   LATR            FLOAT     Array[34, 2]
   LONGR           FLOAT     Array[34, 2]
   LOOKR           FLOAT     Array[34, 2]
   T_CCD           FLOAT         -49.4369


Measurement profile data

Mdata1

   I_CR            FLOAT     Array[6, 34, 2]
   SIGMA_CR        FLOAT     Array[6, 34, 2]
   Z               FLOAT     Array[6, 34, 2]
   FLAGS           BYTE      Array[6, 34, 2]

Mdata2

   K1              FLOAT     Array[2]
   K2              FLOAT     Array[2]
   H               FLOAT     Array[2]
   S_Z0            FLOAT     Array[2]

Mdata3

   NO2             FLOAT     Array[34, 2]
```

[L1_CVD]

Measurement header data

```
   ID              LONG            15416
   UT              LONG      Array[2]
   WT              LONG                3
   FILGR           LONG               13
   FILT            LONG                7
   NBIMA           LONG                1
   NVB             LONG                6
   NHB             LONG               25
   NI              LONG               40
   NJ              LONG                6
   NTOP            LONG               17
   NHO             LONG                7
   APST            LONG      Array[2]
   EXPTIM          LONG             1536
   QUALY           LONG                0
```

Measurement profile data

```
   I_DC            LONG      Array[6, 40, 2]
   DCM             LONG      Array[4]
   T_CCD           FLOAT        -49.4369
   IMATIME         LONG         85687901
   IMQUAL_DC       FLOAT     Array[6, 2]
```

[L1_CVP]

Measurement header data

```
   ID              LONG            15416
   UT              LONG      Array[2]
   WT              LONG                3
   FILGR           LONG               13
   FILT            LONG                7
   NBIMA           LONG                1
   NVB             LONG                6
   NHB             LONG               25
   NI              LONG               40
   NJ              LONG                6
   NTOP            LONG               17
   NHO             LONG                7
   APST            LONG      Array[2]
   EXPTIM          LONG             1536
   QUALY           LONG                0
```

Measurement profile data

```
   I_DC            LONG      Array[6, 40, 2]
   DCM             LONG      Array[4]
```

```
T_CCD           FLOAT         -49.4369
IMATIME         LONG         85687901
IMQUAL_DC       FLOAT     Array[6, 2]
```

[L1_CALINF]

Measurement header data

```
DAYTIME         LONG      Array[2]
QUALI           LONG                 0
NBBYTE          LONG             32706
NBIMA           LONG                 1
*CALHEA         BYTE      Array[36]
```

*CALHEA[36] is the calibration header packet that contains the following information:

calibration ID, Orbit, Filter group, start time, calibration filter, calibration source,number of images, horizontal and vertical bin dimension, vertical height and offset of window, horizontal wide and offset of window, aperture 1 and 2 status, Filter wheel position, exposure time, lase light out voltage, laser current, laser temp, laser PZT,laser consumption, laser stable, white light source out voltage, white light source temperature, mirror error of x,y, and z, mirror integration of x,y, and z, EMAF time tag, and ELS output voltage.

Measurement profile data

```
*CALIMAHEA      BYTE      Array[12]

TB_BIN          BYTE      Array[32706]
```

*CALIMAHEA is the calibration image headers that contains the following information:image ID, measurement number, images number, mirror position, EMAF timetag, calibration source output voltage, and CCD temperature

[L1_CVP]

Measurement header data

```
ID              LONG             24347
UT              LONG      Array[2]
WT              LONG                 4
FILGR           LONG                 7
FILT            LONG                 8
NBIMA           LONG                 4
NVB             LONG                 2
NHB             LONG                25
```

NI	LONG	29
NJ	LONG	6
NTOP	LONG	199
NHO	LONG	7
APST	LONG	Array[2]
EXPTIM	LONG	1536
CALIBSOU	LONG	1
QUALY	LONG	2

Measurement profile data

Mdata

I_CR	FLOAT	Array[6, 29, 2]
DCM	LONG	Array[4]
T_CCD	FLOAT	-49.4369
IMATIME	LONG	86160821
IMANB	LONG	1
CALSOUR	FLOAT	7.20000e-06
FLAGS	BYTE	Array[6, 29, 2]

Mfrq1

J1	FLOAT	Array[6, 29, 2]
J2	FLOAT	Array[6, 29, 2]
J3	FLOAT	Array[6, 29, 2]
SIGMA_J1	FLOAT	Array[6, 29, 2]
SIGMA_J2	FLOAT	Array[6, 29, 2]
SIGMA_J3	FLOAT	Array[6, 29, 2]

Mfrq2

PHI	FLOAT	Array[6, 29, 2]
V	FLOAT	Array[6, 29, 2]
SIGMA_PHI	FLOAT	Array[6, 29, 2]
SIGMA_V	FLOAT	Array[6, 29, 2]
IMQUAL	FLOAT	Array[6, 2]

[L2_FD]

Measurement header data

ID	LONG	44793
UT	LONG	Array[2]
LTIME	FLOAT	10.8662
UTR	LONG	Array[2]
LTIMER	FLOAT	0.00000
OBSCAT	LONG	2
FWDREV	LONG	2
FILGR	LONG	9
FILT	LONG	2

NBIMA	LONG	8
REPT	LONG	0
NHB	LONG	25
NVB	LONG	4
NJ	LONG	6
NI	LONG	49
NHO	LONG	7
NTOP	LONG	17
APST	LONG	0
EXPTIM	LONG	1024
QUALY	LONG	6
QUALYR	LONG	2
REF_NI	LONG	49
ZR	FLOAT	Array[49]
LATR	FLOAT	Array[49]
LONGR	FLOAT	Array[49]
LOOKR	FLOAT	Array[49]
DZR	FLOAT	3.59976
DLAT	FLOAT	0.404438
DLONG	FLOAT	2.08775
HZ	FLOAT	283.930
LZ	FLOAT	104.228
IFLAGDR	LONG	0
N_ALT	LONG	48

Measurement profile data

IDEC1	LONG	1
IDEC2	LONG	1
Z	FLOAT	Array[48]
W	FLOAT	Array[48]
SIG_W	FLOAT	Array[48]
E	FLOAT	Array[48]
SIG_E	FLOAT	Array[48]
T	FLOAT	Array[48]
SIG_T	FLOAT	Array[48]
NV	FLOAT	Array[48]

[L2_CD]

Measurement header data

ID	LONG	44458
UT	LONG	Array[2]
LTIME	FLOAT	99.9900
UTR	LONG	Array[2]
LTIMER	FLOAT	0.00000
OBSCAT	LONG	2
FWDREV	LONG	1
FILGR	LONG	7
FILT	LONG	2
NBIMA	LONG	8

REPT	LONG	0
NHB	LONG	25
NVB	LONG	2
NI	LONG	37
NJ	LONG	6
NHO	LONG	7
NTOP	LONG	203
APST	LONG	0
EXPTIM	LONG	1024
LAT	FLOAT	4.74340
LONG	FLOAT	129.646
SZA	FLOAT	Array[37]
QUALY	LONG	6
QUALYR	LONG	-5
QUFLAG	LONG	1
OTFLAG	LONG	1
OEFLAG	LONG	1
N_ALT	LONG	37

Measurement profile data

Z	FLOAT	Array[37]
E	FLOAT	Array[37]
SIG_E	FLOAT	Array[37]
W	FLOAT	Array[37, 2]
SIG_W	FLOAT	Array[37, 2]
T	FLOAT	Array[37]
SIG_T	FLOAT	Array[37]

[c_cdbi#.dat]

Measurement header data

SFDU	BYTE	Array[40]
DLMC	BYTE	Array[24]
DLUD	BYTE	Array[24]
VER_NUM	BYTE	Array[8]
AUTH_NAME	BYTE	Array[24]
HOR_OFFSET	LONG	2
VER_OFFSET	LONG	0
BIN_HEIGHT	LONG	1
BIN_WIDTH	LONG	5
CCDROW_NUM	LONG	256
CCDCOL_NUM	LONG	31
DESCRIP	BYTE	Array[80]

Measurement profile data

FOV1	FLOAT	Array[32, 256]
FOV2	FLOAT	Array[32, 256]
MAXROW	INT	256

```
   MAXCOL          INT            31
```

[cdbp.dat]

Measurement header data

CDBP_HDR

```
   SFDU            BYTE      Array[40]
   DLMC            BYTE      Array[24]
   DLUD            BYTE      Array[24]
   VER_NUM         BYTE      Array[8]
   AUTH_NAME       BYTE      Array[24]
   HOR_OFFSET      LONG                 2
   VER_OFFSET      LONG                 0
   BIN_HEIGHT      LONG                 1
   BIN_WIDTH       LONG                 5
   CCDROW_NUM      LONG               256
   CCDCOL_NUM      LONG                31
   DESCRIP         BYTE      Array[160]
```

CDBP_VAR

```
   PHASE_STEP_MIRROR4
                   FLOAT     Array[4, 10]
   PHASE_STEP_MIRROR8
                   FLOAT     Array[8, 6]
   OPD_A2222       FLOAT     Array[9]
   FILT4_GROUND_D  FLOAT     Array[3]
   FILT6_GROUND_D  FLOAT     Array[3]
   FILT4_ROT_E     FLOAT     Array[6]
   FILT6_ROT_E     FLOAT     Array[6]
   ROT_TEMP_O2C1   FLOAT           0.00000
   ROT_TEMP_O2C2   FLOAT           0.00000
   CONST_C3_OH4    FLOAT          -13.1840
   CONST_C3_OH6    FLOAT          -13.1840
   CONST_C4_OH4    FLOAT           6.60000
   CONST_C4_OH6    FLOAT           6.60000
   INTEG_POP_OH4   FLOAT     Array[5]
   INTEG_POP_OH6   FLOAT     Array[5]
   FOV_OV_LAP_TIME FLOAT     Array[8]
   ROW_AVE_DEV_LIM FLOAT           100.000
   FOV_VERT_DIMEN  LONG               240
   FOV_HOR_DIMEN   LONG               160
   HOR_ANG_SIZE_FOV
                   FLOAT     Array[2]
   VER_ANG_SIZE_FOV
                   FLOAT     Array[2]
   HOR_LOC_IMAG_OPT_AXIS
                   FLOAT     Array[2]
   VERT_LOC_IMAG_OPT_AXIS
                   FLOAT     Array[2]
```

```
   DELTA_ALPHA     FLOAT     Array[2]
   DELTA_BETA      FLOAT     Array[2]
   DELTA_ALPHA5    FLOAT     Array[2]
   DELTA_BETA5     FLOAT     Array[2]
   OA_ALPHA        FLOAT     Array[2]
   OA_BETA         FLOAT     Array[2]
   OPT_DIS_PARA_ADIS
                   FLOAT           1.00000
   OPT_DIS_PARA_BDIS
                   FLOAT           0.00000
   OPT_DIS_PARA_CDIS
                   FLOAT           0.00000
   OPT_DIS_PARA_AWDIS
                   FLOAT           1.00000
   OPT_DIS_PARA_BWDIS
                   FLOAT           0.00000
   OPT_DIS_PARA_CWDIS
                   FLOAT           0.00000
   DERV_OPD_CLAMDA FLOAT     Array[9]
   OPD_NEUT_VAR    FLOAT     Array[9]
   RAYL_SCAT_REF_ALT
                   FLOAT           85.0000
   DARK_CUR_THRES  FLOAT           10000.0
   DARK_CUR_MONITOR
                   FLOAT           0.00000
   ELEC_COUNT_CONV FLOAT           73.0000
   CONTRI_VARIANCE FLOAT           3.30000
   DC_AVER_STD     FLOAT     Array[2]
   BAD_BIN_CUR_MONITOR
                   LONG      Array[4]
   STAR_DETECT_CRIT
                   FLOAT     Array[32, 2]
   IPF_ROT_TRANS   FLOAT     Array[2, 2, 2]
   IPF_OMF_TRANS   FLOAT     Array[3, 3, 2]
   BAF_SCAT_REF_Z  FLOAT           0.00000
   S_557_551       FLOAT           1.24000
   B_557_551       FLOAT           1.24000
   B_630_551       FLOAT           1.16000
   B_732_737       FLOAT           1.00000
   AVG_WAV_CONV    FLOAT           1.22000
   NO2_557_551     FLOAT           1.36000
   NO2_732_735     FLOAT           0.00000
   NO2_734_735     FLOAT           0.00000
   NO2_737_735     FLOAT           0.00000
   ST_557_551      FLOAT           1.36000
   ST_630_551      FLOAT           1.16000
   ST_732_735      FLOAT           0.00000
   ST_734_735      FLOAT           0.00000
   ST_737_735      FLOAT           0.00000
Measurement profile data
CDBP_BSCM
   BSC             FLOAT     Array[6, 32, 2]
```

< APPENDIX C >

Diagnostics plots for the wave 4 cases – checking the quality of the VER, U and T profiles):

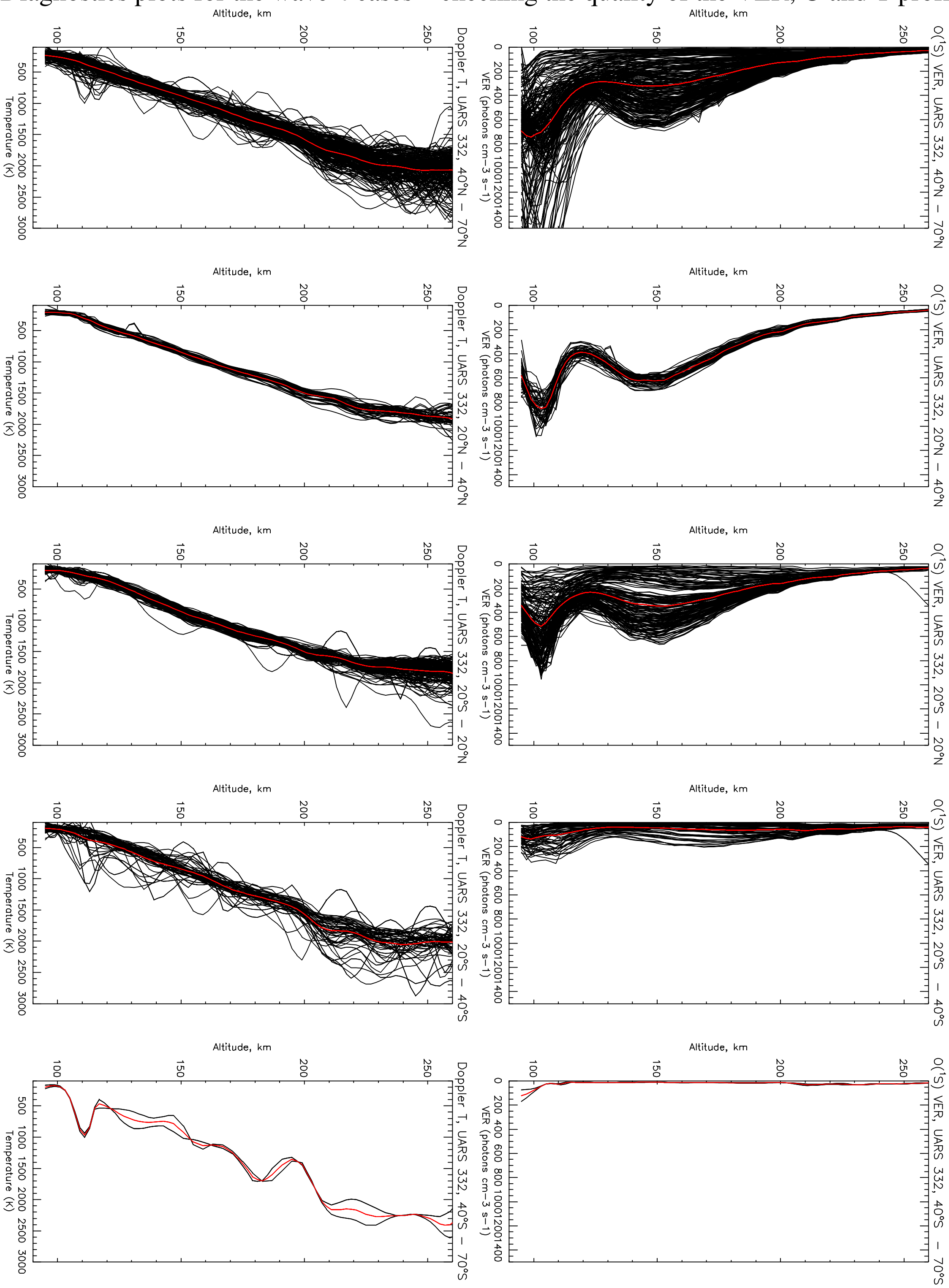

Figure C1: O(^{1}S) VER and Doppler temperature – UARS Day 332 (August 8, 1992)

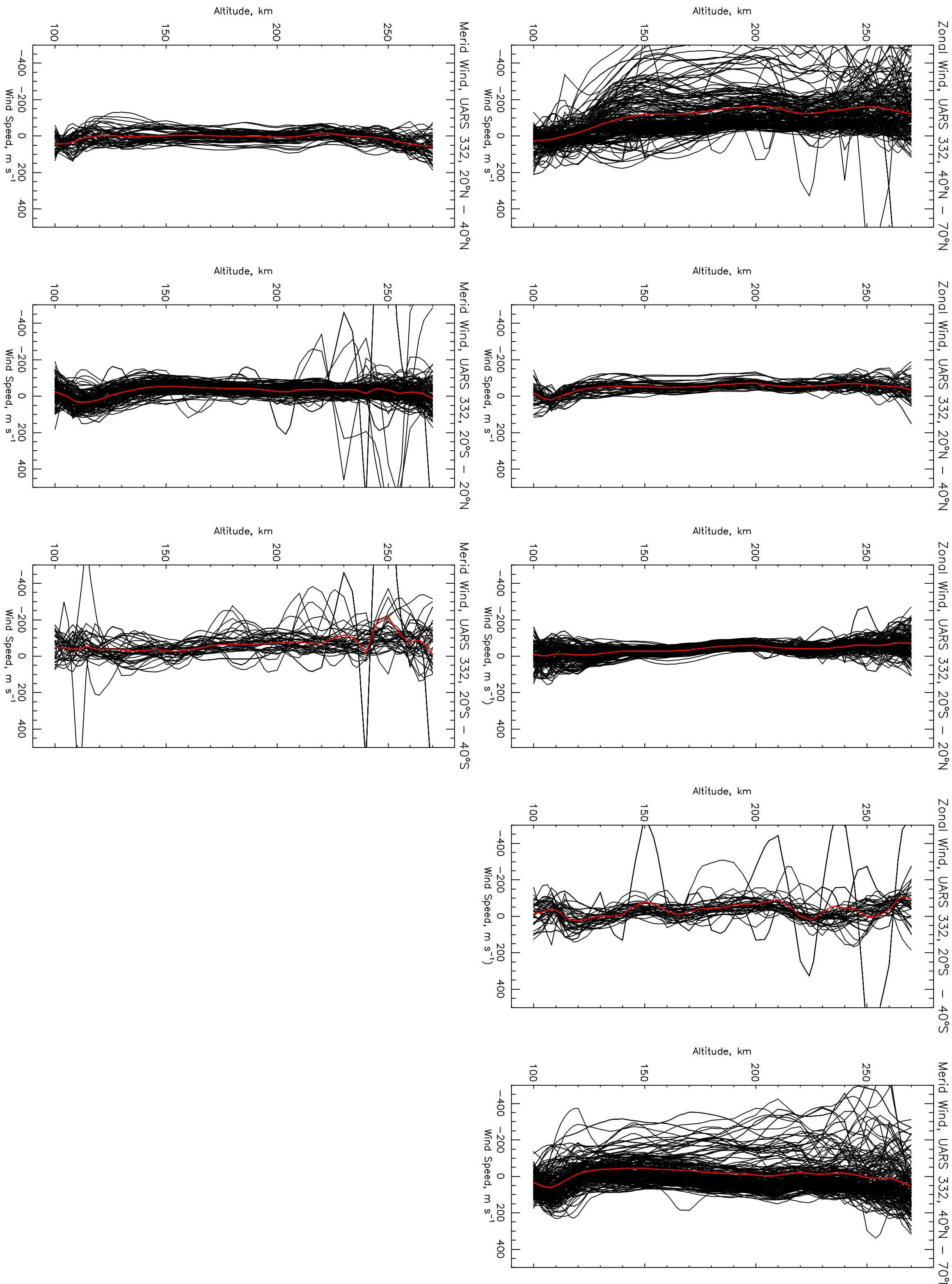

Figure C2: Zonal and meridional winds – UARS Day 332 (August 8, 1992)

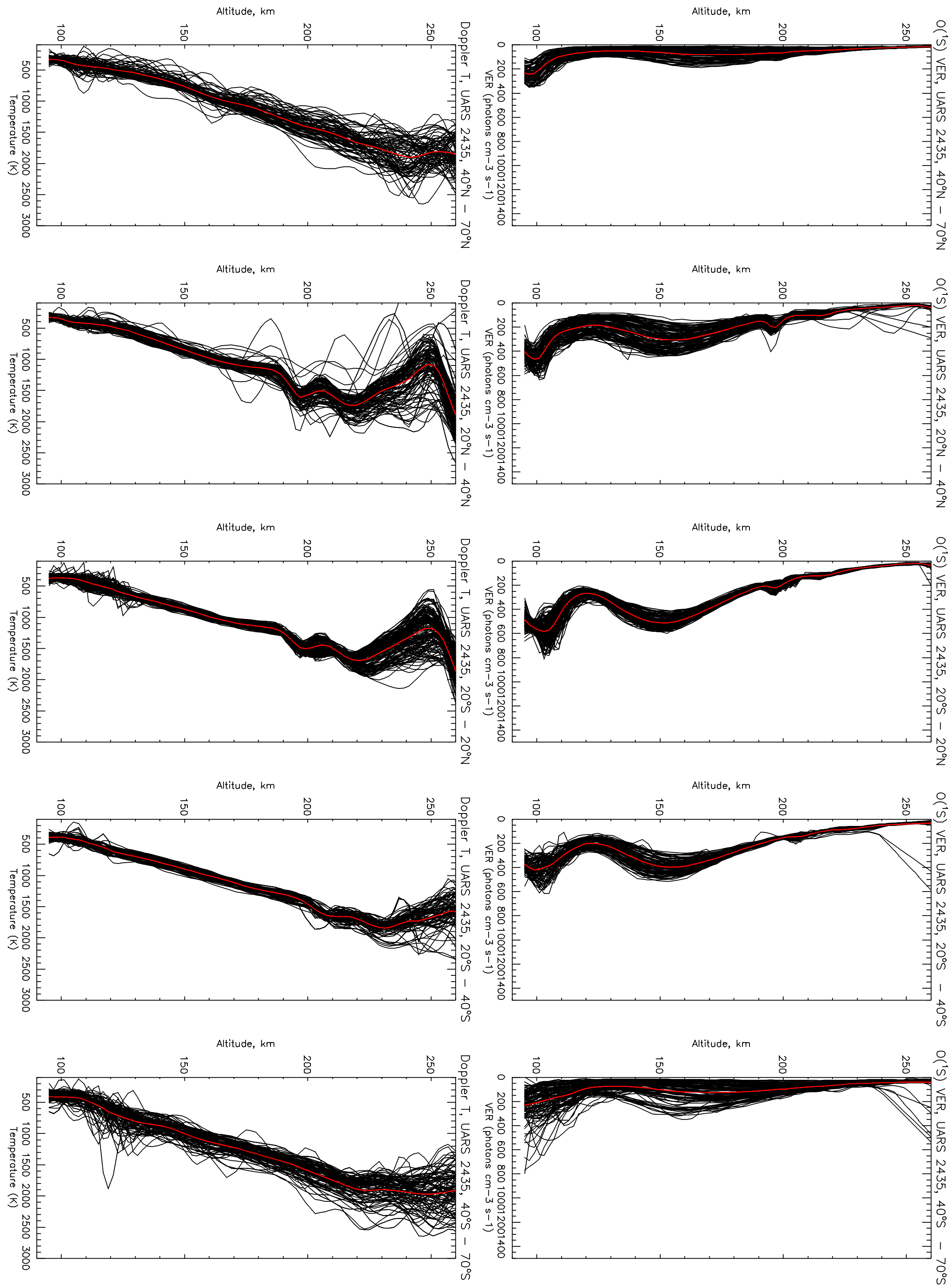

Figure C3: O(^{1}S) VER and Doppler temperature – UARS Day 2435 (May 12, 1998)

< Appendix D >

This Appendix contains a FORTRAN subroutine implemented in the extended CMAM for calculation of the nighttime mesospheric emissions in the OH Meinel and O_2 Atmospheric bands, and in the O green line.

```
C*************************************************************
C*                                                           *
C*                  SUBROUTINE AIRGLOW2                      *
C*                                                           *
C*************************************************************

c   To calculate airglow at one grid-point in:
c 1) O green line (557.7 nm) - based on McDade et al., PSS, 34, 789, 1986 and
c    Melo et al. JGR, 106, 15377, 2001. (Barth mechanism, steady-state conditions);
c 2) O2 Atmospheric (0-1) and (0-0) bands (866 nm and 761.9 nm) - based on
c    Melo et al. JGR, 106, 15377, 2001 and  McDade et al., PSS, 34, 789, 1986.
c    (Barth mechanism, steady-state conditions);
c 3) Meinel OH bands (a bunch of transitions in the NIR region, mainly < 1 um)
c     Steady-state conditions, excitation by O3+H with following quanching; vibrational
c     levels up to 9 are involved
c    (most measurements are for 9-4, 8-3, 7-4, and 6-2, which are passed
c    from this subroutine, also note - only emissions due to transitions from
c    v = 6 and higher can be reasonable estimated, no satisfactory input data
c    for transitions from the lower vibrational states).

C Called by MAMCHMF3
C Calls nothing
      SUBROUTINE AIRGLOW2(AGGR,   AGAB0,  AGAB1,
     &                AGNIR,  AROH94, AROH83,
     &                AROH74, AROH62, AROHP94,
     &                AROHP83,AROHP74,AROHP62,
     &                O,O1D,O2,O3,N2,H,T,P,JO3D,
     &                JO3,JO2)

c INPUT: O,O1D,O2,O3,N2,H - number density (cm-3)
c     T  - temperature (K)
c        JO3  - photolysis rate (O3 -> O + O2 ) (s-1)
c        JO3D - photolysis rate (O3 -> O1D O2* ) (s-1)
c        JO2 - photolysis rate (O2-> ) (s-1)
C        P  - presure (Pa)
C      IMPLICIT NONE
      PARAMETER(JPBND=9)
      INTEGER I,J,JJ
      REAL O,O1D,O2,O3,N2,H, T, JO2,JO3,JO3D, P
      REAL OOO,AK5,AK1,AKO3H,AKOHO,AGABU,AGABB
C
c OUTPUT: AGGR,AGAB0,AGAB1,AGNIR - airglows in O green line, O2 atmospheric
c               (0-0) and (0-1) bands, and J03 photodissociation rate (for day-night mask),
c               respectively; volume emission rates (cm-3 s-1);
c AROH94, AROH83, AROH74, AROH62 - airglows in OH Meinel bands 9-4, 8-3, 7-4,
c                 and 6-2, respectively; volume emission rates (cm-3 s-1);
c AROHP94, AROHP83, AROHP74, AROHP62 - the same as AROH, but but to calculate
c       chemical pumping of the excited OH, model output for O3 and H are used
```

```
c       for AROH,  whereas to calculate AROHP the assumpiton of nighttime
c       photochemical equilibrium is used (i.e., k1*O*O2*M = k2*O3*H)
c
C
      REAL AGGR, AGAB0, AGAB1, AGNIR, AROH94, AROH83, AROH74, AROH62,
     &     AROHP94, AROHP83, AROHP74, AROHP62
C
c INTERNAL ARRAY for OH Meinel bands:
C OHND(9): nascent distribution of excited OH (from reaction O3+OH)
c OHAE(J=1-9, I=1-9): probabilities (in s-1) of optical transition (Einstein
c       coeff) J -> I-1 (e.g. OHAE(9,5) means transition 9-4. Note, J > I-1.
c OHAET(J=1-9): probablities of all optical transitions from level J
c      (this is a sum of AE(J=1-9, I=1-9) over I=1-9, i.e. I-1=0-8), in s-1
c OHQN2(9): collisional quanching of OH(v=1,9) by N2  (sudden death assumption
c      (i.e., only transitions v -> 0 are assumed), in cm3/s.
c OHQO2(J=1-9, I=1-9): quanching of OH(v=J) by O2 resulting in transition
c       J -> I-1 (note, J > I-1), in cm3/s.
c OHQO2T(J=1-9): quanching of OH(v=J) by O2 (this is a sum of
C        OHQO2(J=1-9, I=1-9) over I=1-9, i.e. I-1=0-8), in cm3/s.
c OHV(9): population of the excited OH(v=1,9) level, in cm3
c OHVP(9): population of the excited OH(v=1,9) level, in cm3, in assumpition
c       of chemical equilibrium for nighttime O3 (i.e., k1*O*O2*M = k2*O3*H)
c AROH(J=1-9,I=1-9): VER (cm-3 s-1) for transitions J -> I-1 (e.g., AROH(9,5)
c       means VER for 9-4 band). Note, J > I-1.
c AROHP(J=1-9,I=1-9): the same as AROH, but in assumption of chemical
c       equilibrium for nighttime O3 (i.e., k1*O*O2*M = k2*O3*H)

      REAL  OHND(JPBND),  OHAE(JPBND,JPBND),  OHAET(JPBND),
     &      OHQN2(JPBND), OHQO2(JPBND,JPBND),OHQO2T(JPBND)
C
      REAL OHV(JPBND), OHVP(JPBND), AROH(JPBND,JPBND),
     &      AROHP(JPBND,JPBND)
C
c Data for OH Meinel bands:
      data (OHND(J),J=1,JPBND) /0.00, 0.00, 0.00, 0.00, 0.00,
     &                          0.08, 0.17, 0.27, 0.48/
      data ((OHAE(J,I), I=1,JPBND), J=1,5)/
     & 2.274E+01, 0.000E+00, 0.000E+00, 0.000E+00, 0.000E+00,
     & 0.000E+00, 0.000E+00, 0.000E+00, 0.000E+00,
     & 1.342E+01, 3.242E+01, 0.000E+00, 0.000E+00, 0.000E+00,
     & 0.000E+00, 0.000E+00, 0.000E+00, 0.000E+00,
     & 1.082E+00, 3.860E+01, 3.078E+01, 0.000E+00, 0.000E+00,
     & 0.000E+00, 0.000E+00, 0.000E+00, 0.000E+00,
     & 1.327E-01, 4.082E+00, 7.187E+01, 2.146E+01, 0.000E+00,
     & 0.000E+00, 0.000E+00, 0.000E+00, 0.000E+00,
     & 2.429E-02, 5.882E-01, 9.431E+00, 1.083E+02, 9.288E+00,
     & 0.000E+00, 0.000E+00, 0.000E+00, 0.000E+00/
      data ((OHAE(J,I), I=1,JPBND), J=6,JPBND)/
     & 5.689E-03, 1.212E-01, 1.529E+00, 1.690E+01, 1.416E+02,
     & 1.072E+00, 0.000E+00, 0.000E+00, 0.000E+00,
     & 1.498E-03, 3.111E-02, 3.510E-01, 3.237E+00, 2.627E+01,
     & 1.669E+02, 1.582E+00, 0.000E+00, 0.000E+00,
     & 4.354E-04, 9.309E-03, 9.793E-02, 7.432E-01, 5.264E+00,
```

```
     & 3.658E+01, 1.815E+02, 1.354E+01, 0.000E+00,
     & 1.336E-04, 2.979E-03, 3.153E-02, 2.230E-01, 1.334E+00,
     & 9.809E+00, 4.460E+01, 1.829E+02, 3.693E+01/
      data (OHAET(J),J=1,JPBND) /22.74, 45.85, 70.48, 97.56,
     &                127.7, 161.3, 198.4, 237.8, 275.9/
      data (OHQN2(J),J=1,JPBND) /0.06E-13, 0.10E-13, 0.17E-13,
     &                     0.30E-13, 0.52E-13, 0.91E-13,
     &                     1.60E-13, 7.00E-13, 4.80E-13/
      data ((OHQO2(J,I), I=1,JPBND), J=1,5)/
     & 0.2E-12, 0.0E+00, 0.0E+00, 0.0E+00, 0.0E+00,
     & 0.0E+00, 0.0E+00, 0.0E+00, 0.0E+00,
     & 0.0E+00, 0.4E-12, 0.0E+00, 0.0E+00, 0.0E+00,
     & 0.0E+00, 0.0E+00, 0.0E+00, 0.0E+00,
     & 0.0E+00, 0.1E-12, 0.7E-12, 0.0E+00, 0.0E+00,
     & 0.0E+00, 0.0E+00, 0.0E+00, 0.0E+00,
     & 0.0E+00, 0.1E-12, 0.2E-12, 1.0E-12, 0.0E+00,
     & 0.0E+00, 0.0E+00, 0.0E+00, 0.0E+00,
     & 0.0E+00, 0.1E-12, 0.2E-12, 0.6E-12, 1.6E-12,
     & 0.0E+00, 0.0E+00, 0.0E+00, 0.0E+00/
      data ((OHQO2(J,I), I=1,JPBND), J=6,JPBND)/
     & 0.1E-12, 0.1E-12, 0.3E-12, 0.6E-12, 1.1E-12,
     & 2.2E-12, 0.0E+00, 0.0E+00, 0.0E+00,
     & 0.4E-12, 0.6E-12, 0.9E-12, 1.2E-12, 1.6E-12,
     & 2.3E-12, 3.2E-12, 0.0E+00, 0.0E+00,
     & 0.4E-12, 0.6E-12, 0.8E-12, 1.0E-12, 1.4E-12,
     & 1.9E-12, 2.5E-12, 3.3E-12, 0.0E+00,
     & 2.8E-12, 2.9E-12, 3.1E-12, 3.2E-12, 3.4E-12,
     & 3.6E-12, 3.8E-12, 4.0E-12, 4.2E-12/
      data (OHQO2T(J), J=1,JPBND)/2.00E-13, 4.00E-13, 8.00E-13,
     &                      1.30E-12, 2.50E-12, 4.40E-12,
     &                      1.02E-11, 1.19E-11, 3.10E-11/
C
c initialization
      AGGR  = 0.0
      AGAB0 = 0.0
      AGAB1 = 0.0
      AGNIR = 0.0
      DO J=1,JPBND
       OHV(J) = 0.0
       OHVP(J)= 0.0
       DO I=1,JPBND
        AROH(J,I)  = 0.0
        AROHP(J,I) = 0.0
       ENDDO
      ENDDO
C
c define common parameters:
      TK1 = 300./T
      AK1 = 4.7E-33*TK1*TK1
C
c GREEN LINE:
c ------------------
C
```

```
c constants:
      A5 = 1.18
      A6 = 1.35
      CO = 211.0
      CO2 = 15.0
      AK5 = 4.0E-12*EXP(-865.0/T)
      OOO = O*O*O
C
c VER:
      AGGRu = A5*AK1*OOO*(N2+O2)
      AGGRb = (A6+AK5*O2)*(CO2*O2+CO*O)
      AGGR = AGGRu/AGGRb
C
c ATMOSPHERIC (0-0) and (0-1) BANDS:
C -------------------------------------------------
c
c constants:
      CO    = 19.3333
      CO2   = 6.6666
      AK2O2 = 4.0E-17
      AK2N2 = 2.2E-15
      AK2O  = 8.0E-14
      A2    = 0.083
C
c VER:
c common elements for two bands
      AGABu = AK1*O*O*(N2+O2)*O2
      AGABb = (A2+AK2O2*O2+AK2N2*N2+AK2O*O)*(CO2*O2+CO*O)
c (0-0) BAND:
      A1    = 0.079
      AGAB0 = A1*AGABu/AGABb
c (0-1) BAND:
      A1    = 0.004
      AGAB1 = A1*AGABu/AGABb
C
c JO3 photodisociation rate:
C -------------------------------
      AGNIR   = JO3
C
c OH MEINEL BANDS:
C----------------------------
C
c reaction rates for O3+H -> OH(v)+O2 and OH(v)+O -> H+O2:
      AKO3H = 1.4E-10*EXP(-470/T)
      AKOHO = 2.5E-10
c reaction rate for O+O2+M -> O3+M
      AKOO2M=6.0E-34*TK1**2.3
c calculate population of OHV=OH(v)=OH(v,production)/OH(v,loss)
C
      DO JJ = 1,JPBND
        J = 10-JJ
        JP1 = J+1
C
```

```
c production term
c 1) chemical pumping for model O3 and H  - CP
c    and in the assumption of chemical equilibrium for nighttime O3 - CPP
      CP  = AKO3H*O3*H*OHND(J)
      CPP = AKOO2M*O*O2*(O2+N2)*OHND(J)
c CPP should be zero-ed below 0.01 hPa (1 Pa) and for daytime
c  (note, minimum J, and so JO3, is 1E-30, which a background nighttime value)
      IF((P .GT. 1.0) .OR. (JO3 .GT. 1.0E-29)) CPP = 0.0
c 2) optical pumping (transitions from the higher excited levels)
      OP = 0.0
      OPP= 0.0
      IF(J.EQ.JPBND) GOTO 10
       DO I=JP1,JPBND
         OP = OP+OHV(I)*OHAE(I,JP1)
         OPP= OPP+OHVP(I)*OHAE(I,JP1)
       ENDDO
   10  CONTINUE
c 3) collisional transitions from the higher excited levels
      CT = 0.0
      CTP= 0.0
      IF(J.EQ.JPBND) GOTO 11
       DO I=JP1,JPBND
        CT = CT+OHV(I)*OHQO2(I,JP1)
        CTP = CTP+OHVP(I)*OHQO2(I,JP1)
       ENDDO
       CT = CT*O2
       CTP = CTP*O2
   11  CONTINUE
C
c loss term
c 1) radiative loss
      RL = OHAET(J)
c 2) collisional deactivation
      CD = OHQN2(J)*N2 + OHQO2T(J)*O2
c 3) chemical loss
      CL = AKOHO*O
C
c population of the excited vibrational state OH(v=J) for 2 versions
      OHV(J)  =  (CP+OP+CT)/(RL+CD+CL)
      OHVP(J) =  (CPP+OPP+CTP)/(RL+CD+CL)
     ENDDO
C
c VER for all possible transitions:
     DO J=1,JPBND
      DO I=1,JPBND
       AROH(J,I) =  OHV(J)*OHAE(J,I)
       AROHP(J,I)=  OHVP(J)*OHAE(J,I)
      ENDDO
     ENDDO
C
c OUTPUT: VER for 4 selected transitions (bands)
c force OH airglow to be zero for
c        a) daytime and
```

```
c       b) outside of the 70-105 km (4.54-0.0113 Pa) region.
C
      IF((JO3.GT.1.0E-29) .OR. (P.GT.4.54) .OR. (P.LT.0.0113)) THEN
        AROH94  = 0.0
        AROH83  = 0.0
        AROH74  = 0.0
        AROH62  = 0.0
        AROHP94 = 0.0
        AROHP83 = 0.0
        AROHP74 = 0.0
        AROHP62 = 0.0
      ELSE
        AROH94  = AROH(9,5)
        AROH83  = AROH(8,4)
        AROH74  = AROH(7,5)
        AROH62  = AROH(6,3)
        AROHP94 = AROHP(9,5)
        AROHP83 = AROHP(8,4)
        AROHP74 = AROHP(7,5)
        AROHP62 = AROHP(6,3)
      ENDIF
C
      RETURN
      END
```

< Appendix E >

What WINDII airglow measurements tell us about the upper atmosphere

Airglow is light produced by photochemical processes in the upper atmosphere, where collisions between species are less frequent than at lower altitudes, allowing excited species sufficient time to undergo chemical reactions before they are deactivated. The driver for all of this is sunlight, which ionizes atoms and molecules, and dissociates molecules into atoms, in particular molecular oxygen into its constituent atoms. At altitudes of around 100 km and above, these atoms live for hours to weeks so can create airglow during the night, when the sun is not present. Even during the long polar night the airglow can persist, as atomic oxygen can be transported from lower to higher latitudes. Although there are many airglow emissions, those arising from atomic oxygen are perhaps the most important and all of the emissions observed by WINDII come from the so-called oxygen airglow.

Airglow emission rate

WINDII measures three airglow quantities, 1) emission rate, 2) wind and 3) temperature. The fundamental emission rate quantity is “volume emission rate”, the number of photons emitted from a unit volume per second, usually measured in photons cm^{-3} s^{-1}. This is not an obvious measurement, as an instrument viewing the airglow sees the photons coming from a column around the line of sight, in other words the number of photons emitted per second from a 1 cm^2 column along the line of sight. This quantity is given a special name, the Rayleigh; Lord Rayleigh IV was a pioneer in airglow measurement. One Rayleigh is 10^6 photons per second from a 1 cm^2 column; this is the “integrated emission rate” of the airglow, and from the ground that is all that can be measured. However, from an altitude of 585 km WINDII viewed the Earth’s limb, from 80 up to 300 km above the Earth edge. From these multiple views at different altitudes it is possible to deduce the volume emission rate as a function of altitude through a process called inversion and so obtain the vertical profile of volume emission rate.

WINDII observed the $O(^1S)$ atomic oxygen green line airglow at 557.7 nm, the $O(^1D)$ atomic oxygen red line airglow at 630.0 nm, the hydroxyl radical (OH) emission near 733 nm the O^+ (^2P) emission at 732 nm and the molecular O_2 Atmospheric Band emission at 765 nm. All of these derive from atomic oxygen and so by measuring their airglow volume emission rates one can, by knowing the chemical reactions involved, determine the vertical profiles of atomic oxygen, something that is extremely hard to do in any other way. The peak of production of atomic oxygen through solar photodissociation is around 130 km and it was long thought that the atomic oxygen reached lower levels near 100 km where these airglow emissions occur through diffusion. WINDII observed a tremendous variability in the atomic oxygen profiles (from the volume emission rate profiles), showing that larger scale dynamical motions of the atmosphere are a major driver of downward transport, and had the winds to prove it. What has just been written applies to airglow observed at night. During the daytime additional photochemical processes, driven by the photoelectrons produced by sunlight in the atmosphere, enhance the green and red line atomic oxygen airglows, and produce the O^+ emission that is seen only in the daytime. At higher altitudes, around 200 km the O^+ emission offers the possibility of observing atomic oxygen concentrations, as the O^+ is produced by solar radiation ionizing the neutral atomic oxygen. This capability has not yet been achieved, but success is expected in the coming year.

In summary, observations of volume emission rates yield the concentrations of constituents as a function of altitude, latitude, longitude and local time, which for WINDII has been primarily atomic oxygen. Limited determinations of nitric oxide have also been made and that can be further pursued.

Winds

The atomic oxygen red and green lines are pure spectral lines because there are no isotopic effects, and nuclear spin coupling is absent. If atomic oxygen is carried by the background wind then the airglow emission from it is Doppler shifted, and this can readily be measured because the lines are so narrow. WINDII is unique in using a Michelson interferometer for this satellite measurement. It is not an FTS, where the observed interferogram is Fourier transformed to yield a spectrum. Since the viewed atomic line is a single narrow line, its Fourier transform is just a sinusoid, and one need only measure the phase of the sinusoid to measure the wind, which can be done very accurately. Not only that, but with the limb views, one can determine the wind profiles. The different airglow emissions occur at different altitudes, but by using different emissions one can cover the range from 80 km to 300 km.

Winds are the key observable of dynamics, and the first WINDII observations were of the migrating diurnal tide near the equator, caused by heating in water vapour and ozone near the Earth's surface. Because of conservation of energy the amplitude of this tidal perturbation grows as the atmospheric density decreases and near 100 km WINDII measured 70 m s^{-1}, astounding many researchers as earlier estimates of the tide were much lower. At mid-latitudes the migrating semi-diurnal tide becomes important. These tides are called migrating because they migrate with the sun; the diurnal tide has a single bulge underneath the sun, not two as is the case for lunar ocean tides. WINDII also observes the mean winds, which transport atomic oxygen from lower to higher latitudes, maintaining atomic oxygen in the polar cap during winter. Of current interest are non-migrating tides, not driven by the sun but by effects near the Earth's surface such as strong convection. These have many different wavenumbers, the number of waves around the Earth, and can propagate eastward, westward, or not at all. WINDII also observes winds produced by geomagnetic disturbances, as high as 700 m s^{-1}.

Temperature

The airglow emission lines are inherently extremely narrow, but in the atmosphere have widths solely determined by the thermal motions of the emitting atoms. This means that a measurement of their widths yields the ambient temperature. This is so for the $O(^1S)$ green line, which has a lifetime of about 1 second. Up to about 130 km the excited $O(^1S)$ atoms make sufficient collisions to bring them into thermal equilibrium with their surroundings (but not so many collisions as to deactivate), so yield the true temperature. WINDII measures the Doppler widths indirectly, using the fact that with increasing temperature the ratio of the sinusoidal amplitude to its mean value (which Michelson called the visibility) decreases as the different components of the line increasingly interfere with one another. Above 130 km WINDII observes a continually increasing temperature and it is not yet clear as to how this should be interpreted. For the $O(^1D)$ red line, which has a lifetime of about 110 sec, the Doppler temperatures are valid up to 300 km. For some purposes, such as investigating tides, the absolute value of the temperature is not important, only its variation and this needs to be further explored.

The Future

During the UARS mission the focus was on the middle atmosphere (they used the name upper atmosphere as they thought the public would not understand what was meant by middle atmosphere) and the upper limit was considered to be 110 km. For this reason the WINDII team also focussed on the airglow emissions near 100 km. Now, twenty years later, the upper thermosphere around 250 km is of current interest and there is a wealth of data that have not been investigated. With the new data processing we have a new resource for studying this region.